# Computational Modeling, Design and Synthesis of Selective Cannabinoid Receptor 2 ($CB_2$) Agonists

by

Logan Taylor Neel

A dissertation submitted to the Graduate Faculty of
Auburn University
in partial fulfillment of the
requirements for the Degree of
Doctor of Philosophy

Auburn, Alabama
December 11, 2021

Keywords: computational modeling, cannabinoids, organic synthesis, drug discovery, indoles



Approved by

Dr. Forrest Smith, Chair, Professor of Drug Discovery and Development
Dr. Randall Clark, Gilliland Professor of Drug Discovery and Development
Dr. Jack DeRuiter, Hill Crest Professor of Drug Discovery and Development
Dr. Murali Dhanasekaran, Professor of Drug Discovery and Development

## Abstract

Synthetic cannabinoids that are synthesized and used recreationally are a world-wide health problem. They are synthesized in order to mimic the euphoric effects similar to THC, but due to the higher affinity at the cannabinoid receptors and the unknown mechanism of action, they often cause more severe side effects or even death. Unfortunately, the wide array of starting materials, it is easy to design and synthesize newer synthetic cannabinoids as soon as one is banned. In order to prohibit the use of these designer drugs, they need to be structurally identified. The use of analytical methods such as GC-MS and GC-IR can help with the identification of the synthetic cannabinoids and their respective regioisomers. However, synthetic cannabinoids can also be used therapeutically. Specifically, $CB_2$ selective agonists have become an interesting therapeutic target. Targeting $CB_2$ instead of $CB_1$ is favorable because modulation of $CB_2$ does not elicit unwanted psychotropic effects that are seen with $CB_1$. Designing selective $CB_2$ agonists was more challenging without the publication of the $CB_2$ X-Ray crystal structure. The use of molecular modeling to design a homology model of $CB_2$ in order to design and develop selective $CB_2$ agonists that will be synthesized for therapeutic use is the main goal of this project.

**Acknowledgments**

I would first like to thank my main advisor, Dr. Forrest Smith, for his continuous guidance that he has given me in the past five years. I knew after I volunteered in his lab the summer of 2016 that I wanted to stay at Auburn, specifically in his lab because I knew he would be someone I could learn a lot from. I am glad he gave me the chance and accepted me in his lab as a PhD student. I am truly blessed to have such a caring advisor that provided me with a great deal of knowledge in order for me to grow in my career as a scientist. I appreciate all his time, effort and dedication that I was given and I could not have asked for a better mentor.

Next, I would like to thank my committee members, Dr. Randall Clark, Dr. Jack DeRuiter and Dr. Murali Dhanasekaran for all the support and advice they have given me throughout the duration of my graduate school career.

I also would like to thank the DDD graduate department for their support and also for allowing me to be a Graduate Teaching Assistant.

A special thanks goes to Dr. David Riese for not giving up on me. He gave me the opportunity to volunteer in his lab in 2015 and even though I left his lab saying “this is just not for me”, he continued to guide me and truly help me find my passion. I will always be grateful for him and his passion to help students.

Thank you to CNSi and AFPE for the financial support that I had received in order for me to continue my research.

Last but not least, I would like to thank my family and friends that helped me along the way. This chapter of my life was challenging and without them I would not have made it. A special thanks goes to my husband, Garrett Baker, for being by my side throughout my journey

of obtaining my PhD. You believe in me, you are my biggest supporter and you are my best friend.

## Table of Contents

## List of Tables

## List of Figures

## List of Schemes

## List of Abbreviations

| | |
|---|---|
| THC | Δ9-tetrahydrocannabinol |
| ECS | Endocannabinoid System |
| AD | Alzheimer's Disease |
| PD | Parkinson's Disease |
| HD | Huntington's Disease |
| GPCRs | G-protein coupled receptors |
| AEA | Anandamide |
| 2-AG | 2-Arachidonoylglycerol |
| $CB_1$ | Cannabinoid Receptor 1 |
| $CB_2$ | Cannabinoid Receptor 2 |
| CNS | Central nervous system |
| NAPE-PLD | N-acylphosphatidylethanolamide-specific phospholipase D |
| PLC | Phospholipase C |
| DAGL | Sn-1-diacylglycerol lipase |
| EMT | Endocannabinoid membrane transport |
| FAAH | Fatty acid amide hydrolases |
| MAGL | Monoacylglyceride lipase |
| CBD | Cannabidiol |
| Cryo-EM | Cryogenic electron microscopy |
| CADD | Computer-aided drug design |
| SBDD | Structure-based drug design |
| LBDD | Ligand-based drug design |

| | |
|---|---|
| NMR | Nuclear magnetic resonance |
| SAR | Structure activity relationship |
| ACE | Angiotensin-converting enzyme |
| ACE II | Angiotensin-converting enzyme II |
| GC-MS | Gas chromatography-mass spectrometry |
| GC-IR | Gas chromatography-infrared spectroscopy |
| DMF | Dimethylformamide |
| KOH | Potassium hydroxide |
| EI | Electron ionization |
| EI/MS | Electron ionization mass spectrometry |
| PDC | Pyridinium dichromate |
| $POCl_3$ | Phosphorous oxychloride |
| DMP | Dess Martin Periodinane |
| NaOH | Sodium hydroxide |
| VSGB | Variable-dielectric generalized Born |
| PDB | Protein Data Bank |
| IFD | Induced fit docking |
| POPC | 1-Palmitoyl-2-oleoyl-sn-glycerol-3-phosphocholine |
| SPC | Simple point charge |
| NPT | Isothermal-Isobaric |
| RMSD | Root mean square deviation |
| DUD-E | Database of useful decoys: enhanced |
| BEDROC | Boltzmann-enhanced discrimination of receiver operating characteristic |

ROC Area under the receiver operating characteristic curve

RIE Robust initial enhancement

AUAC Area under the accumulation curve

FBDD Fragment based drug design

HCl Hydrochloric acid

TLC Thin layer chromatography

TsOH p-Toluenesulfonic acid

DMSO Dimethyl sulfoxide

THF Tetrahydrofuran

N-Cbz N-carboxybenzyl

$K_2CO_3$ Potassium carbonate

# Chapter One: Introduction

## *1.1 Overview of the Endocannabinoid System*

The use of *Cannabis sativa* dates back to the B.C. era where it was used recreationally for the psychoactive, euphoric effects [1]. However, it was also used therapeutically for ailments such as depression and pain. Cannabis research developed very slowly due to the unknown chemical structures. Cannabis contains over 100 constituents which are all structurally similar, so the separation and isolation was very difficult to achieve. However, as modern separation techniques improved, the main psychoactive constituent of cannabis, $\Delta^9$-tetrahydrocannabinol (THC) (Figure 1), was first isolated and structurally identified in 1964 by Mechoulam [2,3]. This prompted a dramatic increase in research in the cannabinoid field, which 20 to 25 years later led to the discovery of the endocannabinoid system (ECS).

The ECS consists of three main components which include the endogenous cannabinoids (or endocannabinoids), the cannabinoid receptors and the proteins that are responsible for synthesis, transportation and degradation of the endocannabinoids [4,5]. The ECS is responsible for regulating and balancing many different physiological roles in the human body. Some of these physiological roles include appetite, digestion, immune function, sleep, mood, reproduction, memory and pain. Due to the various biological pathways the ECS influences, it has captured the interest of many scientists as an intriguing drug target. Schizophrenia is one of the disease states the ECS is being studied for due to the altered levels of endocannabinoids in schizophrenic patients [6]. Neuroinflammatory diseases such as Alzheimer's Disease (AD), Parkinson's Disease (PD) and Huntington's Disease (HD) are being studied due to the altered levels of the cannabinoid receptors and/or endocannabinoids in specific areas of the brain during different disease stages. Treatment options for anxiety and depression are being linked to the ECS due to

altered levels of endocannabinoids while taking antipsychotic medications. The ECS is also being studied for anticancer effects due to the expression of altered cannabinoid receptors in brain, gynecological, digestive tract, breast and prostate tumors [7].

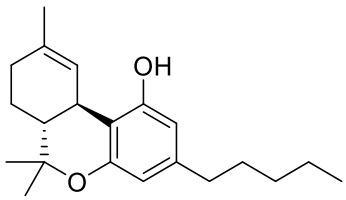


1

**Figure 1.** The chemical structure of $\Delta^9$-tetrahydrocannabinol (THC).

The endocannabinoids are signaling lipids that are naturally produced by the human body. The endocannabinoids mimic the action of THC, meaning they bind to and activate the cannabinoid receptors [8]. However, they do not produce the psychotropic effects that are seen with THC because they are eliminated from the biological system after a period of time. The endocannabinoids do not exclusively interact with the cannabinoids receptors, but they have potential to activate a wide range of g-protein coupled receptors (GPCRs), nuclear receptors and ion channels [4]. The two mainly studied endocannabinoids are anandamide (AEA) and 2-arachidonoylglycerol (2-AG), shown in Figure 2. Interestingly, they are not similar in structure to THC even though they activate the same receptors. Instead, they are long chain polyunsaturated fatty acids with AEA containing an ethanolamide constituent and 2-AG containing a glycerol. Even though they are similar in structure, they play very distinct physiological roles.

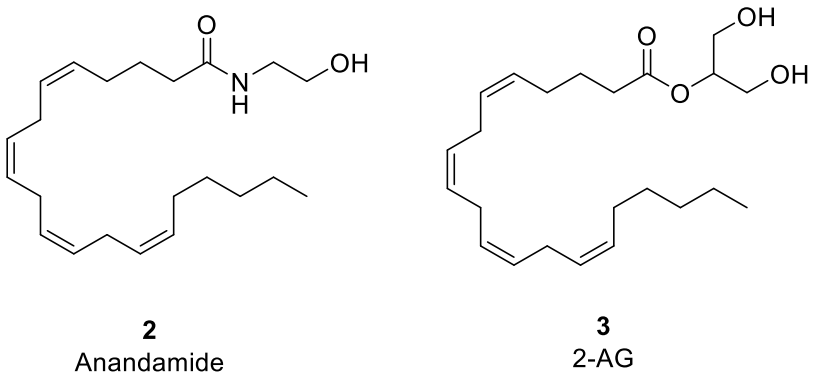


**2**
Anandamide

**3**
2-AG

**Figure 2.** The chemical structures of AEA and 2-AG.

The cannabinoid receptors are GPCRs, which are seven transmembrane helices with an extracellular N-terminus and an intracellular C-terminus. The cannabinoid receptors are primarily coupled to inhibitory G proteins, so upon activation they inhibit adenylyl cyclase, inhibit voltage sensitive calcium channels, stimulate mitogen-activated protein kinases, inwardly rectifying potassium channels and recruit beta arrestins [9]. However, there have been a few studies indicating the receptors can engage in $G_{q/11}$ and $G_s$ pathways. The two main cannabinoid receptors are cannabinoid receptor 1 ($CB_1$) and cannabinoid receptor 2 ($CB_2$), which were cloned in 1991 and 1993, respectively. The $CB_1$ receptor is found primarily in the central nervous system (CNS), with the highest expression on axons and presynaptic terminals of neurons in the amygdala, hippocampus, cortex, basal ganglia and cerebellum [10,11]. The $CB_2$ receptor is found primarily on immune system cells which modulates immunological function, cell migration and cytokine release. $CB_2$ is also found in the CNS, but at a much lower concentration than $CB_1$ [12]. Due to the localization of the receptors, it is evident that $CB_1$ is the receptor responsible for the psychotropic effects that are seen upon binding of THC.

The enzymes responsible for the synthesis and degradation of the endocannabinoids, AEA and 2-AG, are different. AEA is synthesized by different metabolic routes, but the main enzyme responsible is N-acylphosphatidylethanolamide-specific phospholipase D (NAPE-PLD) [13]. The enzymes responsible for the synthesis of 2-AG are phospholipase C (PLC) and sn-1-diacylglycerol lipase (DAGL). The endocannabinoids are too polar to passively diffuse into the intracellular component of a nearby cell and it has been studied that carrier mediated facilitated diffusion utilizing the "endocannabinoid membrane transport (EMT)" is likely the mode of transportation [14]. The degradation of AEA is completed by fatty acid amide hydrolases (FAAH), which produces ethanolamine and arachidonic acid. The enzyme responsible for the degradation of 2-AG is monoacylglyceride lipase (MAGL), which produces arachidonic acid and glycerol.

*1.2 Cannabinoids*

A cannabinoid refers to any chemical that interacts with the cannabinoid receptors. The three main types of cannabinoids are: endocannabinoids, phytocannabinoids and synthetic cannabinoids [15]. There are also classical and nonclassical cannabinoids, whereas the classical cannabinoids are structurally similar to THC. An example of this would be the dibenzopyran derivatives such as THC, its isomers, and any structurally similar analogs. The nonclassical cannabinoids are not structurally similar to THC and consists of groups such as the aminoalkylindoles, diarylpyrazoles, eicosanoids and quinolines [16]. The endocannabinoids are lipid compounds that are naturally produced by the body, with the main two being AEA and 2-AG that were mentioned earlier.

A phytocannabinoid is a plant derived cannabinoid, with the most popular one being THC. THC is one of many phytocannabinoids produced by the cannabis plant, but it is the main

constituent responsible for the euphoric effects when ingesting marijuana [17]. The phytocannabioid, THC, is used recreationally, but it also being evaluated as a medicinal agent. Over the past two decades, attitudes are changing over the recreational and medicinal use of THC [18]. Another phytocannabinoid that was found in *Cannabis sativa* is cannabidiol (CBD), shown in Figure 3. CBD is structurally similar to THC, but interestingly it is considered non psychoactive, which has recently made it therapeutically favorable [19]. CBD has been studied to have antioxidant and anti-inflammatory effects. CBD has shown potential in diseases states such as diabetes, cardiovascular diseases, cancer, anxiety, epilepsy and arthritis.

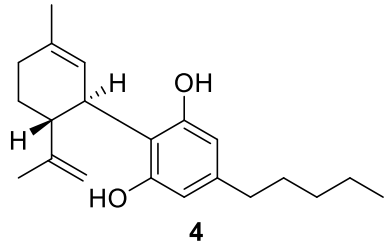


**4**

**Figure 3.** The chemical structure of cannabidiol (CBD).

A synthetic cannabinoid is a man-made chemical that interacts with the cannabinoid receptors and they can be designed for therapeutic or recreational use [20]. An example of a classical synthetic cannabinoid is nabilone, shown in Figure 4. Nabilone also known as, Cesamet, is an FDA approved medication for the treatment of severe nausea and vomiting that is caused by chemotherapy [21]. It is highly similar in structure to THC and acts as an agonist at the cannabinoid receptors. An example of a nonclassical synthetic cannabinoid is CP 55,940, shown in Figure 4. CP 55,940 was designed by Pfizer in 1974, but never went to market due to the enhanced CNS psychoactivity. CP 55,940 acts as a full agonist at $CB_1$ and $CB_2$ receptors and it is 45 times more potent than THC [22]. Another example of a nonclassical synthetic cannabinoid is

WIN 55,212-2, shown in Figure 4. WIN 55,212-2 is considered an aminoalkylindole compound that is not structurally similar to THC but produces the same effects [23]. WIN 55,212-2 is a potent full agonist at the cannabinoid receptors and is currently banned in the United States as a scheduled I drug.

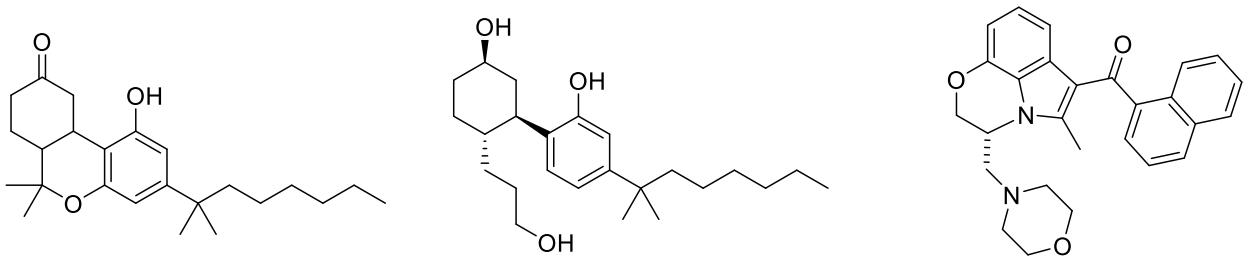


**5** Nabilone **6** CP 55,940 **7** WIN 55,212-2

**Figure 4.** The chemical structures of the classical cannabinoid, nabilone, and nonclassical cannabinoids, CP 55,940 and WIN 55,212-2.

*1.3 Spice*

Synthetic cannabinoids are also designed, synthesized and used for recreational purposes. These synthetic cannabinoids have street names such as Spice, K2 and Magic Gold and are synthesized in underground laboratories [24]. Spice is a dried herbal substance with unknown amounts of chemicals sprayed on them that will then be ingested usually by smoking. Spice is sold in local gas stations in sophisticated packing with the phrase "Not for Human Consumption" written on them. However, the use of spice is increasing which is likely due to the difficulty in detecting the drug on standard drug tests and it also does not produce a smell like THC, which makes it easier to hide [25]. These synthetic cannabinoids are causing an extreme human health concern due to the unpredictable toxicity and abuse potential.

Spice is similar to THC only because it binds to and interacts with the cannabinoid receptors. However, the synthetic cannabinoids in spice are not structurally similar to THC, so they can interact in unpredictable ways, causing unknown side effects [26]. Also, the synthetic cannabinoids that constitute spice often act as full potent agonists at the cannabinoid receptors, whereas THC is only a partial agonist. There has been an increase in hospital admissions and poison control calls associated with spice use that refer to side effects such as chest pains, hallucinations, tachycardia, irritability, and sometimes death [27]. The unpredictable mechanism of action and the increased affinity for the cannabinoid receptors is related to the severe and sometimes fatal side effects that are associated with spice.

An example of a synthetic cannabinoid that is a common constituent found in spice is JWH-018, shown in Figure 4 [28]. JWH-018 is an aminoalkylindole with the chemical formula $C_{24}H_{23}NO$. JWH-018 acts as a full agonist at $CB_1$ and $CB_2$ with binding affinity values of 9 nm and 2.94 nm, respectively. It is considered to be four times more potent than THC and has been associated with psychotic episodes after use. In 2011, shortly after JWH-018 was identified, it was banned in a number of European countries and some American states [29].

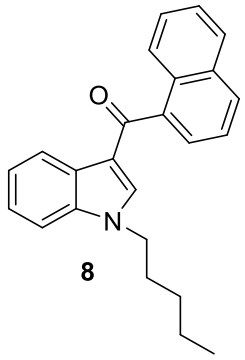


**Figure 5.** The chemical structure of JWH-018.

Only three weeks after JWH-018 was banned in Germany, second-generation products hit the market. These second-generation products are usually slight modifications of the parent drug in order to keep the same euphoric effects, but avoid being detected. An example of a second-generation synthetic cannabinoid is JWH-073, shown in Figure 5 [30]. JWH-073 is also an aminoalkylindole with a chemical formula of $C_{23}H_{21}NO$. JWH-073 is structurally similar to JWH-018, with the exception of a butyl alkyl side chain instead of a pentyl. As soon as JWH-073 was identified in spice products, it was banned as well, but the cycle continues with other derivatives being developed and becoming drugs of abuse. Congress tried to alleviate this problem by the passage of Anti-Drug of Abuse Act, specifically Subtitle E: Controlled Substance Analogue Enforcement Act of 1986, which states "Amends the Controlled Substances Act to provide that controlled substance analogues shall be treated as a schedule I substance" [31]. However, the synthesis, sale and usage of these designer drugs are a challenge to keep up with due to the endless variety of analogs.

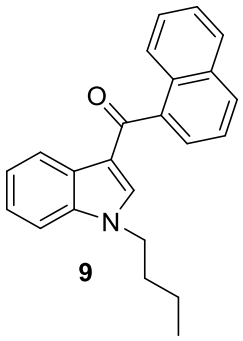


**Figure 6.** The chemical structure of JWH-073.

Another issue of synthetic cannabinoids are the structural isomers. These structural isomers contain the same molecular weight and often coelute on analytical detection methods, which

often causes misidentification [32]. The structural isomers are easily attainable and synthesizable due to the wide availability of the precursor materials. The differentiation of the positional isomers by analytical methods is of importance to the forensic, medical and criminal law field in order to keep the synthetic drug use at a minimum. The development of an isomer specific analytical method is of great value in order to identify isomers that play a role in the synthetic cannabinoid drug chemistry field.

*1.4 $CB_1$ vs. $CB_2$ as a therapeutic target*

The two main cannabinoid receptors, $CB_1$ and $CB_2$, are GPCRs with 48% sequence identity and 68% transmembrane identity [33]. Although both receptors are thought to dimerize or heterodimerize with other GPCRs, this has mainly been investigated with $CB_1$. $CB_1$ has been shown to associate with dopamine $D_2$ receptors, orexin A receptors, adenosine 2A receptors and delta opioid receptors. There is not much known about the allosteric modulation with $CB_2$, but several negative and positive allosteric modulation sites have been identified with $CB_1$. One of the main differences between $CB_1$ and $CB_2$ is the localization of the receptors. $CB_1$ is located primarily in the CNS, but also present in the liver, adipose tissue and skin. $CB_2$ receptors are located primarily on immune cells, but also found in the CNS at a much lower concentration than $CB_1$. The difference in localization of the receptors is suspected to be the reason why $CB_1$ is associated with the unwanted psychotropic effects and $CB_2$ is not. Another unique feature to the $CB_2$ receptor is that it is highly inducible [34]. It has been studied that the $CB_2$ expression increases on microglia in the CNS following any inflammation or injury. This suggests that $CB_2$ could potentially play an important protective role in neuroinflammatory diseases.

As previously stated, targeting the $CB_1$ receptor often leads to unwanted psychotropic effects. Two examples of $CB_1$ targeted drugs are, Rimonabant and Taranabant, shown in Figure 6, which were designed for therapeutic use [35, 36]. Rimonabant is a potent, selective $CB_1$ antagonist/inverse agonist with a binding affinity of 1.98 nm. It was approved in Europe in 2006 for the treatment of obesity and other metabolic disorders. It acts by inhibiting the stimulation of the $CB_1$ receptor, which reduces the overactive ECS that is seen in the obese population. This then will improve lipid and glucose metabolism and regulate food uptake. However, in 2008, it was removed from the market due to the crippling CNS side effects such as suicidal ideation and depression. Taranabant is a $CB_1$ inverse agonist that was developed by Merck for the treatment of obesity [37]. However, it was stopped at phase III clinical trials due to the unwanted CNS side effects of depression, anxiety, fear, and anger.

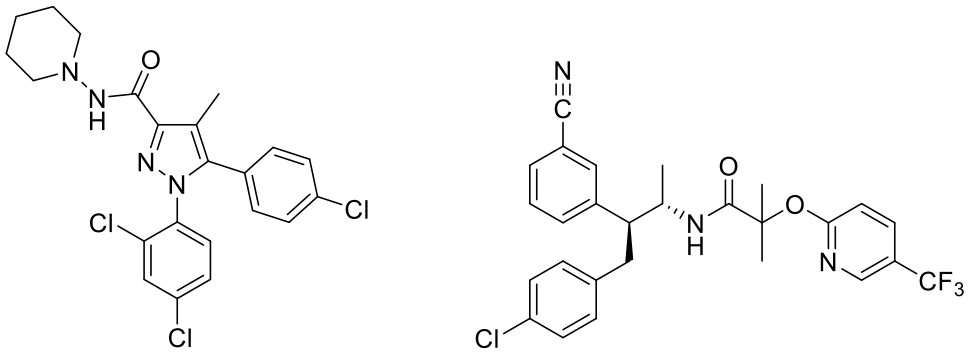


**10**
Rimonabant

**11**
Taranabant

**Figure 7.** The chemical structures of Rimonabant and Taranabant.

Recently, $CB_2$ selective agonists have gained interest as therapeutic agents since they do not elicit the psychotropic effects that are seen with $CB_1$ [38]. Studies have shown that the disease states that $CB_2$ has therapeutic potential in are osteoporosis, cancer, drug addiction, anxiety, liver

disease, pain and neuroinflammation. It is significant that $CB_2$ receptors are highly inducible following inflammation and tissue injury, which suggests potential for neuroinflammatory diseases.

The majority of studies have investigated the $CB_2$ receptor as a therapeutic target for inflammation and pain. Researchers have developed selective $CB_2$ selective agonists with *in vivo* and *in vitro* effectiveness without the psychotropic effects, but further safety and toxicity studies need to be evaluated [39]. The examples include HU-308, AM-1241 and GW-405833, which are shown in Figure 7. HU-308 was the first selective $CB_2$ agonist synthesized in the 1990s. It has a $CB_2$ binding affinity of 22.7 nm and has shown to have anti-inflammatory and peripheral antihyperalgesic properties with no CNS activity. AM-1241 is an aminoalkylindole that acts as a potent, selective $CB_2$ agonist with a binding affinity of 3.4 nm. It produces peripheral mediated antinociception effects and no CNS activity. GW-405833 is another selective $CB_2$ agonist with binding affinity of 14 nm at the $CB_2$ receptor. It displays anti-inflammatory and antihyperalgesic properties as well.

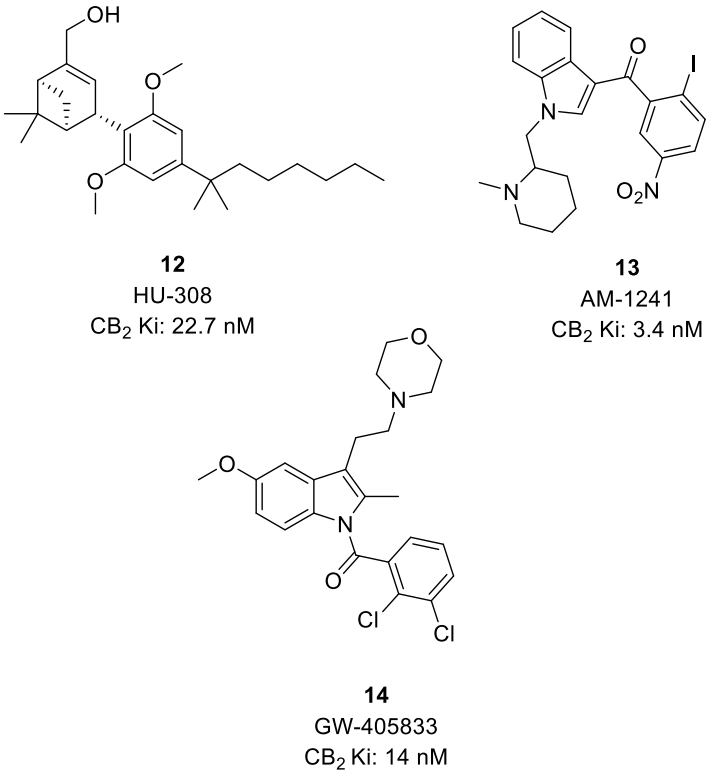


**Figure 8.** The chemical structures of HU-308, AM-1241 and GW-405833 with corresponding $CB_2$ binding affinity values.

Another well studied selective $CB_2$ selective agonist with a variety of therapeutic properties is JWH-133, shown in Figure 8. JWH-133 is a synthetic cannabinoid with a 200-fold greater $CB_2$ selectivity than $CB_1$, with a binding affinity value of 3.4 nm [40]. JWH-133 was designed from the nonselective cannabinoid agonist, HU-210 shown in Figure 8. The removal of the hydroxy groups from HU-210, along with a few minor modifications significantly increased $CB_2$ selectivity and affinity [41]. The pharmacological properties that JWH-133 has shown include neuroprotective, anti-inflammatory, gastroprotective, hepatoprotective, cardioprotective, anti-cancer and nephroprotective properties.

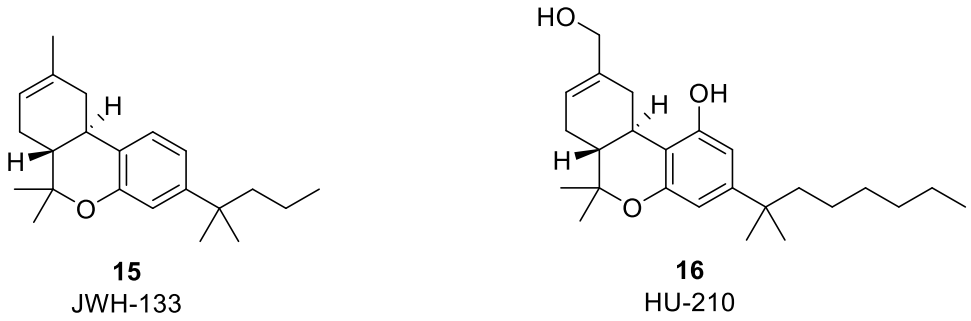


**Figure 9.** The chemical structures of JWH-133 and HU-210.

*1.5 Computer-aided drug design*

Designing selective $CB_2$ agonists for therapeutic use is a difficult task, especially without the crystal structure of the target protein. The cryogenic electron microscopy (cryo-EM) structure of $CB_2$ bound to the agonist WIN 55,212-2 was only recently published in early 2020 [42]. It is hypothesized that the design of selective $CB_2$ agonists will be accelerated due to the publication of the $CB_2$ protein and by use of computer-aided drug design (CADD).

The drug discovery process is a very complex and challenging task that is costly and time consuming [43]. On average, it takes approximately 10-15 years and over one billion dollars to bring one drug to the market. The use of computers to design drugs more efficiently is called computer aided drug design (CADD) and has significantly advanced over the years. CADD is a way for scientists to utilize mathematical models that will help decrease time and money spent on bringing a new drug to market. There are two main categories that define CADD and they are structure-based drug design (SBDD) and ligand-based drug design (LBDD) [44].

SBDD is when the target protein is known, which can then be analyzed in order to determine interactions that are important for binding. This information can be used in order to optimize known compounds or to design novel compounds. The first step of SBDD is target

identification which can be completed by X-Ray crystallography, nuclear magnetic resonance (NMR), or homology modeling. The second step is to analyze and identify the target protein for binding sites. Then completing a virtual screening utilizing a database of compounds, which then will be scored and ranked based on steric, hydrophobic, and electrostatic interactions. This information can then be utilized to further optimize the compound to increase potency at the target protein.

LBDD is when the target protein is unknown, but the ligands of the target are known. The known ligands are used to establish a relationship between their chemical structures and their biological activities. This is also known as structure activity relationship (SAR). This information will then be used to develop a pharmacophore model, which is a model that contains the appropriate steric and electronic features needed for optimal binding. This information will be utilized in order to optimize known ligands or to design novel compounds.

There are numerous drugs that were designed by or optimized by CADD that have been approved. A few examples of this are Fosamprenavir, Nilotinib, Captopril, and Losartan, which are shown in Figure 9 [45]. Fosamprenavir is a sulfonamide and is a prodrug of the antiretroviral protease inhibitor, amprenavir and is used to control HIV infections. Nilotinib is an aminopyridine derivative that acts as an inhibitor at Bcr-Abl tyrosine kinase for the treatment of chronic myeloid leukemia. Captopril is a sulfur containing drug that acts as an angiotensin-converting enzyme (ACE) for the treatment of hypertension. Losartan is an angiotensin-converting enzyme II (ACE II) antagonist that is used also for the treatment of hypertension, but can also be used for diabetic nephropathy and to reduce stroke.

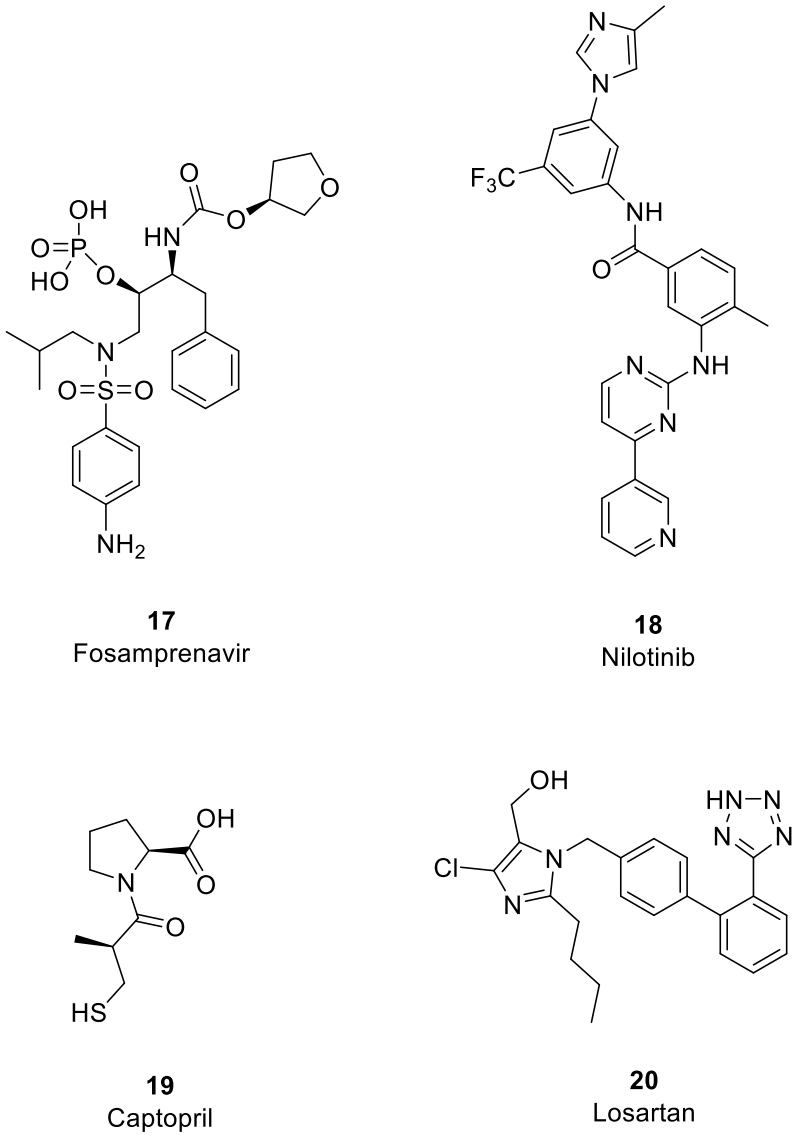


**Figure 10.** The chemical structures of FDA approved medications that were designed and/or optimized by CADD.

## Rational and Research Objectives

Continuous developments of synthetic cannabinoids that will be used as drugs of abuse is a worldwide health concern. The development of analytical methods is a task that will always need to be reevaluated in order to identify newer synthetic cannabinoids. The first objective is to synthesize a variety of regioisomeric aminoalkylindoles. These compounds will then be used in order to develop analytical tools that can be used to help differentiate the isomers from each other.

Based upon previous scientific data, it is evident that the aminoalkylindoles have cannabinoid receptor affinity. It is also evident that selectively targeting $CB_2$ is therapeutically favorable in comparison to $CB_1$. However, the $CB_2$ crystal structure was not available until early 2020. So, CADD can be utilized in order to design a homology model of $CB_2$. The homology model can be validated with a database of known active $CB_2$ agonists and by a series of molecular modeling tools such as: protein structure refinement, molecular dynamics, molecular docking and enrichment studies. This model can then be reevaluated further in order to make any modifications necessary in order to improve accuracy.

This homology model can be used to design novel selective $CB_2$ agonists that will then be synthesized within the laboratory. Once the compounds have been synthesized, pharmacological data at the cannabinoid receptors can be collected.

## Specific Aims

I. Synthesize regioisomeric indoles in order to develop analytical tools that can differentiate the isomers

II. Design and validate an agonist $CB_2$ crystal structure

III. Design and synthesize selective $CB_2$ agonists for therapeutic use

IV. Obtain pharmacological data on selective $CB_2$ agonists.

## Chapter Two: Synthesis, analytical studies and isotope labeling of the regioisomeric substituted indole derivatives

### 2.1) Spectroscopic differentiation and chromatographic separation of regioisomeric indole aldehydes: synthetic precursors

#### 2.1.1) Results and Discussion

A common and easily attainable starting material is a basic indole with an aldehyde at differing positions on the indole ring. An aldehyde can easily undergo a Grignard reaction, which will produce a new carbon-carbon bond. This will lead to a wide array of compounds which can then be further modified. The objective is to synthesize and evaluate the regioisomeric 1-n-pentyl-2-, 3-, 4-, 5-, 6- and 7-formylindoles that are shown in Figure 11. These aldehydes represent the starting materials and synthetic intermediates for the preparation of many regioisomeric indoles [46]. This will provide an analytical framework for the identification of individual aldehydes in this study based on gas chromatography-mass spectrometry (GC-MS) and gas chromatography-infrared spectroscopy (GC-IR) techniques.

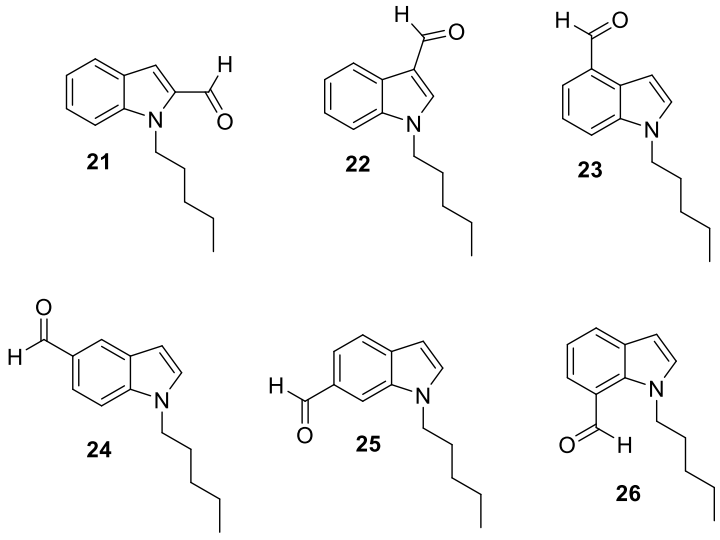


**Figure 11.** The structures of the 1-n-pentylated aldehydes, **21**-**26**.

The indoles 3-,4-,5- and 7-carboxaldehydes were purchased from Alfa Aesar Chemical Company, Ward Hill, MA. The indoles 2- and 6-carboxaldhydes were purchased from Aldrich Chemical Company, Milwaukee, WI. The six regioisomers were synthesized in one step which is shown in Scheme 1 The synthesis consists of dissolving the appropriate substituted aldehyde in dimethylformamide (DMF) and treating with potassium hydroxide (KOH). Then the addition of the alkyl halide, 1-bromopentane, was added in order to yield the desired crude products, **21-26**.

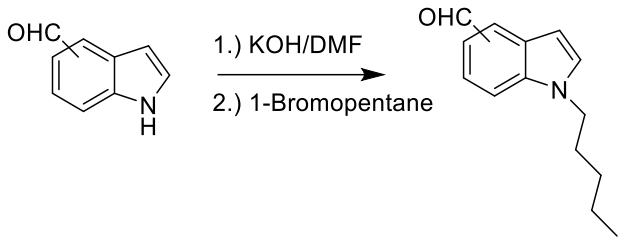


**Scheme 1.** The synthetic route for regioisomers, **21-26**.

The electron ionization (EI) for the six regioisomeric 1-n-pentylindole aldehydes are shown in Figure 12 and the fragmentation pathway is shown in Scheme 2. The molecular radical cation is m/z 215 and is a significant peak in all isomers. The loss of an aldehyde from the molecular radical cation is the fragment ion m/z 186, which is seen in all isomers at a low relative abundance. The fragment ion m/z 158 serves as the base peak for all isomers and results from the loss of $C_4H_9$ (57 Da) due to an alpha cleavage that yields an iminium cation. The loss of the aldehyde from the m/z 158 base peak results in a fragment ion of m/z 130, which is seen in all isomers with the highest abundance being in isomers **22** and **26**. The fragment m/z 144 is the loss of the pentyl chain which is seen in all isomers with varying intensities. Fragment m/z 116 is seen in all isomers but with low abundance and is the loss of the aldehyde and pentyl chain.

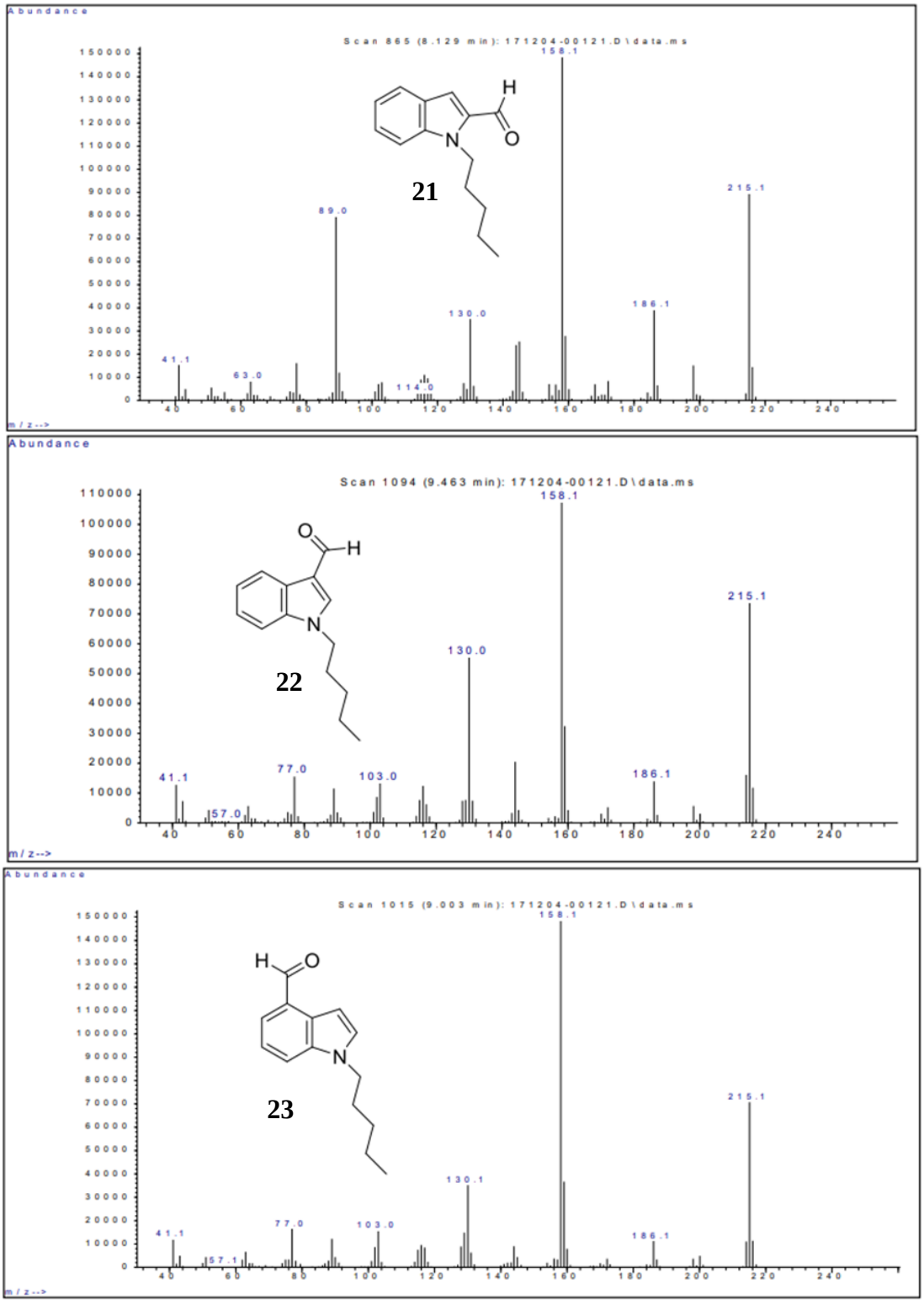


**Figure 12**. The EI mass spectra for the indole aldehydes.

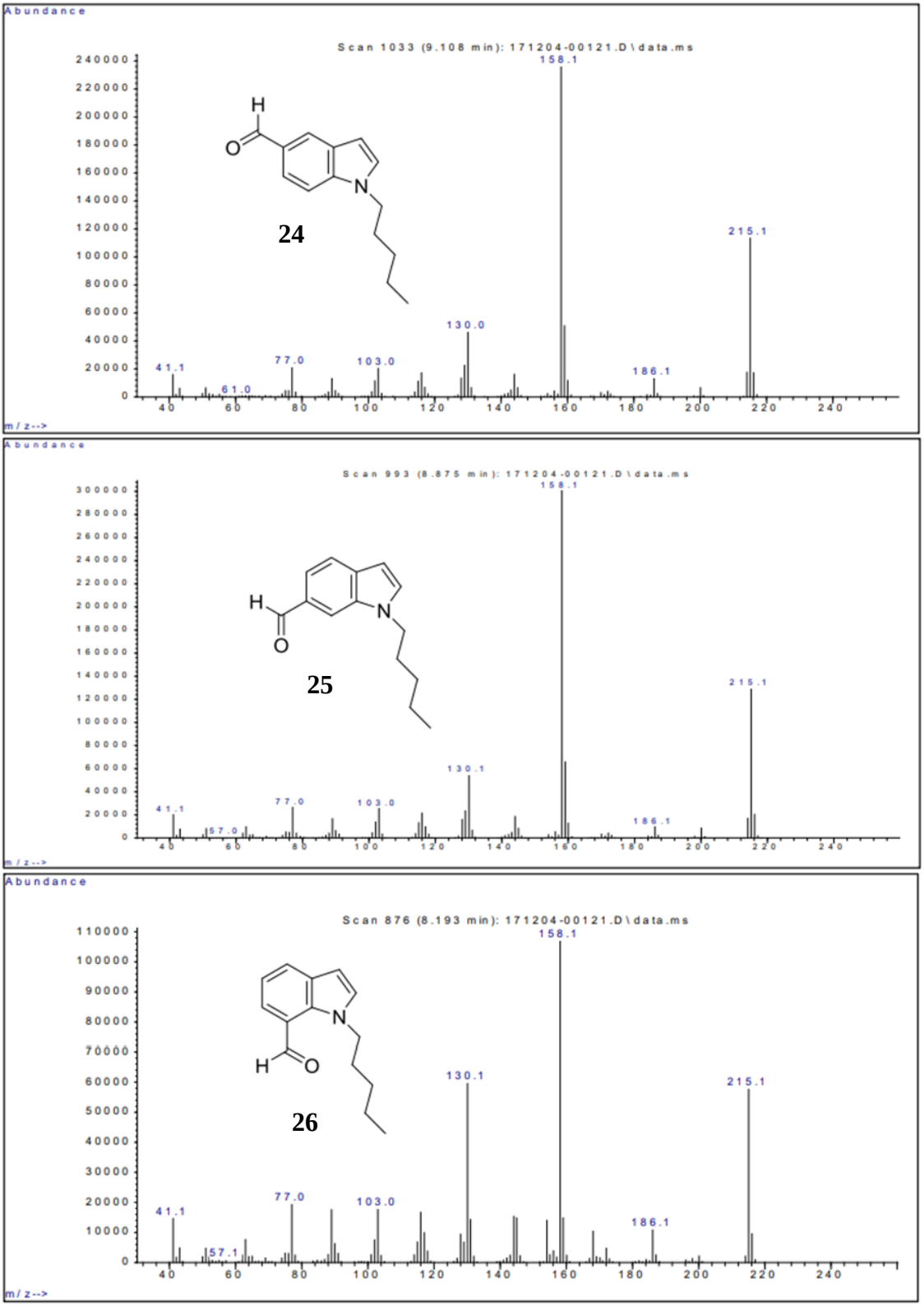


**Figure 12.** Continued.

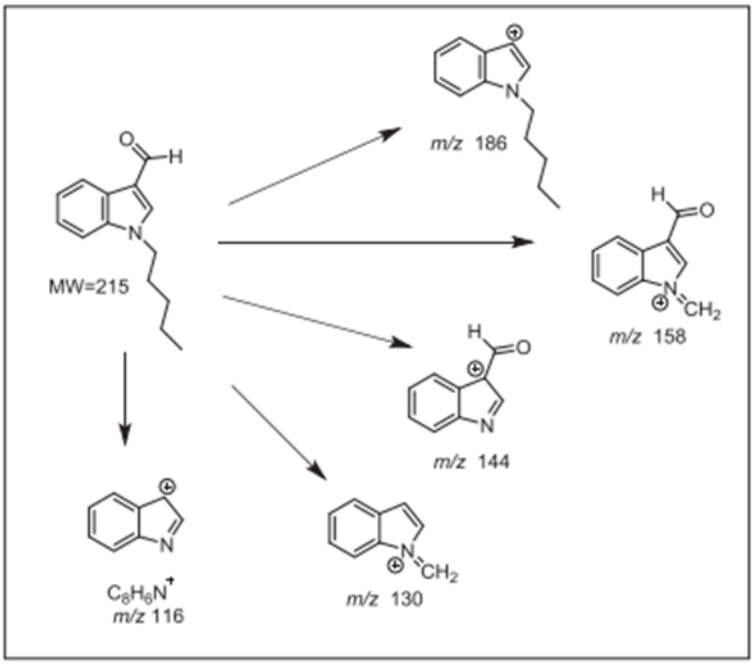


**Scheme 2.** The fragmentation pathway of 1-n-Pentylindole-3-carboxaldehyde, **22**.

In conclusion, the electron ionization mass spectrometry (EI/MS) of all six isomers (**21-26**) are similar with a difference in relative abundance. However, in order to differentiate these isomers other analytical methods must be used. Further studies were completed by other researchers involving the GC-IR analytical method and these six regioisomers (**21-26**). Vapor phase infrared was able to easily distinguish the six regiosiomers from one another by the differences in ring substitution. Not only was this technique able to differentiate these isomers, but it was also used to differentiate their respective regioisomeric indole aldehydes without the pentyl chain.

### 2.1.2) Experimental

#### *2.1.2.1) Instrumentation*

GC–MS system consisted of an Agilent Technologies (Santa Clara, CA) 7890A gas chromatograph and an Agilent 7683B auto injector coupled with a 5975C VL Agilent mass

selective detector. The mass spectral scan rate was 2.86 scans/s. The GC was operated in splitless mode with a helium (ultra-high purity, grade 5, 99.999%) flow rate of 0.48 mL/min and the column head pressure was 10 psi. The MS was operated in the electron ionization (EI) mode using an ionization voltage of 70 eV and a source temperature of 230 °C. The GC injector was maintained at 300 °C and the transfer line at 230 °C. The mass spectra were obtained using a column (30m × 0.25mm i.d.) coated with 0.25 μm film of midpolarity Crossbond silarylene phase; similar to 50% phenyl, 50% dimethylpolysiloxane (Rxi®-17Sil MS) purchased from Restek Corporation (Bellefonte, PA). The mass spectra of the six intermediate 1-n-pentylindolealdehydes were obtained using a temperature program consisting of an initial hold at 80 °C for 1.0 min, ramped up to 300 °C at a rate of 30 °C/min, held at 300°C for 0.50 min then ramped to 340 °C at a rate of 5 °C/min and held at 340 °C for 5.0 min. Samples were dissolved and diluted in high-performance liquid chromatography-grade acetonitrile (Fischer Scientific, Fairlawn, NJ) and introduced via the autoinjector using an injection volume of 1 μL.

*2.1.2.2) Synthetic methods*

**1-n-Pentylindole aldehydes:**

A mixture of potassium hydroxide (1.5 eq) and a solution of the appropriately substituted aldehyde indole in DMF was stirred for 30 minutes at room temperature. 1-Bromopentane (1 eq) was added to the substituted indole/KOH mixture and the resulting mixture was stirred for two hours. This mixture was poured into water and extracted with ethyl acetate (3 x 20 mL). The combined ethyl acetate extracts were washed with water (3 x 20 mL), dried over sodium sulfate and evaporated to yield the desired intermediate 1-n-pentylindole aldehyde product. The resulting compounds were purified by flash chromatography (silica gel) with a 10:90 diethyl

ether-petroleum ether solution as the mobile phase, using Sorbtech (Norcross, GA) purity flash cartridges (granular silica gel, 25 g).

**1-n-Pentylindole-2-carboxaldehyde (21):** Synthesized using the procedure above. 98% yield. GC-MS (EI): 215.1 (molecular ion), 186.1, 158.1 (100%), 130.0, 89.0.

**1-n-Pentylindole-3-carboxaldehyde (22):** Synthesized using the procedure above. 99% yield. GC-MS (EI): 215.1 (molecular ion), 186.1, 158.1 (100%), 130.0, 103.0, 77.0.

**1-n-Pentylindole-4-carboxaldehyde (23):** Synthesized using the procedure above. 98% yield. GC-MS (EI): 215.1 (molecular ion), 186.1, 158.1 (100%), 130.1, 103.0, 77.0.

**1-n-Pentylindole-5-carboxaldehyde (24):** Synthesized using the procedure above. 99% yield. GC-MS (EI): 215.1 (molecular ion), 186.1, 158.1 (100%), 130.0, 103.0, 77.0.

**1-n-Pentylindole-6-carboxaldehyde (25):** Synthesized using the procedure above. 99% yield. GC-MS (EI): 215.1 (molecular ion), 186.1, 158.1 (100%), 130.1, 103.0, 77.0.

**1-n-Pentylindole-7-carboxaldehyde (26):** Synthesized using the procedure above. 97% yield. GC-MS (EI): 215.1 (molecular ion), 186.1, 158.1 (100%), 130.1, 103.0, 77.0.

## 2.2) GC-MS and GC-IR analysis of regioisomeric cannabinoids related to 1-(5-fluoropentyl)-3-(1-naphthoyl)-indole

### 2.2.1) Results and Discussion

AM-2201 (**28**) is a potent, nonselective synthetic cannabinoid with binding affinities of 1.0 nm and 2.6 nm at $CB_1$ and $CB_2$ receptors, respectively [47]. It mimics the mechanism of action similar to THC, except that it is more potent and elicits more severe side effects. Due to its increased potency and toxicity, it is a controlled drug of abuse in the United States. It is also structurally similar to another controlled substance, JWH-018, except that it contains a fluorine at the terminal position of the alkyl chain. The objective is to synthesize AM-2201 (**28**) and the respective regioisomers (**27**, **29**, **30**, **31**, **32**), shown in Figure 13. The compounds will be used to develop an analytical method in order to evaluate the analytical properties of each compound that will help differentiate the isomers from one another [48].

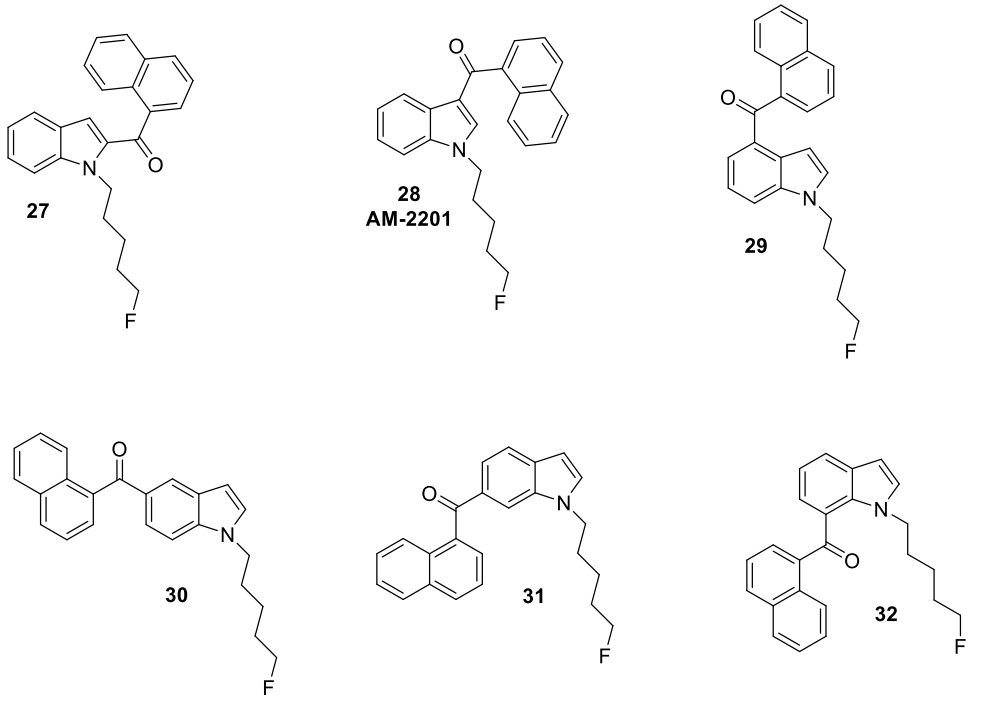


**Figure 13.** The structures of the regioisomeric 1-(5-fluoropentyl)-2-,3-,4-,5-,6- and 7-(1-naphthoyl)-indoles, **27-32**.

The indoles 3-, 4-, 5-, and 7-carboxaldehydes were purchased from Alfa Aesar Chemical Company, Ward Hill, MA. The indole 2- and 6-carboxaldehydes were purchased from Aldrich Chemical Company, Milwaukee, WI. The synthetic route for regioisomers **27-32** are shown in Scheme 3. The first step is an alkylation reaction at the nitrogen of the indole ring, utilizing potassium hydroxide in order to deprotonate the indole. This is followed by the addition of 1-bromo-5-fluoropentane. The next step is a Grignard reaction at the aldehyde utilizing 1-naphthylmagnesium bromide in dry diethyl ether. The last step was the oxidation of the secondary alcohol utilizing pyridinium dichromate (PDC) to yield the crude product.

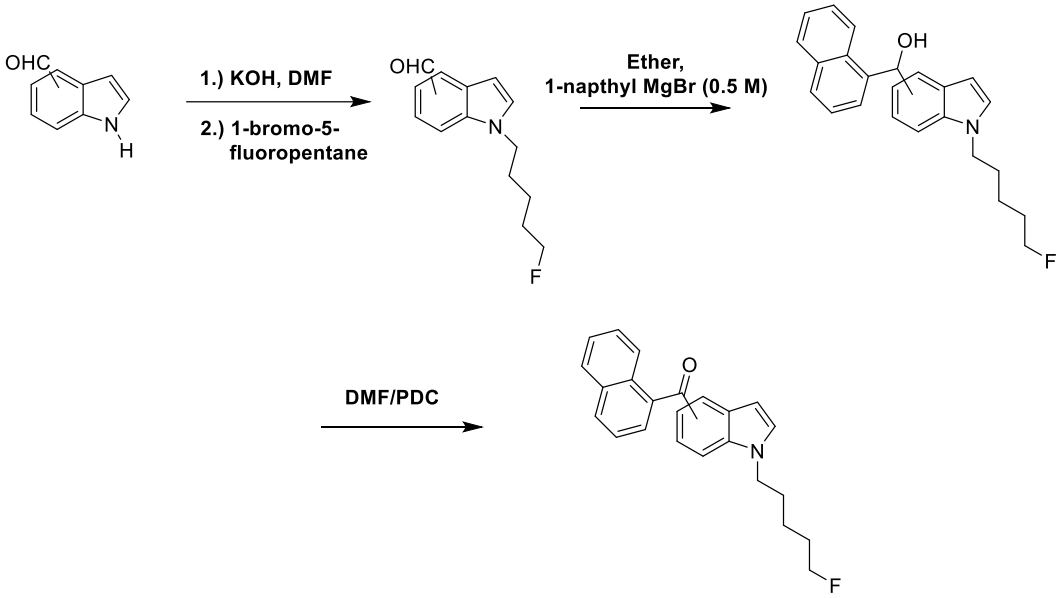


**Scheme 3.** The synthetic route for regioisomeric indoles, **27-32**.

The separation of the six regioisomeric compounds are shown in Figure 14. The separation was done using gas chromatography on a Rtx-200 stationary phase. These compounds eluted within a four-minute range starting at approximately 12 minutes to approximately 16 minutes. The first compound to elute was regioisomer **32** with a retention time of 12 minutes, followed by regioisomer **27** with a retention time of 12.5 minutes. It is suggested that they eluted first because the two substituents are close as possible to each other, which causes for an increased intramolecular interactions and decreased interaction with the stationary phase. The next two compounds to elute were **31** and **29** with retention times of 14.4 minutes and 14.9 minutes, respectively. These retention times are similar due to the naphthoyl substituent being meta to the indole nitrogen in both compounds. The last two compounds to elute were **28** and **30** with retention times of 15.4 minutes and 15.9 minutes, respectively. Compound **30** has the two substituents farthest away from each other which suggests decreased intramolecular interactions and increased stationary phase interaction which is indictive of the highest retention time. Also,

in compound **30**, the carbonyl group is para to the indole nitrogen which allows for increased electronic interactions between the two groups. This is also seen in regioisomer **28** because position 3 of the indole ring is highly electron rich due to the resonance effects with the indole nitrogen. When the carbonyl is at position 3 or 5, this will increase the electronic interactions between the two substituents, which may result in increased retention times. In summary, the elution order appears to be due to the intramolecular and steric interactions between the naphthoyl and pentyl substituents. A previous study was done on the six 1-naphthoyl and six 2-naphthoyl substituted indole regioisomers having the non-fluorinated n-pentyl chain and the same elution order and pattern have been reported [49, 50].

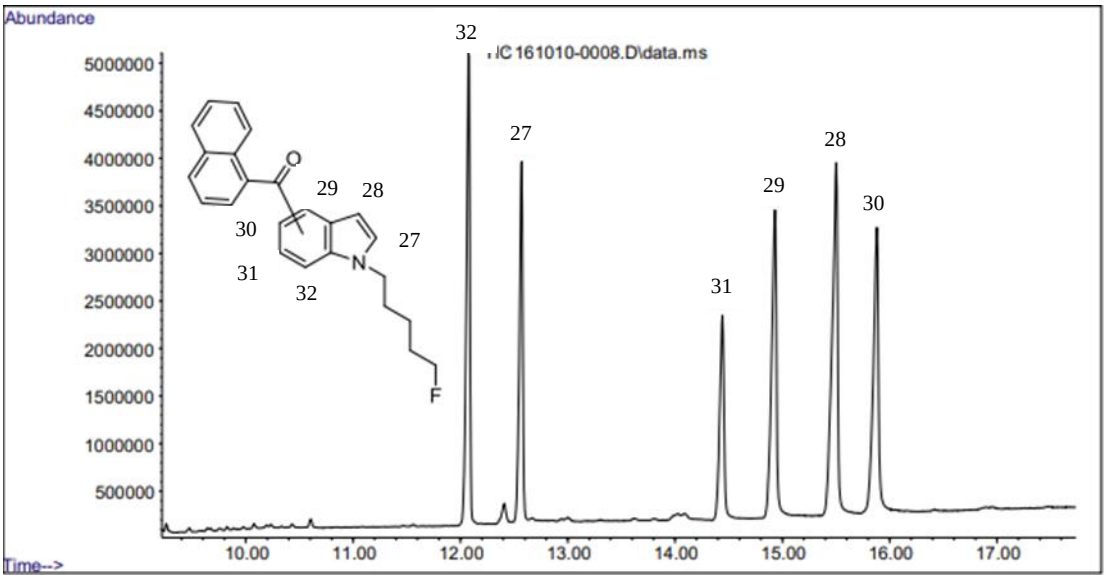


**Figure 14.** The capillary gas chromatographic separation of the six regioisomeric indoles using an Rtx-200 stationary phase.

The electron ionization for all six regioisomers is shown in Figure 15 and the fragmentation pathway is shown in Scheme 4. All six regioisomers have the molecular radical cation of 359 m/z and this serves as the base peak for all isomers except compounds **27** and **32**.

The common fragmentation ions seen in all six isomers are: m/z 342, m/z 284, m/z 270, m/z 232, m/z 155 and m/z 127 with varying intensities for each compound.

Fragment ion m/z 342 is seen in all compounds except compound **32** and has the highest intensity in compound **28**. This is the loss of a hydroxy group (17 Da) from the molecular radical cation. This results from the hydrogen migration from the 8-position of the naphthalene ring to the carbonyl oxygen followed by the hydroxyl elimination. This same fragmentation pattern is seen in the study with the non-fluorinated analogue, JWH-018 [51].

Fragment ion m/z 284 is a significant peak seen in all compounds. It serves as the base peak for compound **27** and is the least intense in compound **31**. This is the loss of $C_4H_8F$ (75 Da), which results in the radical cation formation starting at the indole nitrogen followed by an alpha cleavage which yields an iminium cation. The fragment ion m/z 270 is seen in all isomers with varying intensity. This is the loss of the entire pentyl chain, $C_5H_{10}F$ (90 Da). This fragment ion is not as significant as m/z 284, except in compound **31**.

The fragment ion m/z 232 is a significant peak in all compounds except for compounds **27** and **32**. This is the loss of the naphthyl radical (127 Da) from the molecular radical cation m/z 359. The fragment ion m/z 144 is a significant peak in compound **28** which was also observed in the non-fluorinated analog, JWH-018. This is the result of a hydrogen rearrangement from the fragment ion peak m/z 232 with the elimination of the entire fluorinated side chain. Previous labeling [51, 52] and MS/MS studies [53] have confirmed the proposed structure and suggested mechanism for this fragment ion. The minor fragment ion m/z 204 is the loss of the naphthoyl radical (155 Da) or may result from the loss of CO from the fragment ion m/z 232.

The fragment ions m/z 127 and m/z 155 are the naphthyl and naphthoyl cations, respectively. These are significant peaks in all six isomers, with m/z 127 more intense than m/z 155.

The unique fragment ion m/z 141 is common in isomers **27** and **32** and serves as the base peak for compound **32**. Deuterium labeling studies [49] confirm that this fragment ion consists of the naphthalene ring and a methylene group, thus involving an interaction and rearrangement of the two groups in close proximity on the indole ring.

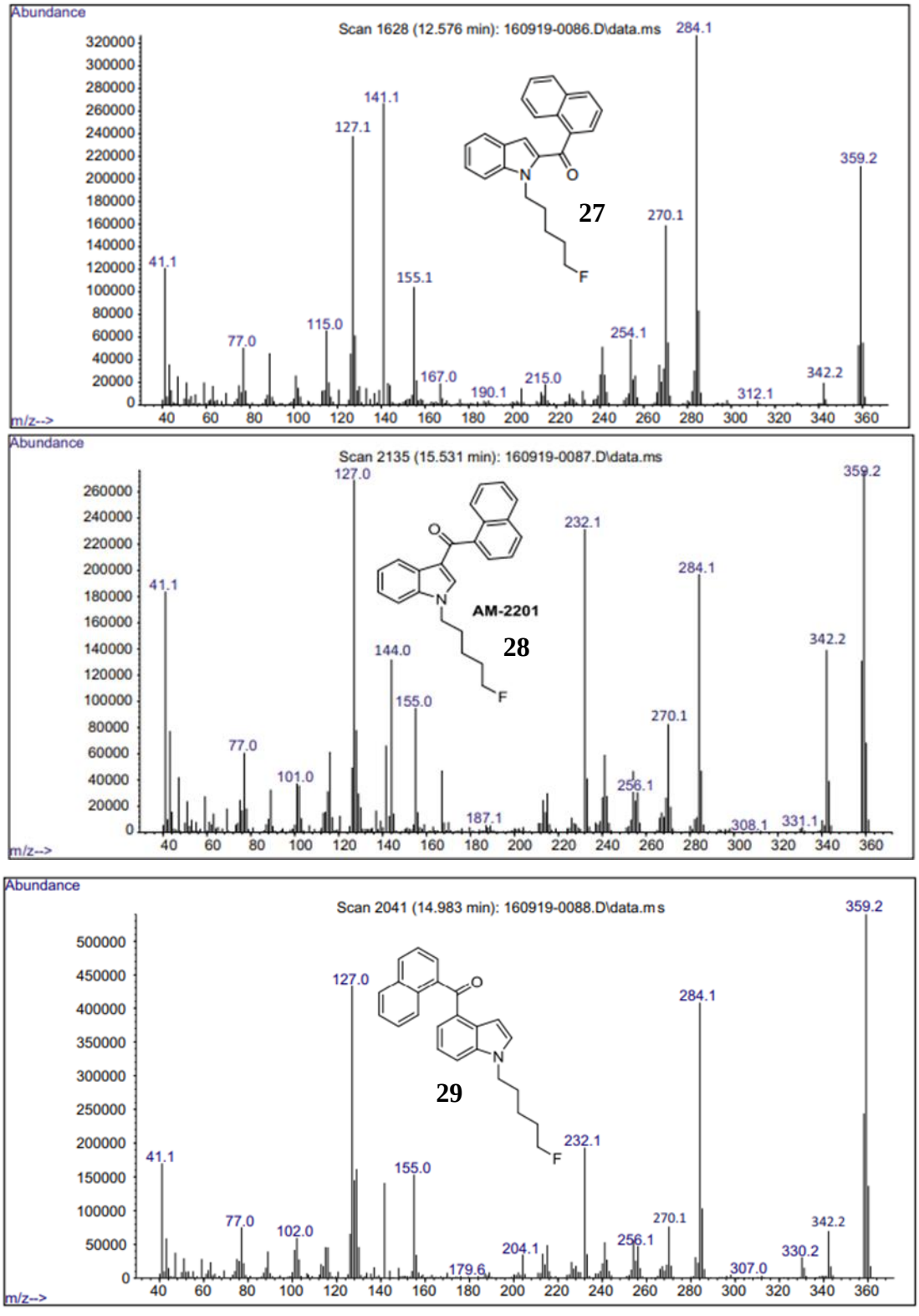


**Figure 15.** The EI mass spectra of the six regioisomeric compounds.

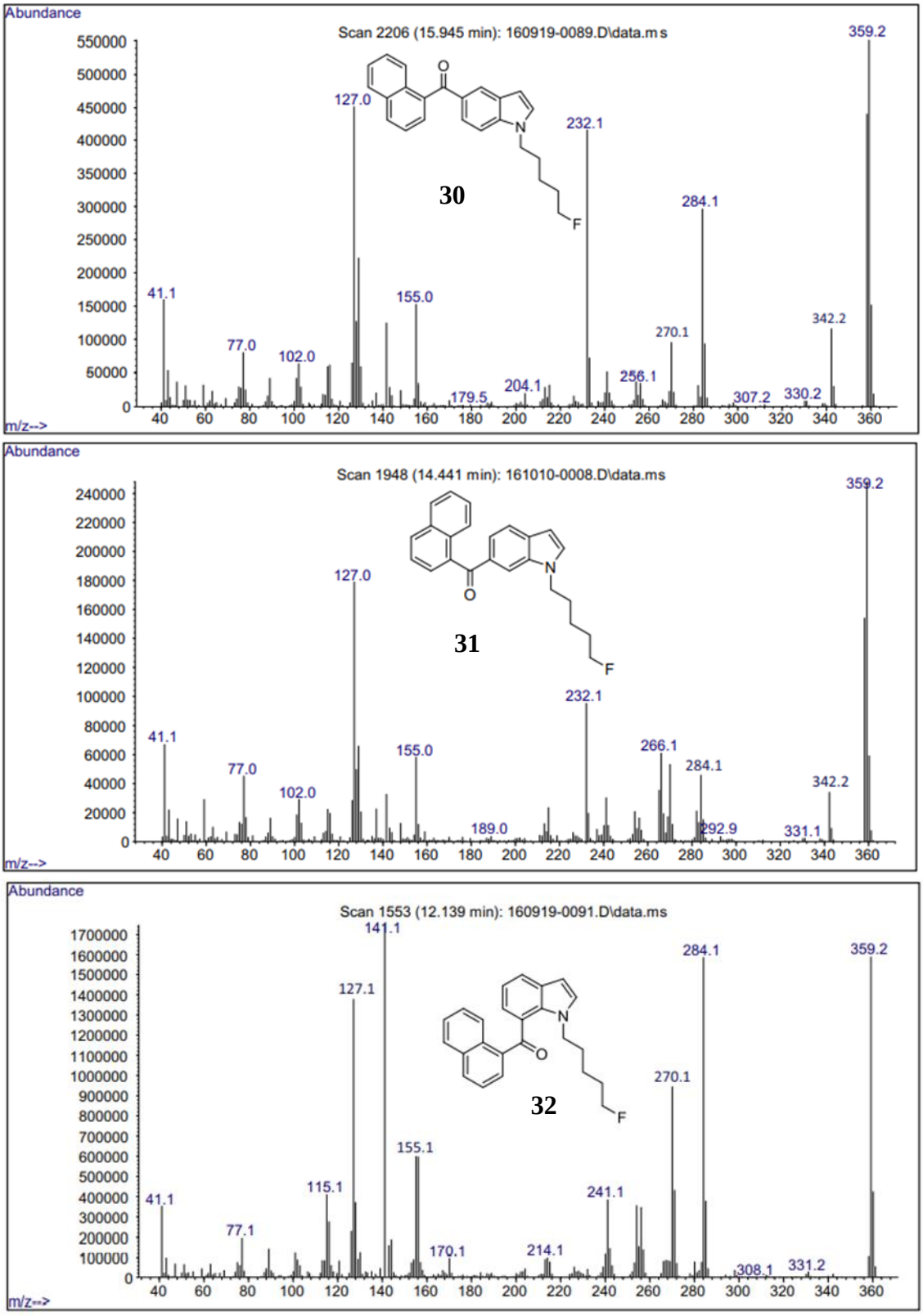


**Figure 15.** Continued.

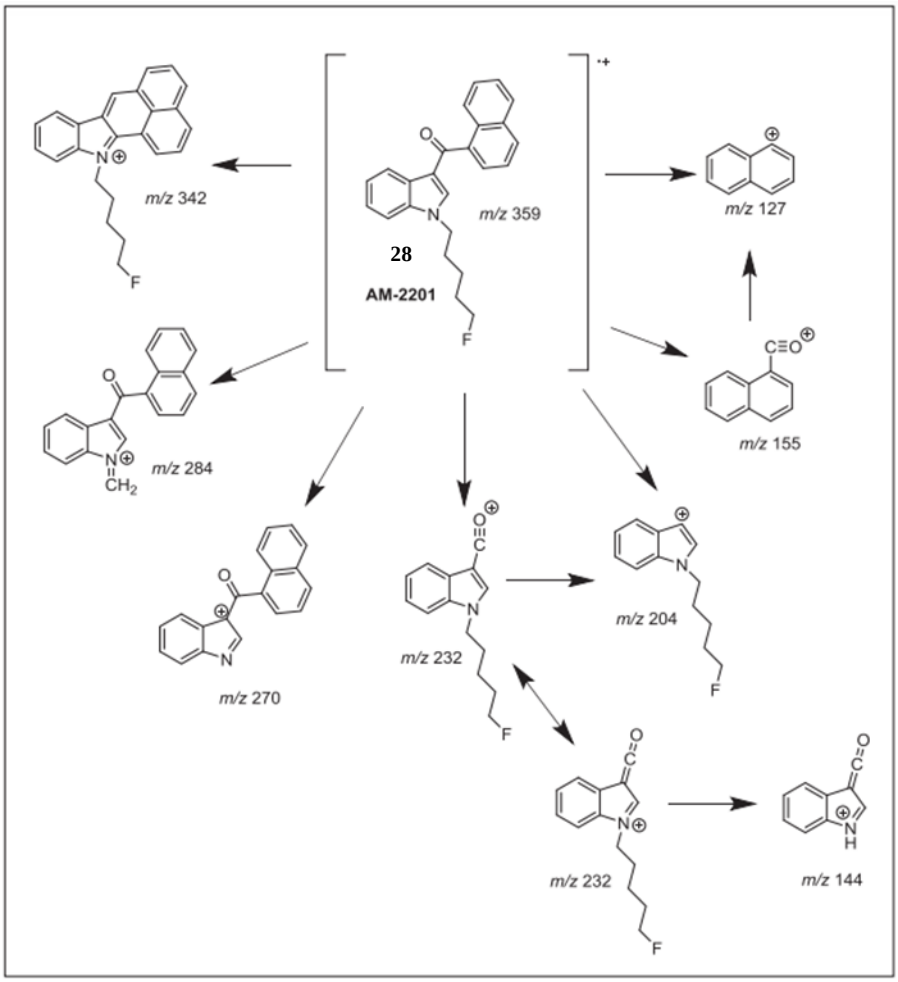


**Scheme 4.** The representative fragmentation pathways in the EI-MS for AM-2201 (**28**).

Vapor phase infrared spectroscopy was done on the six regioisomers as another method of differentiating the isomers, however this work was completed by other researchers. The completion of this work can be viewed in published literature at: https://doi.org/10.1016/j.forc.2018.07.005 , but it was determined that vapor phase infrared spectroscopy could be used in order to easily differentiate all six isomers.

In conclusion, the six regioisomeric compounds were easily differentiable by different analytical techniques such as gas chromatography separation, electron ionization mass spectra

studies and gas chromatography infrared studies. The GC/MS separation was able to identify an elution order that was similar to the non-fluorinated (JWH-018) series of compounds. The elution order appears to be related to the steric hinderance of the substituents on the indole ring. The EI/MS were able to distinguish the six isomers by the varying intensities of fragment ion peaks such as, m/z 232 which was seen in high abundance only in compounds **28-31**. The compounds **27** and **32**, did not have fragment ion m/z 232, but instead had the unique fragment ion of m/z 141. Fragment ion m/z 144 was only seen in high abundance in compound **28**, which is similar to what was seen in JWH-108. The vapor phase IR spectroscopy studies were easily able to identify the isomers based on the position of the carbonyl absorption band.

### 2.2.2) Experimental

#### *2.2.2.1) Instrumentation*

The GC-MS system consisted of an Agilent Technologies (Santa Clara, CA) 7890A gas chromatograph and an Agilent 7683B autoinjector coupled with a 5975C VL Agilent mass selective detector. The mass spectral scan rate was 2.86 scans/s and the mass spectrometer was tuned using the autotune mode. The GC was operated in splitless injection mode with a helium (ultra-high purity, grade 5, 99.999%) flow rate of 0.7 mL/min and the column head pressure was 10 psi. The MS was operated in the electron ionization (EI) mode using an ionization voltage of 70 eV and a source temperature of 230 °C. The GC injector was maintained at 300 °C and the transfer line at 325 °C.

Chromatographic separation was carried out on a column (30 m x 0.25 mm i.d.) coated with 0.25 μm 100% trifluropropylmethyl polysiloxane (Rtx-200) purchased from Restek Corporation (Bellefonte, PA). The mass spectra were obtained using a temperature program

consisting of an initial hold at 80 °C for 1.0 min, ramped up to 300 °C at a rate of 30 °C/min, held at 300 °C for 0.5 min then ramped to 340 °C at a rate of 5 °C/min and held at 340 °C for 5.0 min with a total run time of 21.0 minutes. Samples were dissolved and diluted in high-performance liquid chromatography grade acetonitrile (Fisher Scientific, Fairlawn, NJ) and introduced via the auto injector using an injection volume of μl. The chromatographic separation of the six regioisomeric compounds was carried out using the above described temperature program.

*2.2.2.2) Synthetic Methods*

**1-(5-Fluoropentyl)-indole aldehydes:**

A mixture of potassium hydroxide (1.5 eq) and a solution of the appropriate substituted indole aldehyde in dimethylformamide (DMF) was stirred under nitrogen for 30 minutes. 1-Bromo-5-fluoropentane (1 eq) was added to the substituted indole/potassium hydroxide mixture and the resulting solution was stirred for two hours. This mixture was poured into water and extracted with ethyl acetate (3 x 25 mL). The combined ethyl acetate extracts were washed with water (3 x 25 mL), dried over sodium sulfate and evaporated to yield the desired intermediate.

**1-(5-Fluoropentyl)-2-, 3-, 4-, 5-, 6-, 7-(1-naphthoyl)-indoles:**

A solution of the appropriate 1-(5-fluoropentyl)-indole aldehyde was dissolved in dry diethyl ether, added to a dry flask under a nitrogen atmosphere and then cooled by an ice bath. A solution of 0.5 M 1-naphthylmagnesium bromide in dry ethyl ether was added via syringe/septum over a period of 5 minutes under nitrogen and the resulting solution was stirred at room temperature for 2 hours. The reaction mixture was quenched by the addition of water and

the resulting solution was extracted with ethyl acetate (3 x 25 mL). The combined ethyl acetate extracts were washed with water (3 x 25 mL), dried over sodium sulfate and evaporated to yield a yellow oily residue. This intermediate was dissolved in DMF and then was mixed with pyridinium dichromate (PDC) in DMF at room temperature and the reaction was stirred for 30 minutes. The reaction was quenched with water and extracted with ethyl acetate (3 x 25 mL). The organic layers were combined, washed with water (3 x 25 mL), dried over sodium sulfate and evaporated. The resulting compounds were purified by preparative thin layer chromatography with 10:90 diethyl ether-petroleum ether solution was the mobile phase, using AnalTeach (Newark, DE) glass backed 20 x 20 cm plates with a 500 μm layer of silica as the stationary phase and an inorganic fluorescent 254 nm indicator.

**1-(5-Fluoropentyl)-2-(1-naphthoyl)-indole (27):**

Synthesized using the method described above. 89% yield. GC-MS (EI): 359.2 (molecular ion), 342.2, 284.1 (100%), 270.1, 254.1, 155.1, 141.1, 127.1.

**1-(5-Fluoropentyl)-3-(1-naphthoyl)-indole (28):**

Synthesized using the method described above. 83% yield. GC-MS (EI): 359.2 (molecular ion and 100%), 342.2, 284.1, 270.1, 232.1, 155.0, 144.0, 127.0.

**1-(5-Fluoropentyl)-4-(1-naphthoyl)-indole (29):**

Synthesized using the method described above. 92% yield. GC-MS (EI): 359.2 (molecular ion and 100%), 342.2, 284.1, 270.1, 232.1, 155.0, 127.0.

**1-(5-Fluoropentyl)-5-(1-naphthoyl)-indole (30):**

Synthesized using the method described above. 80% yield. GC-MS (EI): 359.2 (molecular ion and 100%), 342.2, 284.1, 270.1, 232.1, 155.0, 127.0.

**1-(5-Fluoropentyl)-6-(1-naphthoyl)-indole (31):**

Synthesized using the method described above. 91% yield. GC-MS (EI): 359.1 (molecular ion and 100%), 342.2, 284.1, 232.1, 155.0, 127.0.

**1-(5-Fluoropentyl)-7-(1-naphthoyl)-indole (32):**

Synthesized using the method described above. 87% yield. GC-MS (EI): 359.2 (molecular ion), 284.1, 270.1, 241.1, 155.1, 141.1, 127.1.

## 2.3) GC-MS and GC-IR Analyses of the methoxy 1-n-pentyl-3-(1-naphthoyl) -indoles: regioisomeric designer compounds

### 2.3.1) Results and Discussion

Numerous structure activity relationships have been done by varying the substituent on the indole template and some of these studies include: modification of the pentyl chain [54,55], naphthoyl ring [56, 57], or by the addition of small alkyl ethers or halogens [58-60]. The most commonly studied modification is the variation of different substituents on the 3-position of the indole ring. A study done by DeRuiter, J., et. al., indicated that the addition of a 4-methoxy group to the 1-naphthoyl ring of JWH-018 increased $CB_1$ affinity by approximately 7-fold [61].

A previous study was completed by Thaxton-Weissenfluh, et. al. on the analytical properties for the 4-, 5-, 6-, and 7-methoxy substituted indole ring analogs of JWH-018 (Figure 16) [62]. During this study, it was found that the 4-methoxy compound **33** had a unique fragment ion of 324 m/z that was not seen with the other three isomers **34-36**. This study will focus on comparing the 4-, 5-, 6-, and 7-methoxy compounds, but with a focus on the 4-methoxy indole **33** and the $D_3$-4-methoxy compound **37** (Figure 17) that will validate an appropriate fragment ion.

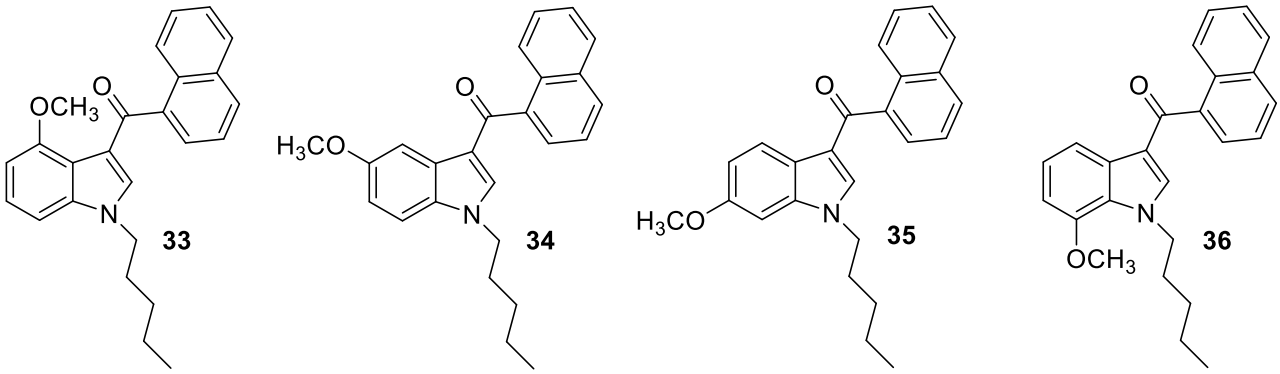


**Figure 16.** The structures of the regioisomeric 4-, 5-, 6-, and 7-methoxy-1-pentyl-3-(1-naphthoyl)-indoles, **33-36**.

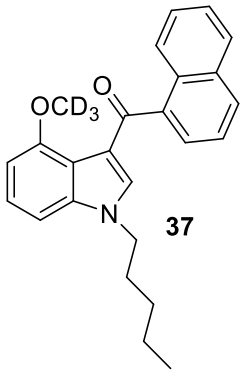


**Figure 17.** The structure of $D_3$-4-methoxy-1-pentyl-3-(1-naphthoyl)-indole, **37**.

The synthesis of the 4-methoxy indole product **33** is shown in Scheme 5. The first step is the Vilsmeier-Haack reaction that is used to add an aldehyde to an electron rich aromatic ring. Phosphorus oxychloride ($POCl_3$), DMF and the starting indole **38** are reacted under an ice bath. The phosphorus oxychloride and DMF form an iminium salt *in situ*, which is also known as the Vilsmeier reagent [63]. The electron rich aromatic ring **38** will then react with the iminium salt. This is followed by an aqueous work up which leads to the aldehyde product, **39**. The next step is an alkylation reaction which is completed by deprotonating the indole, **39**, with potassium hydroxide in DMF and using the alkyl halide, 1-bromopentane to yield the pentylated indole **40**. The next step is a Grignard reaction utilizing 1-naphthylmagnesium bromide in dry diethyl ether,

which will attack the aldehyde in compound **40** in order to yield the secondary alcohol intermediate **41**. The last step is the oxidation of the secondary alcohol intermediate **41** using PDC in DMF to yield the crude product, **33**.

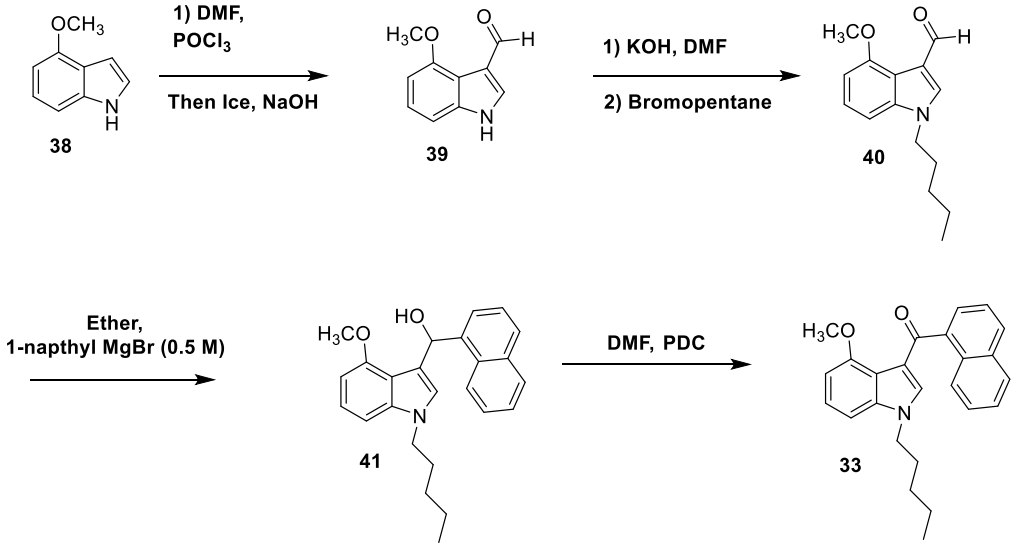


**Scheme 5.** The synthetic route for 4-methoxy indole, **33**.

The synthesis of the deuterated 4-methoxy indole, **37**, is shown in Scheme 6. The first step is the deprotonation of the phenol on the 4-hydroxyindole, **42**, using potassium carbonate in acetone. This is followed by the addition of iodomethane-$D_3$, which yields the $D_3$-4-methoxy indole, **43**. The next three steps are similar to the previous synthetic route, which includes the Vilsmeier-Haack reaction to yield **44**, the alkylation reaction to yield **45**, followed by the Grignard reaction to yield **46**. However, the procedure for the oxidation step is different than what was shown previously. Instead of PDC, the hypervalent iodine, Dess Martin periodinane (DMP), was utilized due to ease of separation of byproducts [64].

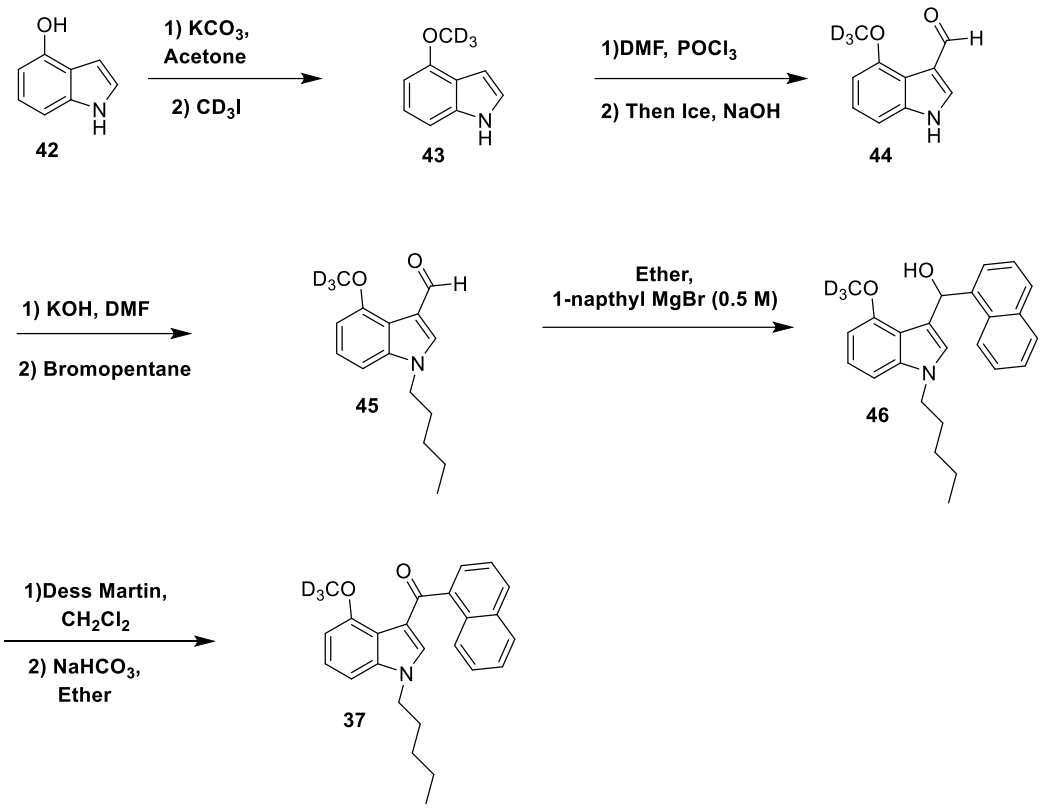


**Scheme 6.** The synthetic route for the $D_3$-4-methoxy, **37**.

The electron ionization mass spectra for regioisomeric 4-, 5-, 6- and 7-methoxy-1-pentyl-3-(1-naphthoyl) indole are shown in Figure 18 and the fragmentation pathway is shown in Scheme 7. The 5-, 6-, and 7- isomers (**34-36**) were completed by Thaxton-Weissenfluh et. al. but are included in this report for comparison. The four isomers, **33-36**, all have a molecular radical cation and base peak of m/z 371. The other fragment ion peaks that are similar between isomers are: 314, 244, 155 and 127.

Fragment ion m/z 354 is seen in all isomers and is the loss of an OH group (17 Da), the oxygen coming from the carbonyl and the hydrogen coming from the 8-position on the naphthalene group. This same pattern has been seen in other studies [49-51, 65, 66] and isotope labeling [51] has been done in order to confirm that it is the hydrogen from the 8-position on the

naphthalene group. Fragment ion m/z 314 is seen in all isomers, but with lower intensity in the 4-methoxy isomer **33**. This is the loss of a butyl ($C_4H_9$) radical (57 Da), which is the result from an alpha cleavage when starting with a radical at the indole nitrogen. Fragment ion m/z 300 is a minor fragment in all isomers and this is the loss of $C_5H_{11}$ (71 Da). Fragment ion m/z 244 is seen in all isomers and is the loss of the naphthoyl ring (127 Da). The loss of the entire pentyl chain from fragment ion m/z 244 is the fragment ion m/z 174. This is a minor fragment that is seen in all isomers. The fragment ion m/z 216 is a minor fragment seen in all isomers and it is the loss of the naphthoyl radical (155 Da). The fragment ions m/z 127 and m/z 155 are the naphthyl and naphthoyl cations, respectively. These are seen in all isomers with relatively high abundance, with fragment ion m/z 127 always more abundant than fragment ion m/z 155.

The electron ionization mass spectra are similar between all four isomers except for a unique fragment ion of m/z 324 that is only seen in one of the methoxy isomers. The fragment ion is only seen in the 4-methoxy isomer **33**, which suggests the close proximity of the carbonyl and methoxy group substituents is an important structural feature in the formation of this fragment ion. High resolution MS analysis of this ion gave a value of 324.1754 corresponding to an elemental composition of $C_{24}H_{22}N$ (calculated 324.1754, 0.6 ppm). The fragment ion m/z 324 is the loss of 47 Da from the molecular radical cation. This unique fragment ion is consistent with the migration of the methoxy group to the carbonyl oxygen with subsequent loss of the methoxy peroxy radical (CH3OO·). In order to validate this idea, an isotope labeling experiment was done and will be explained in the next section.

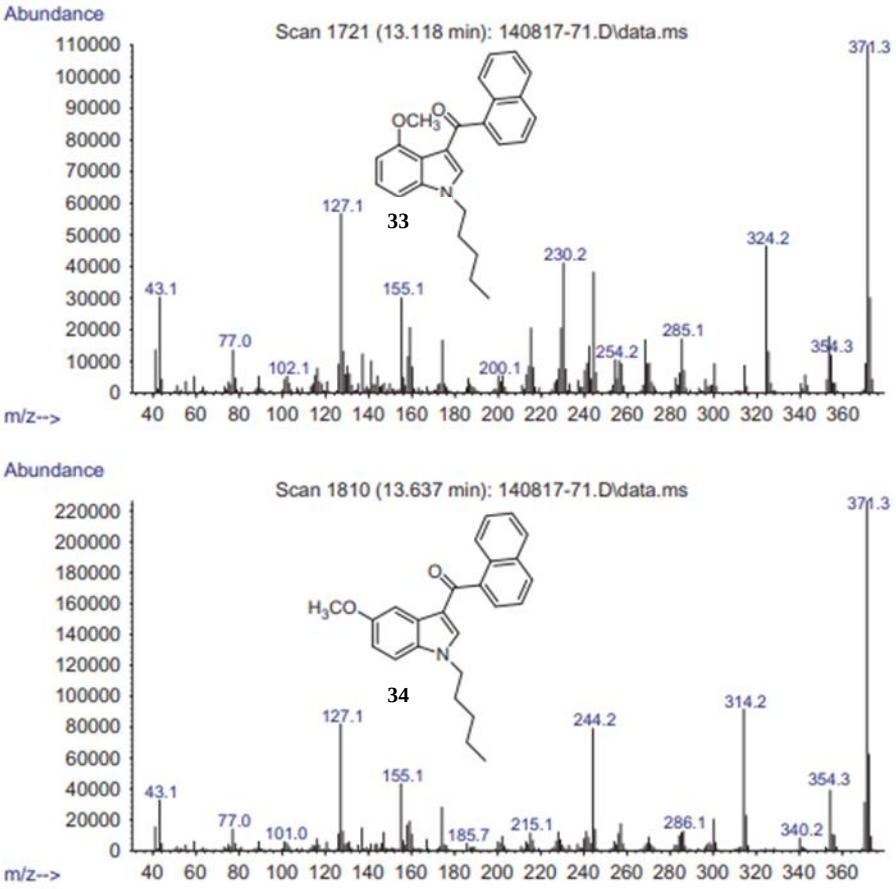


**Figure 18.** The EI mass spectra for methoxy indoles, **33-36**.

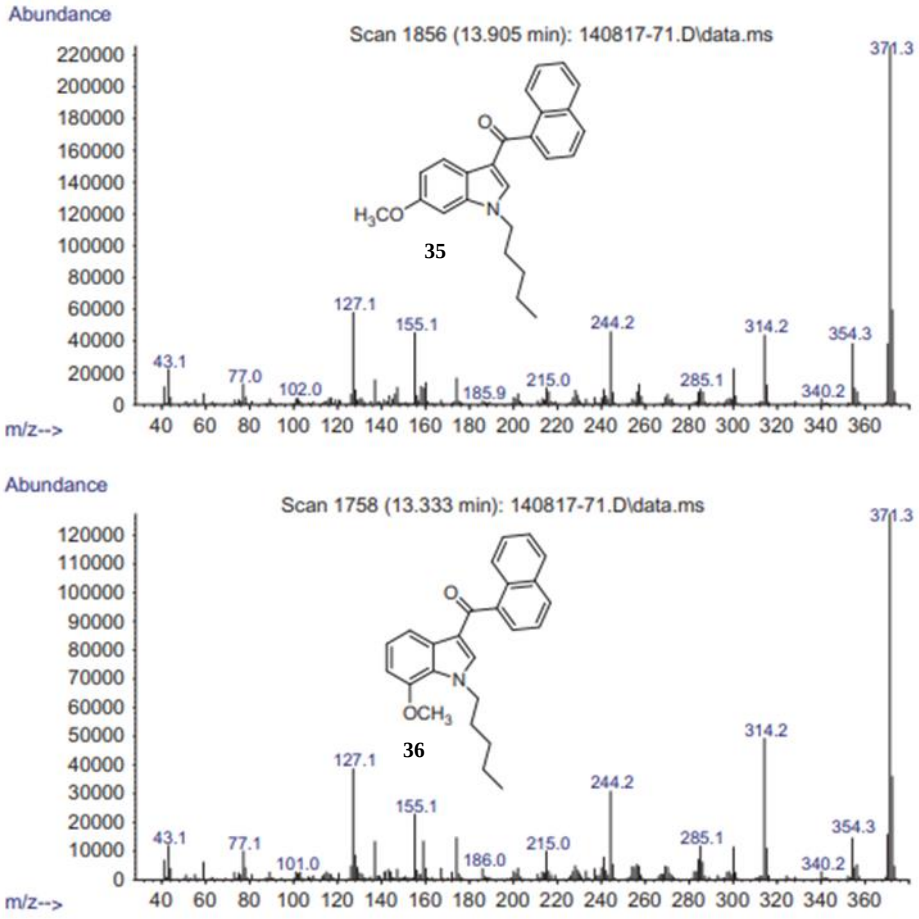


**Figure 18.** Continued.

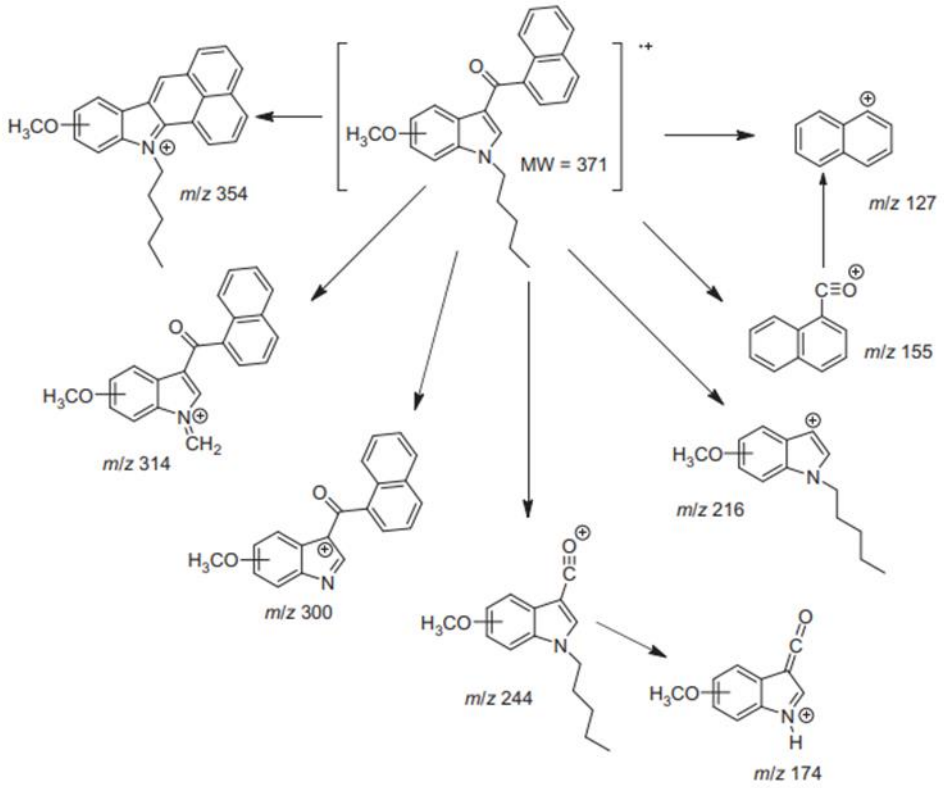


**Scheme 7.** The fragmentation pathway for the methoxy indoles.

The electron ionization mass spectra for the $D_3$-4-methoxy-1-pentyl-3-(1-naphthoyl) indole, **37**, is shown in Figure 19. The molecular radical cation is m/z 374 which is consistent with a compound three mass units higher than the non-deuterated methoxy isomers which had a molecular radical cation of m/z 371. The fragment ion that is of concern is m/z 325 and the suggested fragmentation pathway for this ion is shown in Scheme 8. The first step is the migration of the $OCD_3$ group to the carbonyl of the naphthoyl substituent, followed by migration of one deuterium back to the four-position on the indole ring. The next step is a hydrogen migration from the 8-position of the naphthalene ring to the carbonyl followed by elimination of the methyl peroxy radical ($CD_2HOO\cdot$).

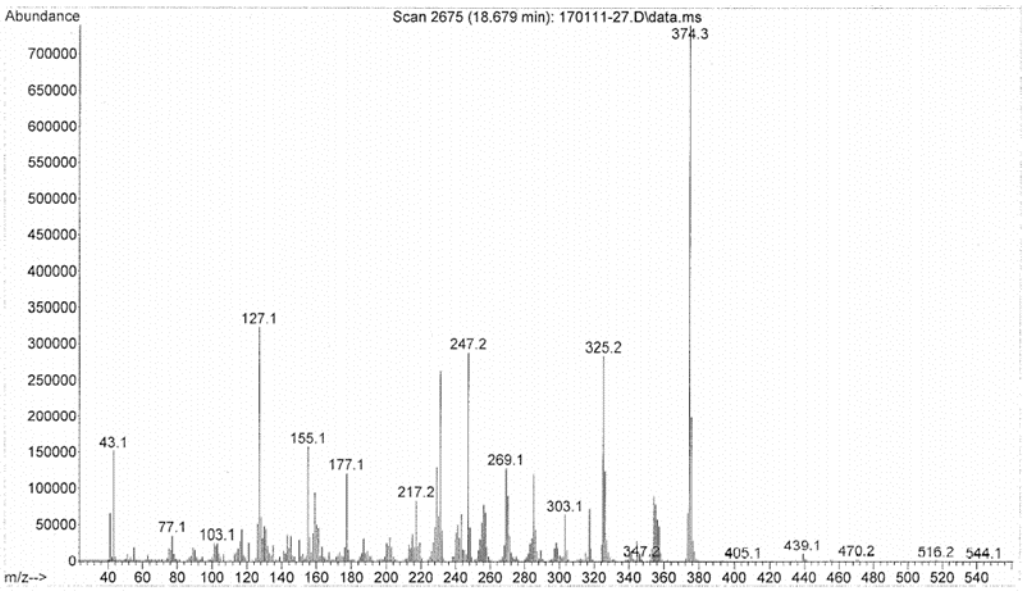


**Figure 19.** The EI mass spectra for the deuterated methoxy, **37**.

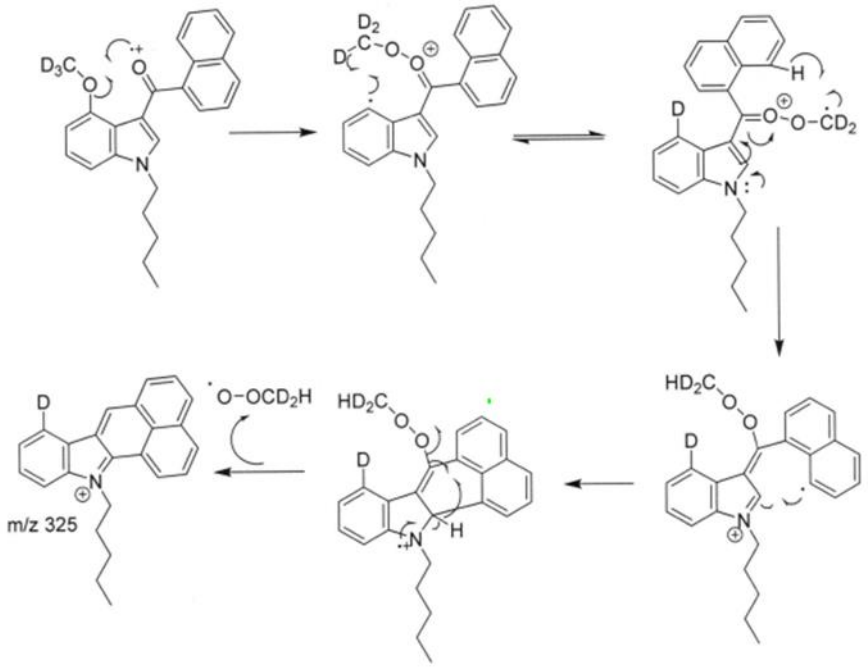


**Scheme 8.** The fragmentation pathway for the deuterated methoxy, **37**.

In conclusion, the 4-, 5-, 6- and 7- methoxy-1-n-pentyl-3-(1-naphthoyl) indoles (**33-36**) were synthesized and analytically evaluated by previous researchers and it was concluded that the electron ionization mass spectra were similar between all isomers except for one unique fragment ion of m/z 324. This fragment ion was only associated with the 4-methoxy isomer **33**, which suggests the close proximity of the methoxy and carbonyl substituents plays an important role when determining the fragment. The predicted fragmentation pattern for this ion is consistent with the migration of the methoxy group to the carbonyl, with one hydrogen from the methoxy group migrating back to the 4-position of the indole ring. Then another hydrogen migration from the naphthalene ring to the carbonyl followed by the loss of the methyl peroxy radical (CH3OO·). In order to prove this theory, an isotope labeling experiment was done by synthesizing the $D_3$-4-methoxy isomer **37** and analytically evaluating this compound by GC/MS. The EI/MS of this compound proved this theory.

### 2.3.2) Experimental

#### *2.3.2.1) Instrumentation*

The same instrumentation method from 2.2.2.1 was used.

#### *2.3.2.2) Synthetic methods*

**4-Methoxy-3-carboxaldehyde-indole (39):**

Phosphorus oxychloride (3.5 mL) was added dropwise to a stirred mixture of DMF (30 mL) and 4-methoxyindole **38** (1 g) at 0°C. The solution was stirred at 0°C for 30 minutes then at 40°C for 1 hour. Ice was added, followed by 2M sodium hydroxide (NaOH) (7 mL) and the mixture was heated under reflux for 5 minutes. Upon cooling, the mixture was extracted with ethyl acetate (3 x 20 mL). The organic layers were washed with water (3 x 20 mL), dried over sodium sulfate

and evaporated to yield the desired intermediate. 91% yield. GC-MS (EI): 175.0 (molecular ion and 100%), 129.0, 104.0, 77.0.

**4-Methoxy-1-pentyl-3-carboxaldehyde-indole (40):**

The aldehyde **39** (0.88g) was dissolved in DMF (8 mL) and treated with potassium hydroxide (1.5 eq). The resulting solution was stirred for 30 minutes at room temperature. 1-Bromopentane (1 eq) was added to the indole/KOH mixture and the resulting solution stirred at room temperature for two hours. The reaction was quenched with water and the product was extracted with ethyl acetate (3 x 20 mL). The organic layer was washed with water (3 x 20 mL), dried with sodium sulfate and evaporated to yield the desired intermediate. No further purification was done. 98% yield. GC-MS (EI): 245.1 (molecular ion and 100%), 199.1, 160.1, 117.1, 89.0.

**4-Methoxy-1-pentyl-3-methanol-(1-naphthalenyl)-indole (41)**

Intermediate **40** (0.70 g) was dissolved in dry diethyl ether (5 mL), added to a dry flask under a nitrogen atmosphere and then cooled by an ice bath. A solution of 0.5 M 1-naphthylmagnesium bromide (0.57 mL) in dry diethyl ether (2 mL) was added via syringe/septum over a period of 5 min. under nitrogen and the resulting solution was stirred at room temperature for two hours. The reaction mixture was quenched by the addition of water and the product was extracted with ethyl acetate (3 x 20 mL). The combined ethyl acetate extracts were washed with water (3 x 20 mL), dried over sodium sulfate and evaporated to yield a yellow residue in 79% yield. No further purification was done.

**4-Methoxy-1-pentyl-3-(1-naphthoyl)-indole (33):**

Intermediate **41** (0.5 g) was dissolved in DMF (5 mL) and then was mixed with pyridinium dichromate (0.55 g) in DMF (2 mL) at room temperature and the reaction was stirred for 30

minutes. The reaction was quenched with water and the product was extracted with ethyl acetate (3 x 20 mL). The organic layers were combined, washed with water (3 x 20 mL), dried over sodium sulfate and evaporated. The resulting compound was purified by column chromatography (silica gel) with a 10:90 ethyl acetate-petroleum ether solution as the mobile phase. 85% yield. GC-MS (EI): 371.3 (molecular ion and 100%), 354.3, 324.2, 285.1, 254.2, 230.2, 200.1, 155.1, 127.1, 102.1, 77.0.

**$D_3$-4-Methoxy-indole (43):**

Potassium carbonate (1.2 g) was added to a solution of 4-hydroxyindole **42** (1 g) in acetone (10 mL) and was stirred for 30 minutes. Iodomethane-$D_3$ (0.47 mL) was added and the solution was stirred overnight at room temperature. The reaction was quenched with water and the product was extracted with ethyl acetate (3 x 20 mL). The combined organic layers were washed with water (3 x 20 mL), dried over sodium sulfate and evaporated to yield the desired intermediate. No further purification was done. 96% yield. GC-MS (EI): 150.1 (molecular ion), 132.1 (100%), 117.1, 104.1, 90.1, 77.1.

**$D_3$-4-Methoxy-3-carboxaldehyde-indole (44):**

Phosphorus oxychloride (0.25 mL) was added dropwise to a stirred mixture of DMF (1 mL) and $D_3$-4-methoxyindole **43** (0.3 g) at 0°C. The solution was stirred at 0°C for 30 minutes then at 40°C for 1 hour. Ice was added, followed by 2 M NaOH (7 mL) and the mixture was heated under reflux for 5 minutes. Upon cooling, the product was extracted with ethyl acetate (3 x 20 mL). The organic layers were washed with water (3 x 20 mL), dried over sodium sulfate and evaporated to yield the desired intermediate. No further purification was done. 93% yield.

**$D_3$-4-Methoxy-1-pentyl-3-carboxaldehyde-indole (45):**

A mixture of potassium hydroxide (1.5 eq) and a solution of the $D_3$-4-methoxy-3-carboxaldehyde indole **44** (0.27 g) in DMF (5 mL) were stirred for 30 minutes. 1-Bromopentane (1 eq) was added to the indole/KOH solution and stirred at room temperature for two hours. The reaction was quenched by the addition of water and the product was extracted with ethyl acetate (3 x 15 mL). The combined organic layers were washed with water (3 x 15 mL), dried with sodium sulfate and evaporated to yield the desired intermediate. No further purification was done. 98% yield. GC-MS (EI): 248.2 (molecular ion and 100%), 219.2, 191.1, 145.0, 117.0, 89.0.

**$D_3$-4-Methoxy-1-pentyl-3-methanol-(1-naphthalenyl)-indole (46):**

The aldehyde **45** (0.25 g) was dissolved in dry diethyl ether (7 mL), added to a dry flask under a nitrogen atmosphere and then cooled by an ice bath. A solution of 0.5 M 1-naphthylmagnesium bromide (2 mL) in dry diethyl ether (3 mL) was added via syringe/septum over a period of 5 minutes under nitrogen and the resulting solution was stirred at room temperature for two hours. The reaction mixture was quenched by the addition of water and the product was extracted with ethyl acetate (3 x 15 mL). The combined ethyl acetate extracts were washed with water (3 x 15 mL), dried over sodium sulfate and evaporated to yield a yellow residue in 91% yield. No further purification was done.

**$D_3$-4-Methoxy-1-pentyl-3-(1-naphthoyl)-indole (37):**

The intermediate **46** (0.20 g) was dissolved in methylene chloride (8 mL) and the Dess Martin reagent (1.3 eq) was added at 0°C. After 10 minutes, the reaction was warmed to room temperature and was allowed to stir for 1.5 hours. The mixture was poured into saturated sodium

bicarbonate and the product was extracted with diethyl ether (3 x 10 mL). The organic layers were combined, washed with water (3 x 10 mL), dried over sodium sulfate and evaporated. The resulting compound was purified by column chromatography (silica gel) with a 10:90 ethyl acetate-petroleum ether solvent as the mobile phase. 88% yield. GC-MS (EI): 374.3 (molecular ion and 100%), 325.2, 303.1, 269.1, 247.2, 217.1, 177.1, 155.1, 127.1.

## Chapter Three: Computational Modeling and Design of $CB_2$ homology model

### 3.1) Results and Discussion

During the beginning of this work in 2017, the crystal structure of $CB_2$ was not published, so the primary goal was to design and validate a $CB_2$ homology model that would be used to develop selective $CB_2$ agonists. However, in 2020, the crystal structure of $CB_2$ was published, so the latter parts of this report will be focused on comparing the designed homology model and the crystal structure of $CB_2$.

#### *3.1.1) Homology Modeling*

The $CB_2$ amino acid sequence was imported into the homology model tool in Schrodinger and was submitted to the NCBI BLAST server in order to search for templates with the greatest sequence identity. Once the template was chosen an alignment, using ClustalW, was performed between the $CB_2$ amino acid sequence and the amino acid sequence of the template. Once the alignment had been completed, the model was built using the "Knowledge Based" method which will build insertions, close gaps and predict side chain conformations with any non-conserved residues. The model was further refined by identifying loop regions and refining them using a variable-dielectric generalized Born (VSGB) solvation model and the OPLS3e force field. The last step of building the model is running a minimization, which produces the lowest energy and most stable conformation of the protein [67]. Three different homology models were produced using different templates, which are shown in Table 1. These were the templates identified from the BLAST search that had the greatest homology with primary sequence of $CB_2$.

| PDB ID | Identity % | Gap % | X-Ray Crystal Structure |
|---|---|---|---|
| 5XR8 | 43 | 11 | $CB_1$ agonist AM841 bound |
| 2RH1 | 21 | 12 | Beta2- adrenergic- inactive |
| 3SN6 | 20 | 11 | Beta2- adrenergic- active |

**Table 1.** The different templates used in order to build three different homology models.

The protein data bank (PDB) ID, 5XR8, is the X-ray crystal structure of $CB_1$ with agonist AM841 bound and has an identity percent of 43 and a gap percent of 11 to $CB_2$ amino acid sequence. The identity percent is the percentage of residues that are identical between the sequences and the gap percent is the percentage of gaps between the template and homolog. The other two PDB ID's, 2RH1 and 3SN6, are crystal structures of the beta 2 adrenergic receptor in the inactive and active forms, respectively. They each have a lower percent identity of $CB_2$ than 5XR8, which was expected, but were included in this study for comparison purposes. The three homology models are shown in Figure 20 with the corresponding Ramachandran plots. A Ramachadran plot is a useful tool that helps identify residues of proteins that have disfavorable dihedral angles [68]. In Figure 20, the Ramachandran plot has a red (favored) region, yellow (allowed) region and white (disallowed) region. The Ramachandran plot for 5XR8 homology model shows two amino acids, Ile 27 and Met 237, in the disallowed region, but because these amino acids are not in close proximity to the binding pocket, they were ignored. The Ramachandran plot for 3SN6 shows one amino acid, Pro 176, in the disallowed region. The amino acid proline is ignored in Ramachandran plots because it is the only amino acid that has a five membered ring as a side chain, which highly restricts its dihedral angle to limited regions,

therefore it is not generally considered [69]. The Ramachandran plot for 2RH1 shows one amino acid, Ala 88, in the disallowed region and since it is not near the binding pocket, it was ignored.

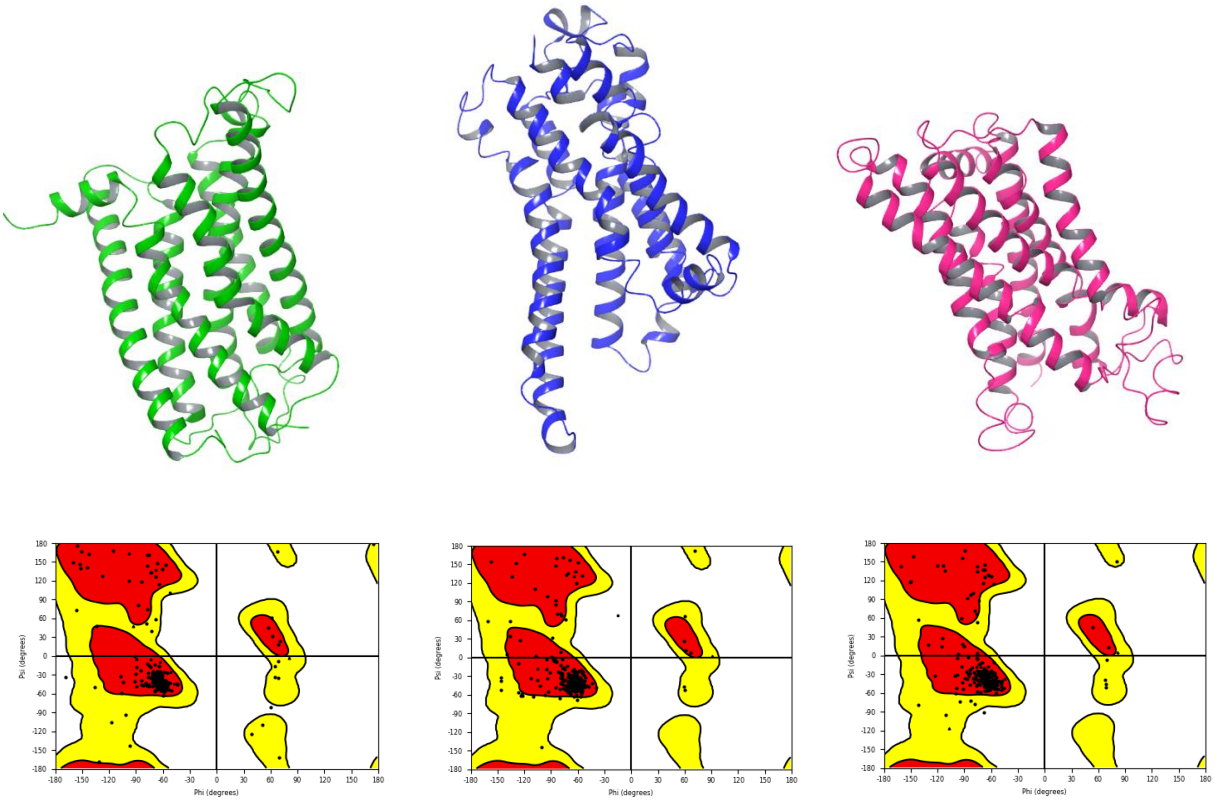

**Figure 20.** Left to right: 5XR8 homology model (green), 3SN6 homology model (blue), 2RH1 homology model (pink) with the corresponding Ramachandran plots.

*3.1.2) Receptor Generation and Docking*

The first step that needs to be performed before any docking is to identify the active site in each homology model. In order to do this, the specific amino acids that make up the binding site have to be identified. This was done in each homology model separately; the receptor grid generation task was opened and centroid of selected residues option was chosen. The amino acids selected in order to identify the active site were:  phenylalanine 94, threonine 114, serine 285, tryptophan 194, valine 164, tryptophan 258. These amino acids were chosen based upon

previous binding energy analysis study, that identified six major domains that contributed to WIN 55,212-2 binding [70]. Specifically, tryptophan 194 in TM5 had shown to be crucial for $CB_2$ binding and adenylyl cyclase activity. Also, tryptophan 258 plays a role in $CB_2$ activation and may be associated in distinguishing agonists versus antagonists. Once the active site was selected, three different $CB_2$ agonists shown in Figure 21 with known binding affinities were docked into each homology model. The Induced Fit Docking (IFD) tool was used with set parameters of OPLS3e force field and SP precision. These three agonists were chosen based on the diversity of their chemical structure. CP 55,940 is a nonselective synthetic cannabinoid that acts as a full agonist at $CB_1$ and $CB_2$ receptors [71]. Out of the three compounds chosen, this is the most structurally similar to THC and it mimics the similar psychotropic effects as well. Indole 38084 is an amino alkyl indole that was synthesized in our labs. WIN 55,212-2 is a potent synthetic cannabinoid that produces similar effects to THC, but with a completely different chemical structure [72].

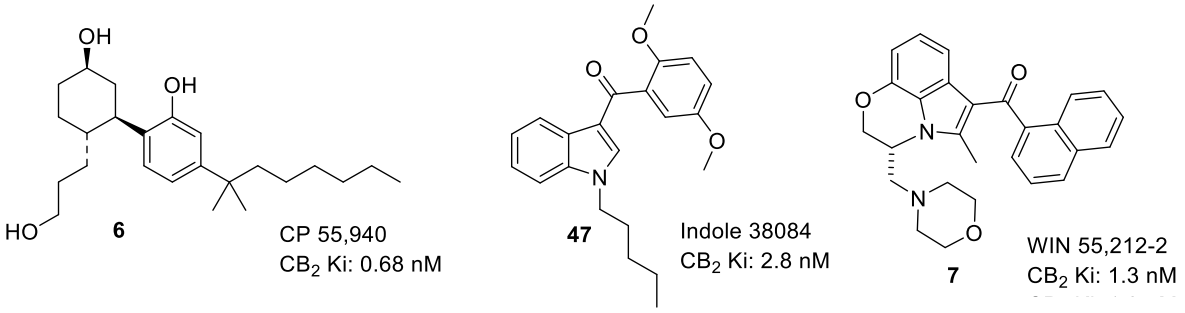


**Figure 21.** The three agonists with their corresponding $CB_2$ binding affinity values.

The results produced from the IFD is the ligand bound to the active site of the homology model. Figure 22, shows an example of CP 55,940 bound to the active site of the 5XR8 homology model. The picture on the left is a 2-D ligand-protein interaction diagram and can

easily visualize the two hydroxyl groups of CP 55,940 hydrogen bonding with Pro 184 and Ile 186. The picture of the right is a 3-D visualization tool of the same interaction.

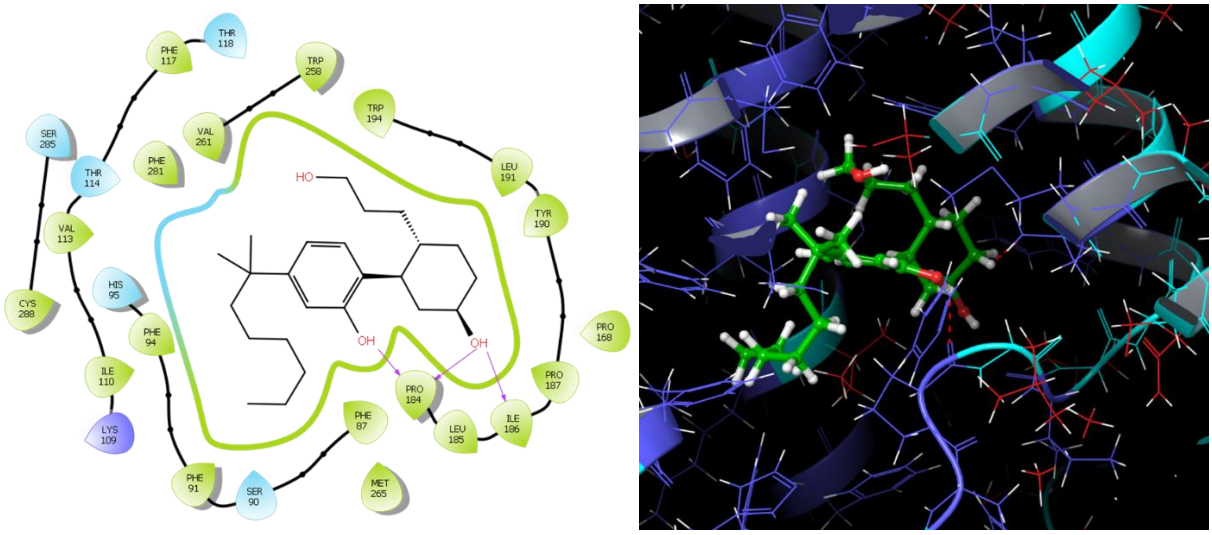


**Figure 22.** The 2-D (left) and 3-D (right) ligand –protein interaction diagram of CP 55,940 and homology model 5XR8.

*3.1.3) Molecular Dynamics and Clustering*

The homology models in complex with either CP 55,940, Indole 38084 or WIN 55,212-2 obtained from the induced fit docking studies was investigated by molecular dynamic simulations. The homology model/ligand complex was imported into the workspace and System Builder was used in order to set up the lipid bilayer membrane. The membrane model used was 1-palmitoyl-2-oleoyl-sn-glycero-3-phosphocholine (POPC, 300K) and it was placed automatically. The solvent model was predefined using a simple point change (SPC) water model. The boundary conditions used were an orthorhombic box shape and the force field was OPLS3e. Any additional ions were added in order to neutralize the protein/ligand complex. An example of the protein/ligand complex surrounded with the lipid bilayer and water is shown in Figure 23.

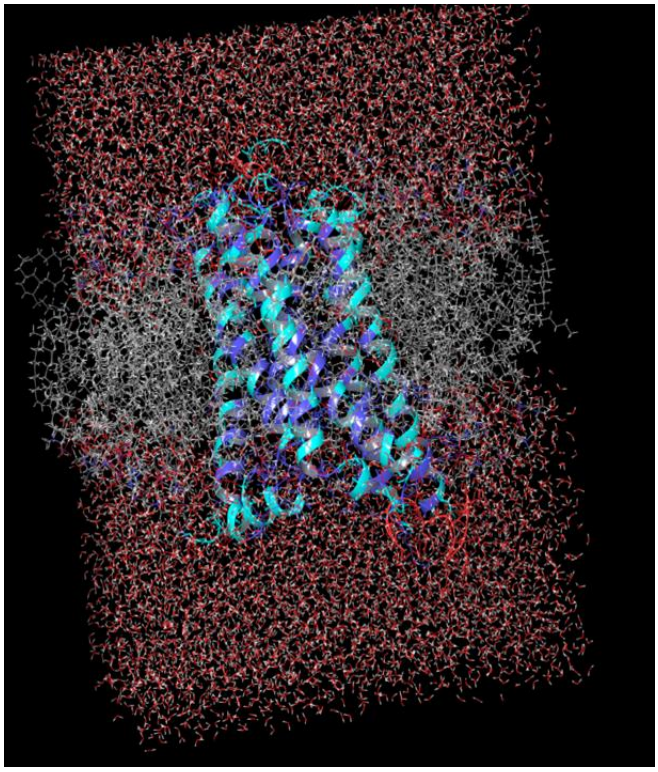

**Figure 23.** The ligand/protein complex surrounded by lipid bilayer and water.

Once the system builder job had completed, the output was used in order to set up the molecular dynamics simulation. The simulation time was set for 100 ns, which produced approximately 1,000 frames. The ensemble class was set for Isothermal-Isobaric (NPT), with a temperature of 300 K and a pressure bar of 1.01325. The model system was relaxed before simulation. At the end of the molecular dynamic simulation, a trajectory file was obtained that displayed 1,000 frames. In order to examine the 1,000 frames more efficiently, the trajectory frame clustering task was used. The trajectory frame clustering is a tool that clusters frames into representative groups based on the root mean square deviation (RMSD) matrix of a specified set of atoms and in this case, the backbone of the protein was the specified set of atoms. Table 2, shows how many representative groups were chosen for each homology model/ligand complex.

In total, 95 frames will be examined based on different homology model templates and different ligands bound when doing molecular dynamic simulations.

| **Homology Model 1: 5XR8** | | | |
|---|---|---|---|
| CP 55,940 | Indole 38084 | WIN 55,212-2 | TOTAL |
| 1-15 frames | 1-15 frames | 1-15 frames | 45 |
| **Homology Model 2: 3SN6** | | | |
| CP 55,940 | Indole 38084 | WIN 55,212-2 | TOTAL |
| 1-10 frames | 1-10 frames | 1-10 frames | 30 |
| **Homology model 3: 2RH1** | | | |
| CP 55,940 | Indole 38084 | WIN 55,212-2 | TOTAL |
| 1-10 frames | 1-10 frames | 1-10 frames | 30 |

**Table 2.** Total amount of frames exported from the molecular dynamics simulations per model.

*3.1.4) Creation of a $CB_2$ agonist database and correlation values*

From the literature, forty $CB_2$ agonists with known binding affinities were chosen (Figure 24) [73]. These compounds were imported into Schrodinger and then prepared using Ligand Preparation, which is a task that converts 2-D structures to 3-D and ionizes the compounds to physiological pH using Epik, where appropriate. These compounds were chosen due to their wide range of binding affinity values, which ranged from 0.032 nM to 3000 nM. This database was docked into the 95 frames (shown in Table 2) and then evaluated based upon the correlation of docking scores versus binding affinity. A docking score is calculated based upon the lipophilic-lipophilic, hydrogen bonding, Coulomb-Van der Waals interactions between the receptor-ligand complex and the rotatable bond penalties [74]. It is primarily used to generate an accurate pose of the ligand-receptor complex and to rank compounds from strong binders to

weak binders. There is not an exact cutoff value for docking scores because different systems will produce a variety of results, but generally a score of -10 or lower is considered a good binder. Figure 25 shows scatter plots of the frame that produced the best correlation value from each homology model. The purpose in doing this study was to determine which frame is more accurate in predicting the crystal structure of $CB_2$. As expected, 5XR8 gave the best correlation value of 0.21. This is a typical correlation value that has been reported in the literature for other docking studies [75-78]. As stated previously, glide docking is generally used to predict poses of the ligand-receptor complex and to separate strong binders (<10 um) from inactive compounds. However, predicting and/or correlating binding affinity with docking scores has shown to have a poor relationship due to the scoring being limited on predicting entropy gains and/or losses and omitting thermodynamics of free energy binding. In certain circumstances, the correlation value may be higher or lower depending upon the target protein and ligands used, which can sometimes be improved.

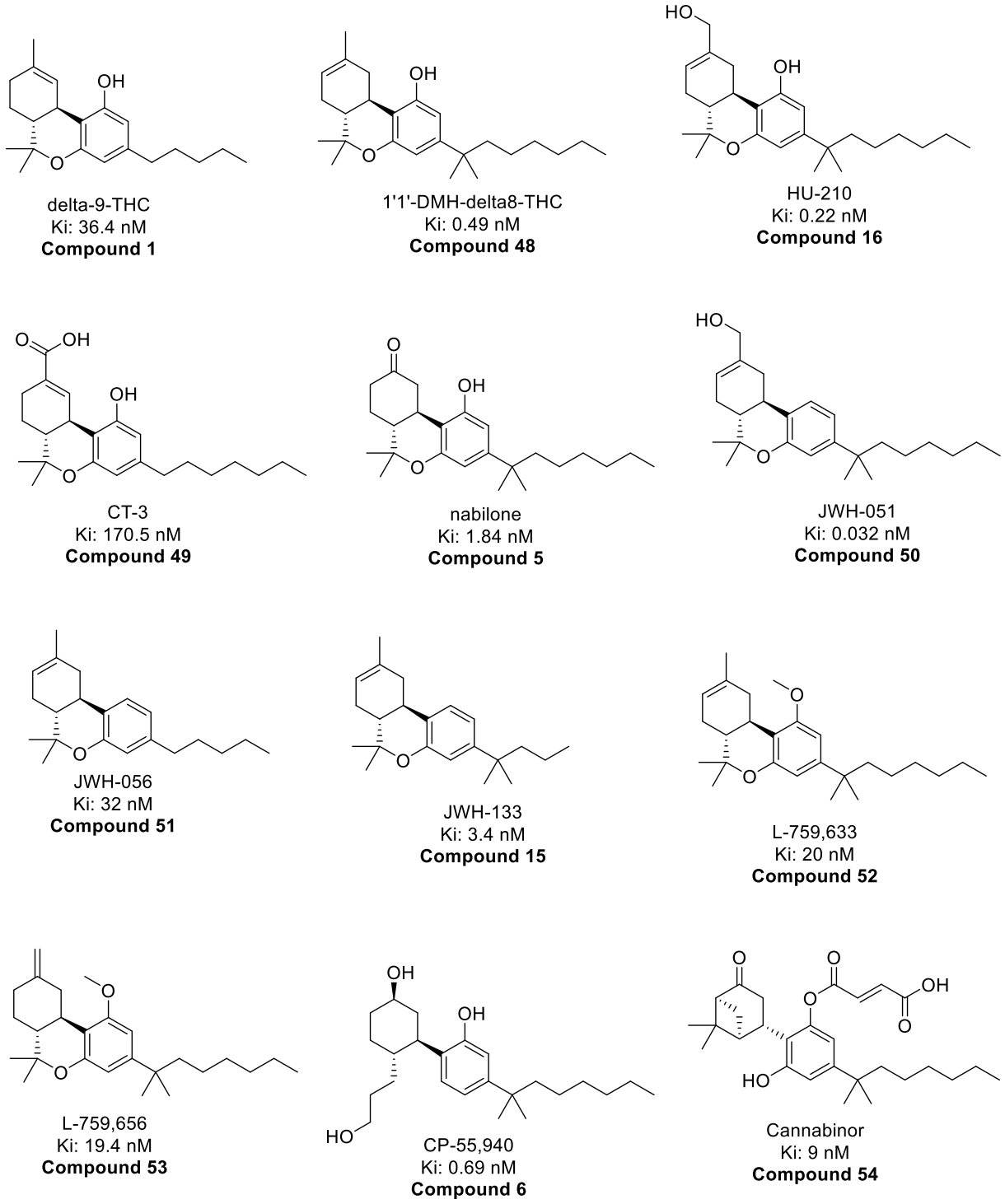


**Figure 24.** $CB_2$ agonist database with the corresponding $CB_2$ binding affinity values.

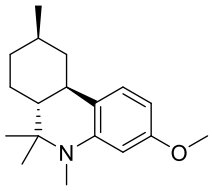

L-759,632
Ki: 54 nM
**Compound 55**

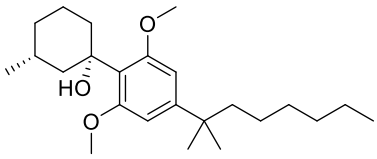

O-1966
Ki: 23.1 nM
**Compound 56**

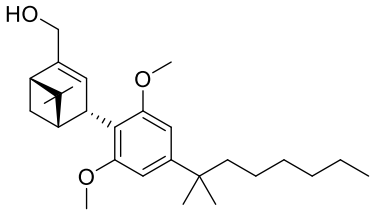

HU-308
Ki: 22.7 nM
**Compound 12**

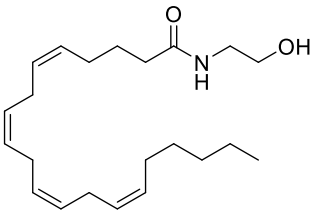

Anandamide
Ki: 371 nM
**Compound 2**

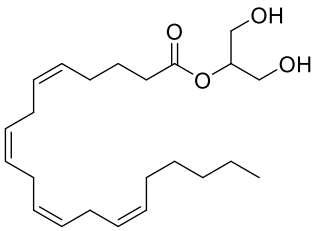

2-AG
Ki: 1400 nM
**Compound 3**

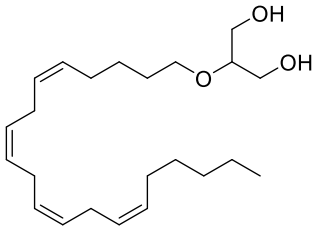

Noladin Ether
Ki: 3000 nM
**Compound 57**

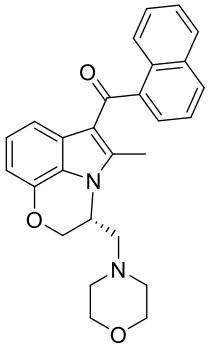

WIN 55212-2
Ki: 0.3 nM
**Compound 7**

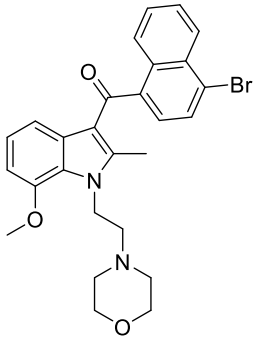

30
Ki: 1.8 nM
**Compound 58**

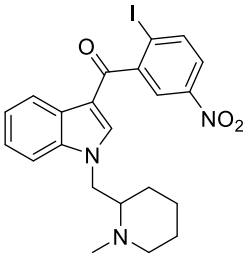

AM-1241
Ki: 7.1 nM
**Compound 13**

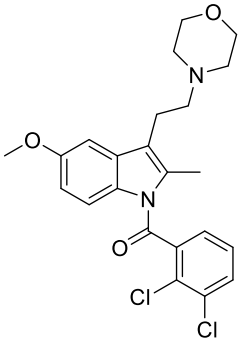

GW-405,833
Ki: 3.8 nM
**Compound 14**

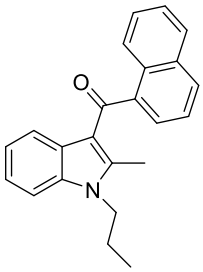

JWH-015
Ki: 14 nM
**Compound 59**

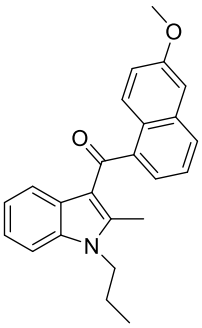

JWH-151
Ki: 30 nM
**Compound 60**

**Figure 24.** Continued.

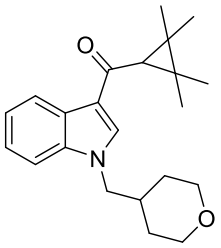

36
Ki: 0.21 nM
**Compound 61**

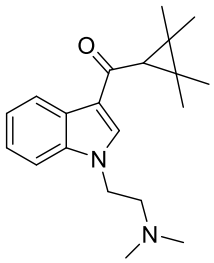

37
Ki: 1.9 nM
**Compound 62**

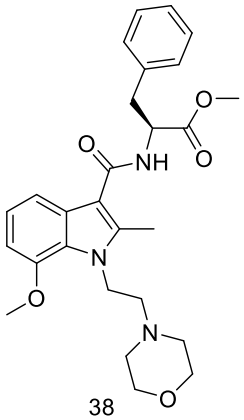

38
Ki: 8 nM
**Compound 63**

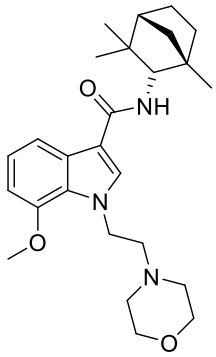

39
Ki: 11 nM
**Compound 64**

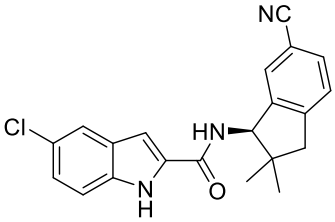

41
Ki: 0.71 nM
**Compound 65**

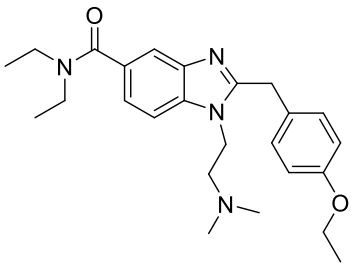

42
Ki: 38 nM
**Compound 66**

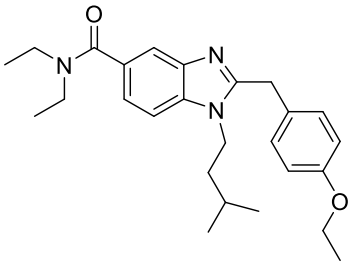

43
Ki: 4.5 nM
**Compound 67**

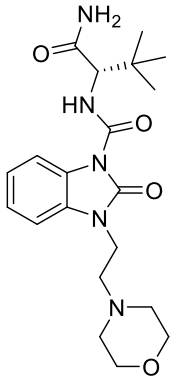

54
Ki: 5 nM
**Compound 68**

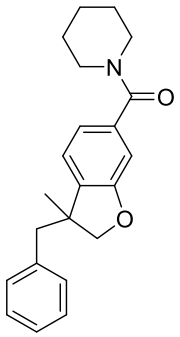

MDA-7
Ki: 422 nM
**Compound 69**

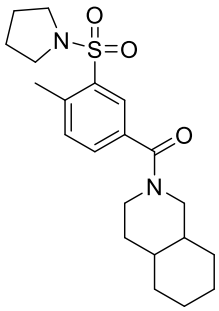

101
Ki: 130 nM
**Compound 70**

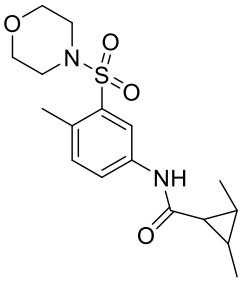

102
Ki: 23 nM
**Compound 71**

**Figure 24.** Continued.

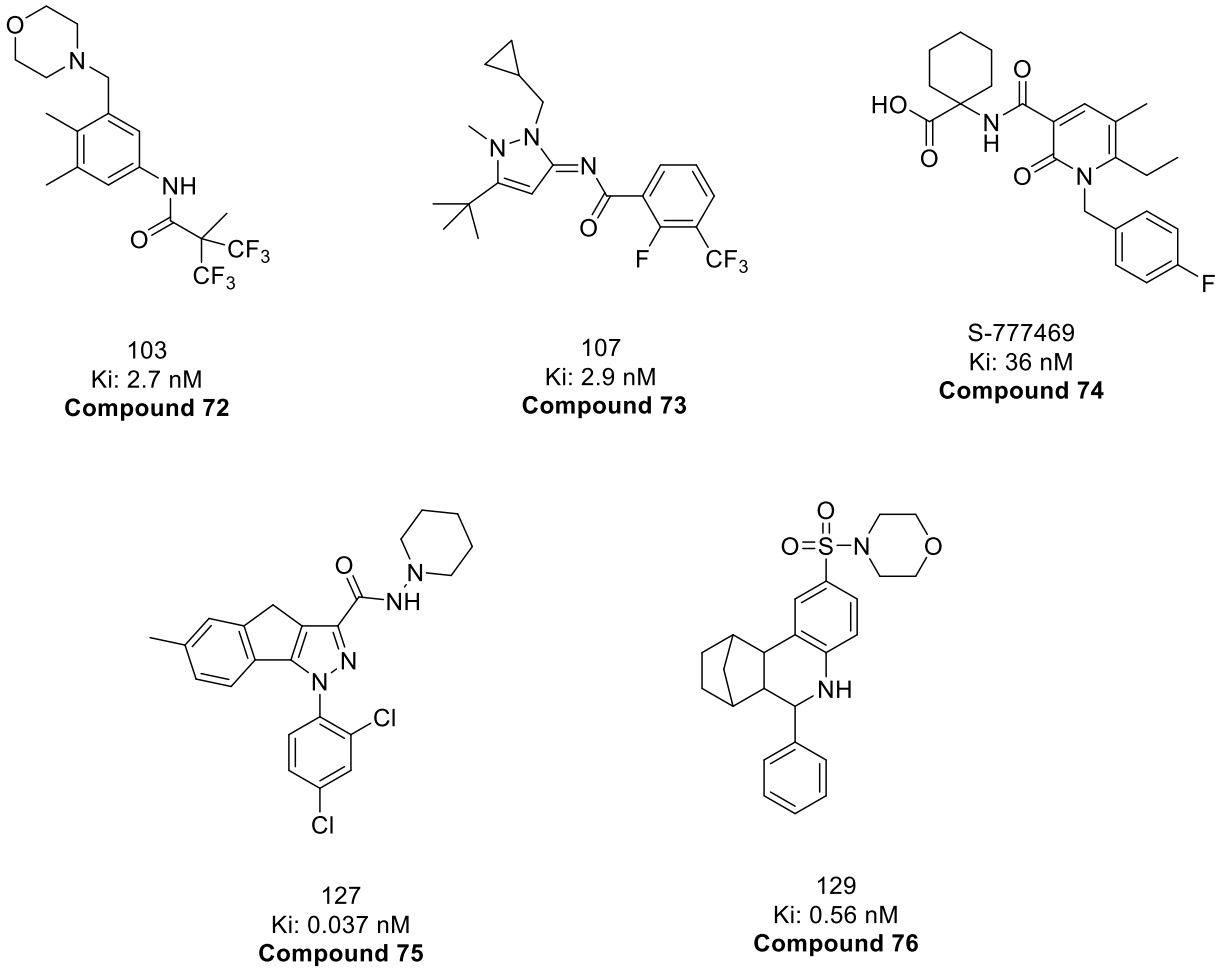


**Figure 24.** Continued.

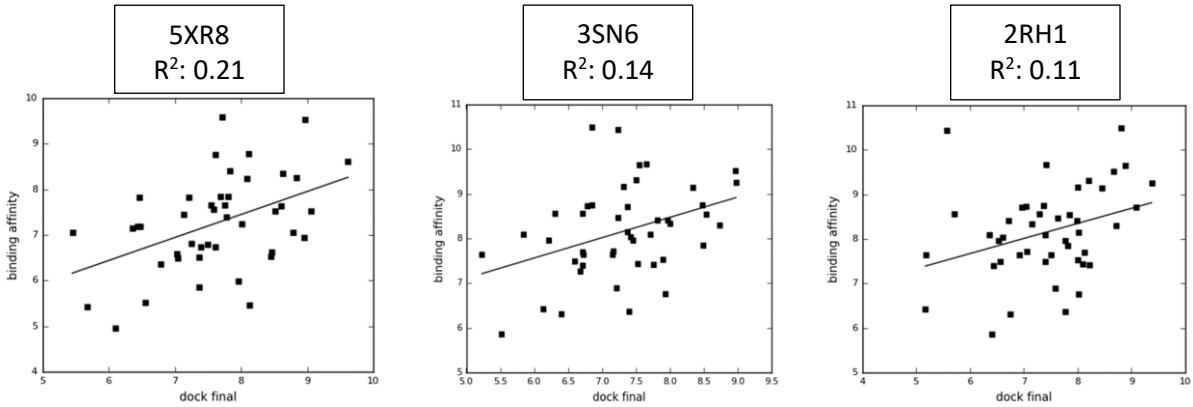


**Figure 25.** Docking scores vs. binding affinity correlation values for each homology model.

*3.1.5) Enrichment Studies*

An enrichment study in molecular modeling is used to evaluate the ability of a target protein to rank or prioritize active compounds over decoy compounds [79]. The active compounds are combined with a set of decoy compounds, docked into the specific receptor and evaluated by a set of enrichment factors. In this study, two decoy databases were created. The first set of decoys was a Drug-Like database that was downloaded from Schrodinger's website [80, 81]. This database consisted of 750 decoy compounds that were random in structure to $CB_2$ active compounds that are shown in Figure 24. The second set of decoy compounds were downloaded from a website known as the database of useful decoys: enhanced (DUD-E). This website requires a submission of known binders and it will generate decoy compounds that are structurally similar. This database also had a total number of 750 decoys. The Drug-Like and DUD-E decoy sets each had an additional 15 $CB_2$ active compounds added to them to give a total number of 765 compounds per decoy set. The metrics that are commonly used to evaluate the performance of ranking actives versus decoys are: area under the receiver operating characteristic curve (ROC), robust initial enhancement (RIE) and area under the accumulation curve (AUAC) [82]. The ROC score is the probability that an active will be ranked before an inactive with a scoring value of 0 to 1, with 1 being ideal. A score of 0.5 or lower is considered a bad prediction and random. The RIE scores with the higher the number is the better. The AUAC scoring is from 0 to 1, with 1 being ideal. The AUAC scores a model on the ability to classify compounds into classes (actives vs decoys). A score of 0.5 is random and any score above 0.7 is considered acceptable. However, these metrics do not consider the early recognition problem, which is ranking actives very early in the ordered list [83, 84]. As an example, large pharmaceutical companies have databases containing millions of compounds to be virtually screened. Most

likely, only the top 0.1% of the ranked compounds will be considered. Therefore, the actives must be ranked early or the virtual screening is useless. In order to take into consideration the early performance, the metric Boltzmann-enhanced discrimination of receiver operating characteristic (BEDROC) was derived. This metric contains an early recognition parameter, alpha. The BEDROC 1 is when alpha=160.9, which means the top 1% of the ranked compounds accounts for 80% of the total score, BEDROC 2 is when alpha=20.0, which means the top 8% of ranked compounds accounts for 80% of the total score and BEDROC 3 is when alpha=8.0, which means the top 20% of the ranked compounds accounts for 80% of the total score. The BEDROC scoring is from 0 to 1, with 1 being ideal.

Both decoy sets, Drug-Like and DUD-E, were individually docked into the forty-five 5XR8 frames that were generated in the previous section. Once the decoy set had been docked into the frames, each frame was analyzed individually by using an Enrichment Calculator in Schrodinger. The following metrics were compared for Drug-Like and DUD-E in Table 3 at one specific frame using the 5XR8 homology model.

| | BEDROC 1 | BEDROC 2 | BEDROC 3 | ROC | RIE | AUAC |
|---|---|---|---|---|---|---|
| Drug-Like | 0.425 | 0.467 | 0.611 | 0.87 | 7.72 | 0.86 |
| DUD-E | 0.037 | 0.121 | 0.258 | 0.71 | 2.01 | 0.71 |

**Table 3**. The enrichment scoring of Drug-Like and DUD-E decoys at one frame using the 5XR8 homology model.

The BEDROC, ROC, RIE and AUAC scores are extremely higher when utilizing the Drug-Like decoy set. It was hypothesized that the Drug-Like decoy set would produce greater enrichment results than the DUD-E decoy set due to the structural difference seen in the Drug-Like versus actives. In other words, it would be easier for the homology model to pick out active compounds when combined with compounds that were not structurally similar.

Another way to evaluate the performance is by a percent screen plot, which is shown in Figure 26. This plot evaluates the percent of actives found in *n* percent of compounds screened and anything below the grey diagonal line represents random.

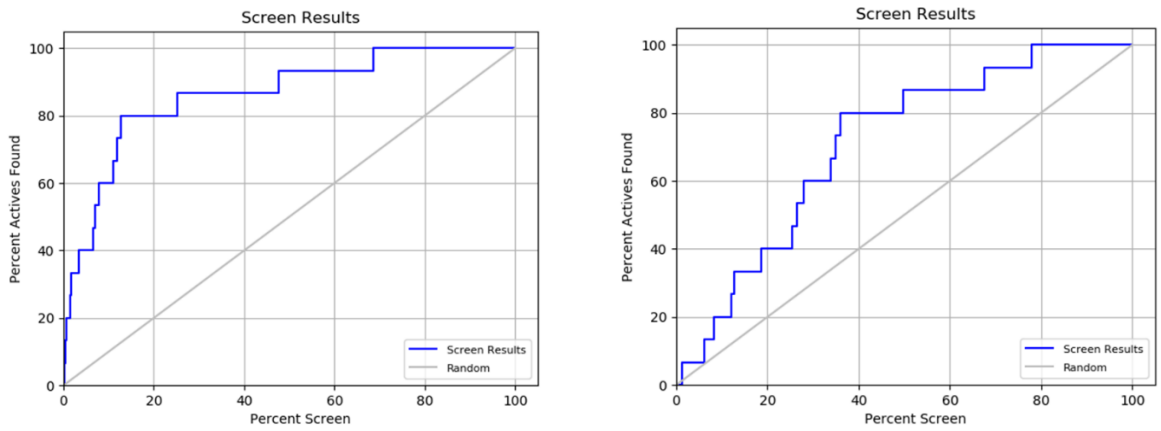


**Figure 26.** The percent screen plot for Drug-Like Decoy set (left) and DUD-E decoy set (right).

When evaluating the percent screen plot, the Drug-Like decoy set found a higher percent of actives quicker than the DUD-E decoy set. In other words, more actives were found sooner when using the Drug-Like decoy set versus the DUD-E decoy set. At 20% screen, the 5XR8 homology model found 80% of actives with the Drug-Like decoy database, but only found 40% of actives with the DUD-E database. Again, this was expected that the Drug-Like decoy set would be better than the DUD-E decoy set due to the structural differences.

In order to test the homology model performance even more, the X-ray crystal structure of $CB_1$ was utilized. The rationale for this study was because it is now a known crystal structure using ligands with known $CB_1$ binding affinities. Therefore, this should be an accurate way to test the ability of the docking and scoring of active versus decoy compounds. A total number of 765 compounds, 15 $CB_1$ active compounds and 750 DUD-E decoys, were docked into the $CB_1$ crystal structure. After the database was docked, the enrichment calculator was used in order to

produce the same scoring as before. The enrichment results for $CB_1$ versus $CB_2$ are shown in Table 4 and the percent screen plot is shown in Figure 27.

| | BEDROC 1 | BEDROC 2 | BEDROC 3 | ROC | RIE | AUAC |
|---|---|---|---|---|---|---|
| $CB_1$ | 0 | 0.086 | 0.256 | 0.74 | 1.44 | 0.74 |
| $CB_2$ | 0.037 | 0.121 | 0.258 | 0.71 | 2.01 | 0.71 |

**Table 4.** The enrichment scoring of $CB_1$ and $CB_2$ using the DUD-E decoy set.

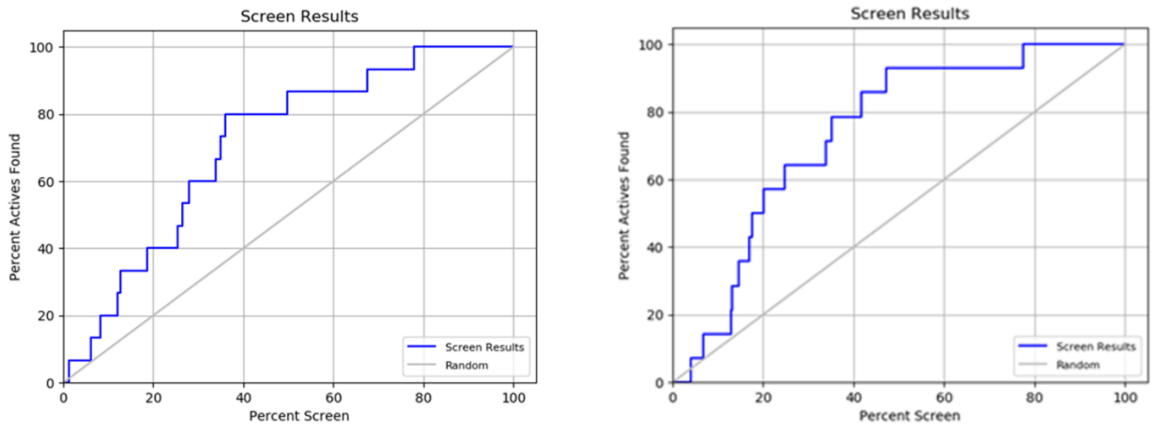


**Figure 27.** The percent screen plot for $CB_2$ (left) and $CB_1$ (right).

The enrichment results between $CB_1$ and $CB_2$ are similar, with the BEDROC and RIE scores being slightly better for $CB_2$. The ROC and AUAC scores are only slightly higher in $CB_1$, but not by a significant amount. The percent screen plot shows that $CB_1$, finds active compounds only slightly sooner than $CB_2$. In $CB_1$, at 60% total screen, approximately 95% of active compounds were found and in $CB_2$, approximately 85% were found. This concludes that our homology model is a good starting point, but that there is room for improvement.

*3.1.6) Modifications made to homology model*

In order to improve the homology model, two structural modifications were made. The first modification was shifting two amino acids upwards in order to adjust the position of phenylalanine 197. As seen in Figure 28, the blue side chain represent PHE 197 before any modifications were done and the green side chain represents PHE 197 after the amino acids were shifted upwards by two. The shifting of the amino acids, fixes the position of PHE 197 towards the binding pocket and it has been previously studied that side chain, PHE 197, is necessary when binding agonists [85].

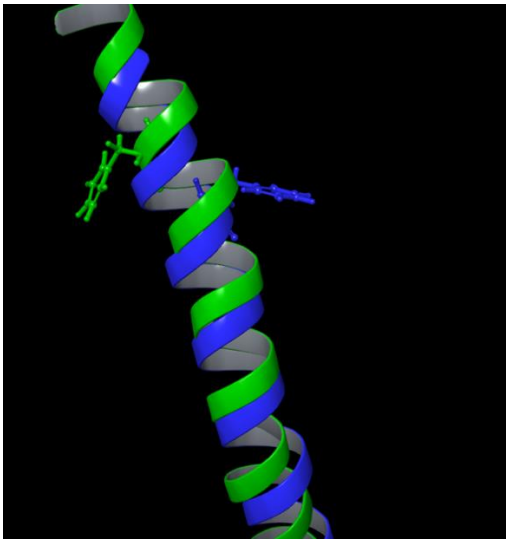

**Figure 28.** The position of side chain PHE 197 in the modified model (green) and pre-modified model (blue).

The second modification that was made is patching the internal disulfide bond between CYS 174 and CYS 179. In figure 29, the yellow bond represents the disulfide patch that was made. This modification was made because the internal disulfide bond of CYS 174 and CYS 179

stabilizes extracellular loop 2, which maintains a key conformational lock of the binding site to enable a ligand binding conformation [86].

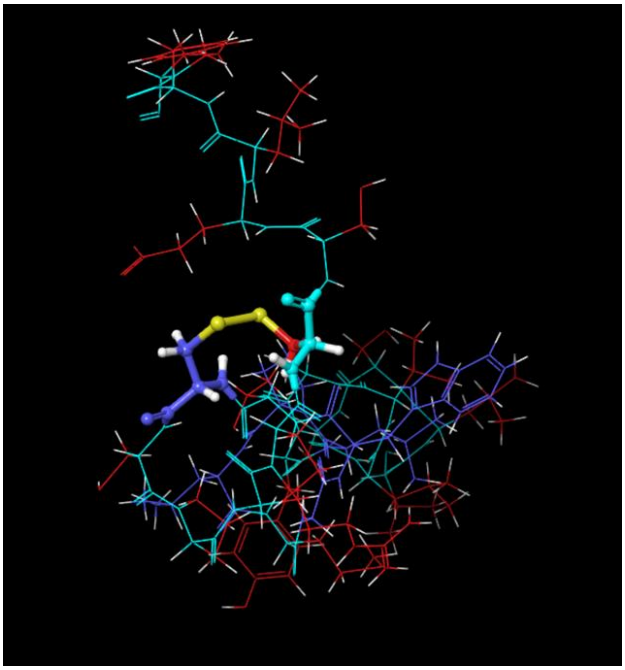

**Figure 29.** The disulfide bond between CYS 174 and CYS 179 patched.

Once these modifications were made, the homology model went through the process of molecular dynamics, clustering of frames, docking of decoy plus actives databases (Drug-Like and DUD-E) and enrichment calculation. The enrichment results of the pre-modified model and post-modified model are compared and shown in Table 5.

| | BEDROC 1 | BEDROC 2 | BEDROC 3 | ROC | RIE | AUAC |
|---|---|---|---|---|---|---|
| Pre-Modification DUD-E decoys | 0.037 | 0.121 | 0.258 | 0.71 | 2.01 | 0.71 |
| Post-Modification DUD-E decoys | 0.294 | 0.321 | 0.432 | 0.74 | 5.32 | 0.73 |
| Pre-Modification Drug-Like decoys | 0.425 | 0.467 | 0.611 | 0.87 | 7.72 | 0.86 |
| Post-Modification Drug-Like decoys | 0.516 | 0.581 | 0.665 | 0.88 | 9.61 | 0.87 |

**Table 5.** The enrichment scores for the pre-modified model and post-modified $CB_2$ homology model utilizing the DUD-E decoy database and Drug-Like decoy database.

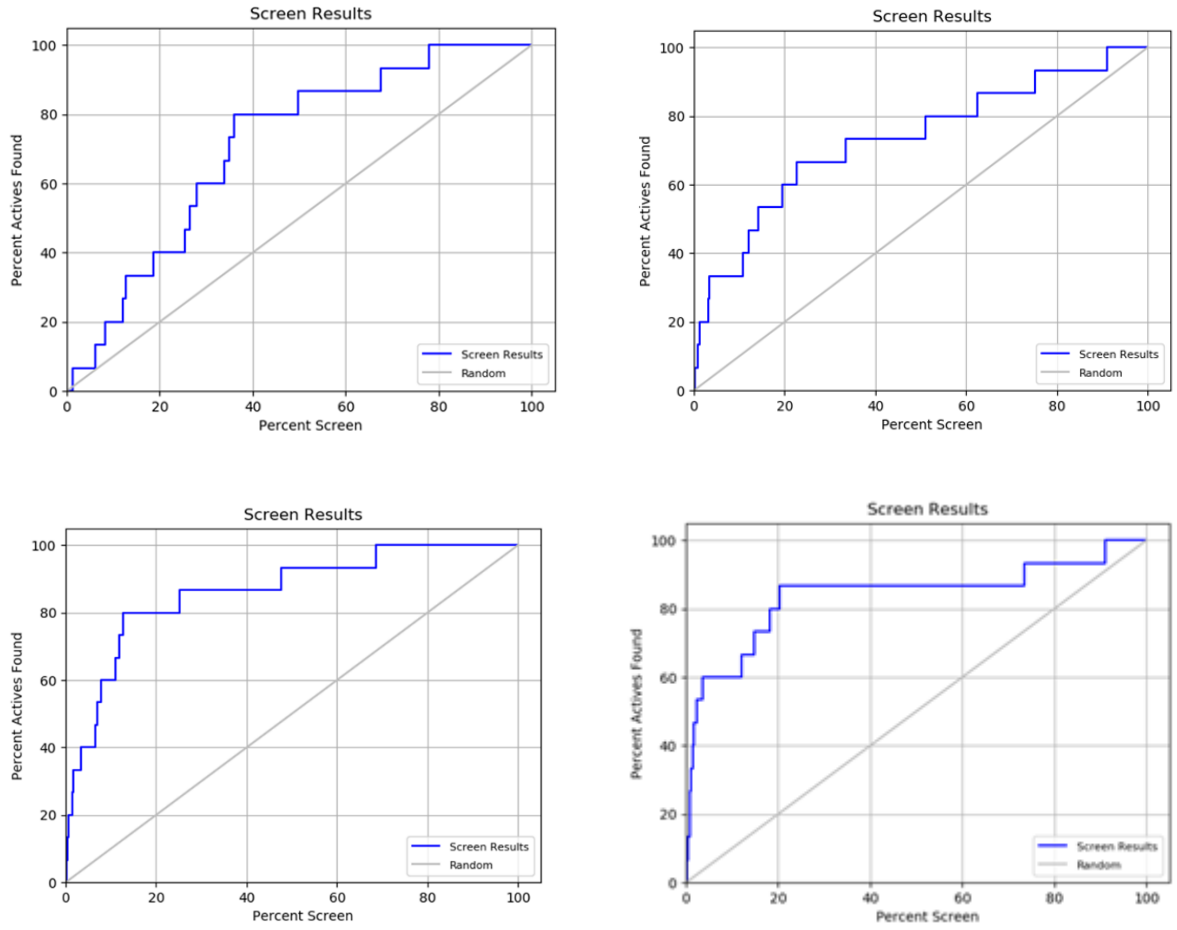


**Figure 30.** The percent screen plot for pre-modified model (top, left) and post-modified model (top, right) utilizing the DUD-E decoy database. The percent screen plot for the pre-modified model (bottom, left) and post-modified model (bottom, right) utilizing the Drug-Like decoy database.

When comparing the pre- and post- modified homology model with the DUD-E database in Table 5, the enrichment scores are higher for the post-modified model. The ROC and AUAC scores are close, but still higher for the post-modified. This same pattern is seen for the pre- and post-modified model with the Drug-Like decoy set. However, the Drug-Like decoy database still scores higher than the DUD-E decoy database. The percent screen plot is shown in Figure 30. When comparing the pre- and post-modified model utilizing the DUD-E decoy (top plots), at 10% screen, the post-modified model found approximately 35% actives and the pre-modified

model only found 20% actives. At 20% screen, the post-modified model found 60% actives and the pre-modified model found 40% screen. When comparing the pre- and post-modified model utilizing the Drug-Like decoy (bottom plots), at 5% screen, the post-modified found 60% screen and then pre-modified model found 40% screen. With both the Drug-Like and DUD-E decoy databases, the modified model has shown improvement and this post-modified model will be used in order to design novel selective agonists.

*3.1.7) Development of indole compounds*

The aminoalkylindole, JWH-018, is a well-known potent, nonselective agonist at the cannabinoid receptors [87]. The compound has been heavily studied due to its common and frequent appearance in different spice products on the market. The known cannabinoid receptor activity and the familiarity with indoles is the reason why JWH-018 was used to design a set of novel indoles as selective $CB_2$ agonists. JWH-018 was docked into the highest scoring enrichment frame from the 5XR8 model. In order to design a selective $CB_2$ agonist, JWH-018 docked into $CB_1$ binding site was evaluated and taken into consideration. The goal was to enhance $CB_2$ binding while reducing binding at $CB_1$. The 2-D interaction of JWH-018 and the proposed $CB_2$ binding pocket are shown in Figure 31. The only predicted interactions between JWH-018 and $CB_2$ are pi-pi interactions between the aromatic indole and PHE 87 and PHE 281. The 6th position on the indole ring has room for growth and is near the amino acid SER 285. It was hypothesized by the addition of a hydroxyl or amino group that a hydrogen bond interaction would form with SER 285.

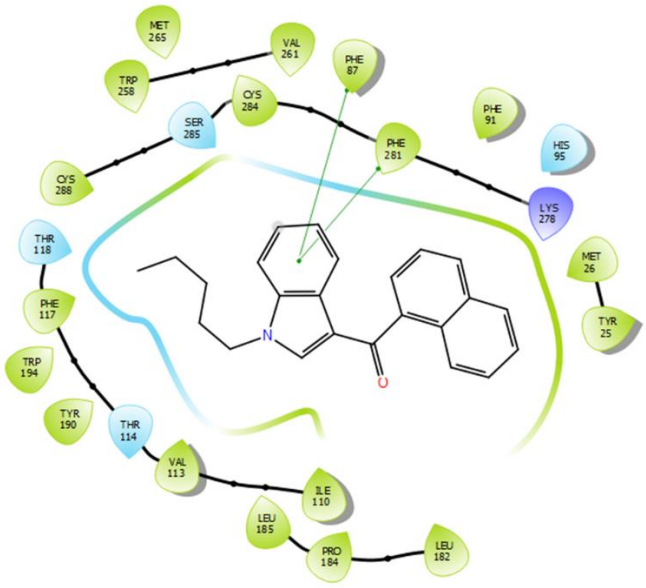


**Figure 31.** The aminoalkylindole, JWH-018, bound to $CB_2$ binding pocket.

The proposed set of substituted indole target compounds are shown in Figure 32. The proposed compounds have the same structural composition of JWH-018, but with the addition of a methyl ester or amide at position 6 on the indole. These four compounds were docked into the $CB_2$ binding pocket and the 2-D interaction diagram, along with the corresponding docking scores are shown in Figure 33. Indole **80** has a docking score of -10.111. The important interactions shown are pi-pi binding with aromatic residues PHE 117 with the naphthoyl ring and PHE 87 with the indole core along with hydrogen bonding between the amino group of the amide and SER 90. Indole **78** has a docking score of -10.918. The interactions shown are pi-pi bonding between the naphthoyl ring and PHE 200. Also, hydrogen bonding between the carbonyl of the amide and SER 90 and another hydrogen bond between the amino functionality of the amide with PHE 106. Indole **79** has a docking score of -9.394. The only interactions shown are hydrogen bonding with the carbonyl of the methyl ester between amino acids ASN 93 and LYS 109. Indole **77** has a docking score of -10.435 and shows one hydrogen bond

interaction between the carbonyl of the methyl ester and SER 90. It is important to keep in mind that these interactions are only predictions and the only way to verify these are by doing extensive biological testing. Even though the hypothesis of hydrogen bonding with SER 285 did not seem to play an important role in the docking evaluations, it still is predicted in all cases that the addition of the methyl ester and amide groups have hydrogen bonding potential. The lone pairs on the carbonyl oxygen of the methyl esters and/or amides can potentially play a role in hydrogen bonding. Also, the lone pairs on the oxygen of the ester or the nitrogen of the amide have potential to hydrogen bond with the receptor. It was also of interest to investigate the hindered rotation by the addition of the double bond. These compounds will be synthesized and shown in the next section.

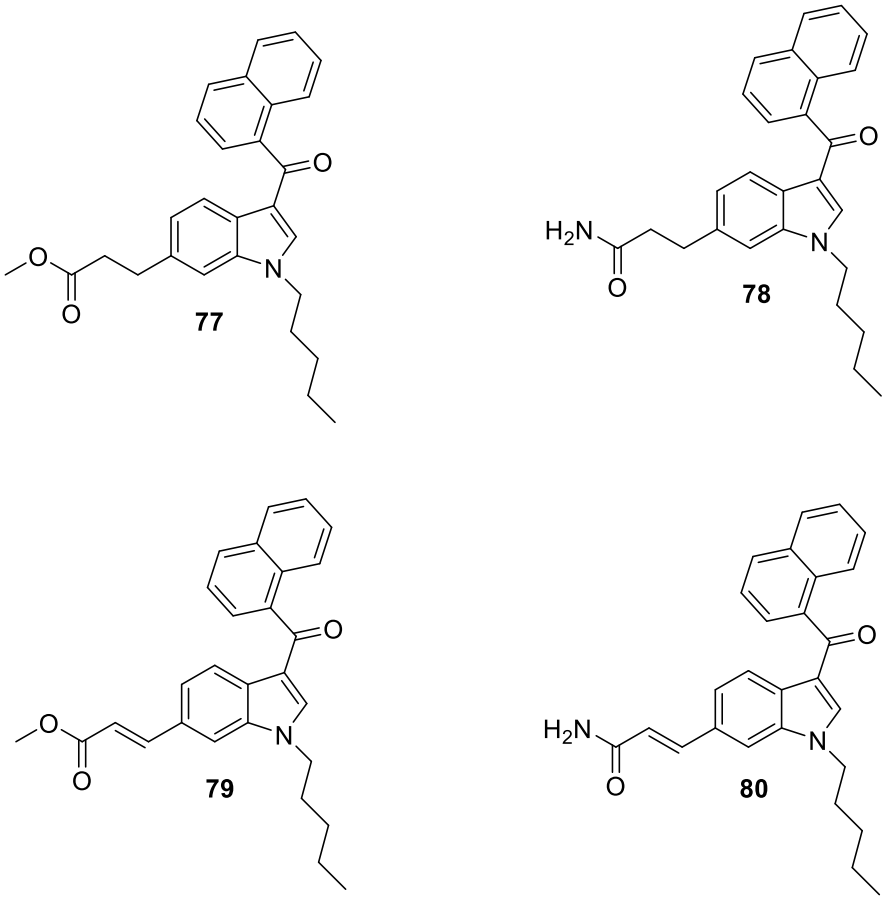


**Figure 32.** The proposed set of indole target compounds.

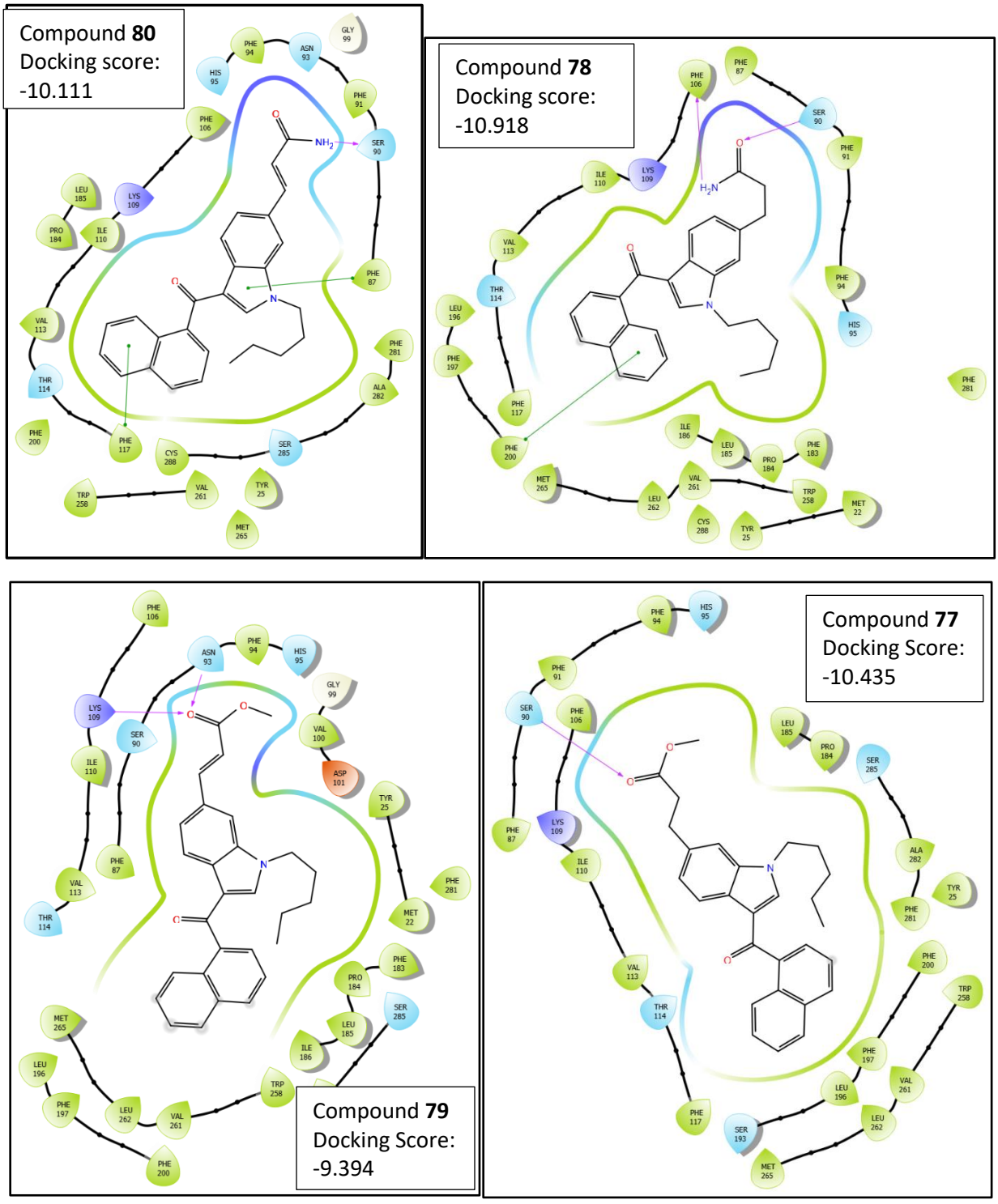


**Figure 33.** The 2-D ligand interaction diagram of the proposed indoles bound to $CB_2$ along with the corresponding docking scores.

*3.1.8) Antagonist and agonist crystal structure of $CB_2$ published.*

Early in 2019, Li, X. et. al., published the X-ray crystal structure of $CB_2$ with antagonist AM10257 bound (PDB ID: 5ZTY) [88]. Being that the $CB_2$ homology model created during this study was based off an agonist bound, it was of interest to compare the two. The PDB ID, 5ZTY, was downloaded and prepared using protein preparation in Schrodinger. The prepared protein, 5ZTY, and the pre-modified $CB_2$ homology model after molecular dynamics were superimposed and a protein structure alignment was done. The protein structure alignment gave a score of 0.387 and a root mean square deviation (RMSD) of 3.101 angstroms. It is hypothesized that these scores are high because the homology model did not contain all the amino acids that the crystal structure contained. The smaller the alignment score, the better. Any alignment score less than 0.6-0.7 is considered a good alignment and any score more than 0.7-0.8 is considered a failed attempt [89].

The prepared protein 5ZTY and the post-modified $CB_2$ homology model created during this study were superimposed and a protein structure alignment was done. The protein structure alignment of 5ZTY and the post-modified $CB_2$ homology model is shown in Figure 34. The protein structure alignment gave an alignment score of 0.266 and a RMSD of 2.576 angstroms. The amino acid TRP 258 is a highly conserved residue in Class A GPCRs and has been reported to have a crucial role in GPCR activation [42, 90]. This particular amino acid is considered a toggle switch and plays a crucial role in the inactive/active states of $CB_2$. It was published, that the inactive $CB_2$ TRP 258 undergoes a 64-degree clockwise rotation compared to the active $CB_2$ GPCR. The differences in rotation of TRP 258 between the inactive $CB_2$ crystal structure and the $CB_2$ active homology model are shown in Figure 34. The post-modified $CB_2$ homology model

that was created during this study predicted the toggle switch in the correct orientation for the active state.

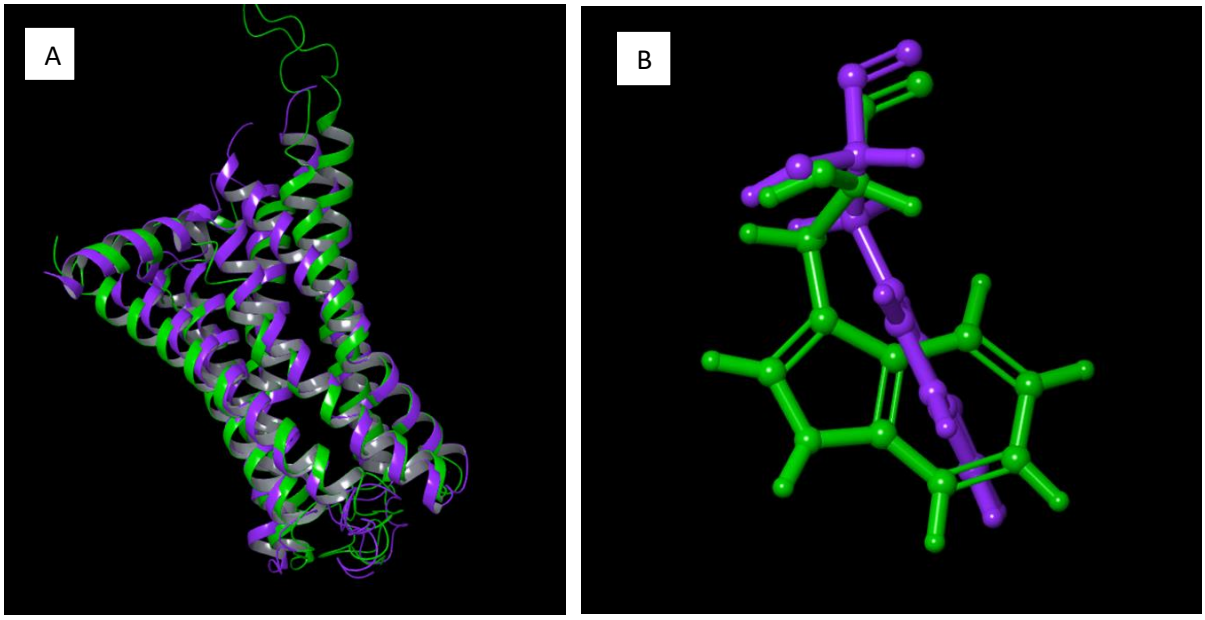


**Figure 34.** A) The protein structure alignment of 5ZTY (purple) and the post-modified $CB_2$ homology model (green). B) TRP 258 orientation for 5ZTY (purple) and the post-modified $CB_2$ homology model (green).

An enrichment study was done of 5ZTY using the same process as before with only the DUD-E decoy database combined with 15 active $CB_2$ agonists, which was done in order to compare to the pre- and post-modified homology model enrichment scores. The enrichment results are shown in Table 6 and the percent screen plot is shown in Figure 35. The pre- and post-modified $CB_2$ homology model both show much higher enrichment scores than for 5ZTY and the percent screen plot shows a higher percent of actives were found quicker with both homology models than for 5ZTY. At 20% screen, the pre-modified model found approximately 40% active compounds, the post-modified homology model found approximately 60% active compounds and the antagonist crystal structure found approximately 15% actives. This was expected since

the active compounds in the decoy database were agonist compounds. In other words, it was expected that the $CB_2$ homology model based off an agonist would give higher enrichment scores than a crystal structure in the antagonist form when the active compounds are composed of $CB_2$ agonists.

| | BEDROC 1 | BEDROC 2 | BEDROC 3 | ROC | RIE | AUAC |
|---|---|---|---|---|---|---|
| 5ZTY | 0 | 0.008 | 0.086 | 0.57 | 0.14 | 0.57 |
| Pre-Modified $CB_2$ homology | 0.037 | 0.121 | 0.258 | 0.71 | 2.01 | 0.71 |
| Post-Modified $CB_2$ Homology | 0.294 | 0.321 | 0.432 | 0.74 | 5.32 | 0.73 |

**Table 6.** The enrichment scores between 5ZTY and the $CB_2$ homology model (pre- and post-modified).

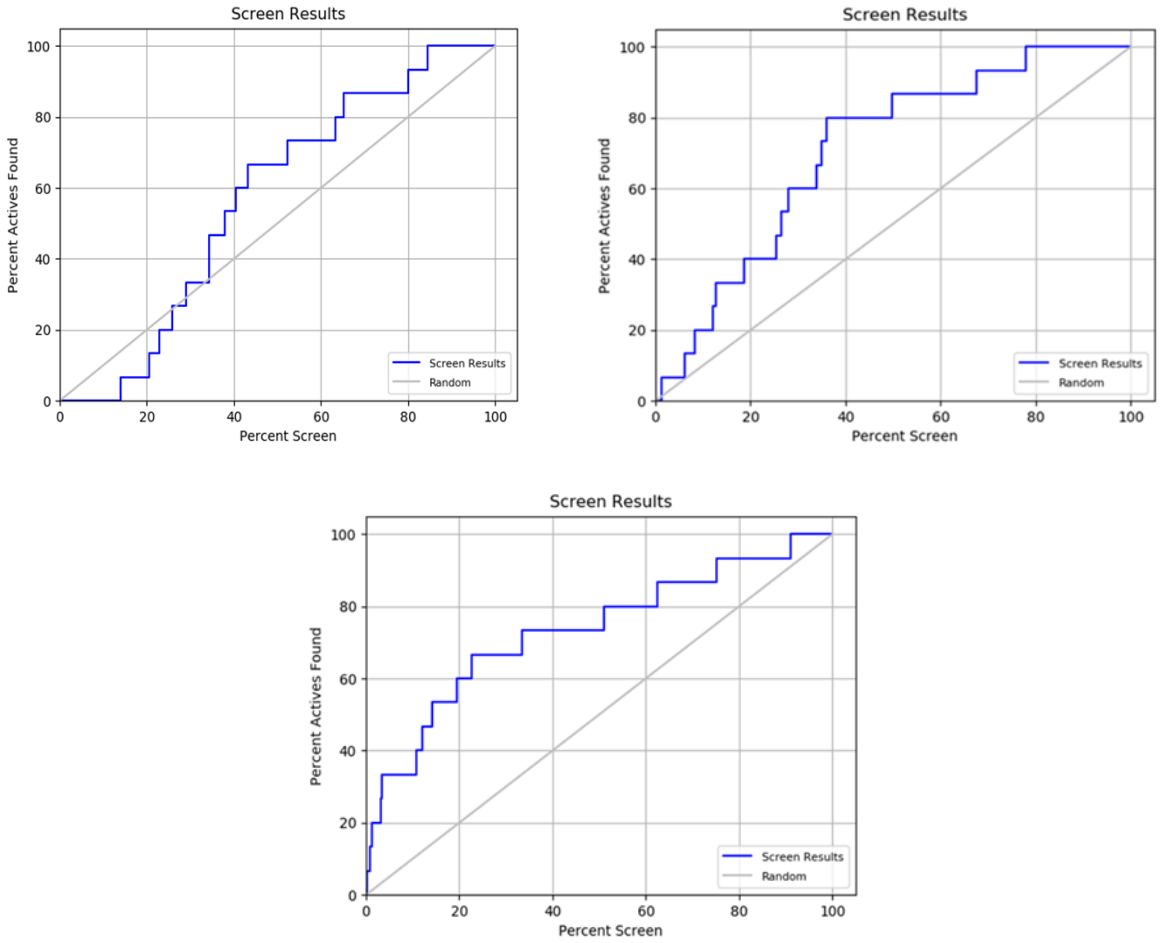


**Figure 35.** The percent screen plot of 5ZTY (top left), pre-modified $CB_2$ homology model (top right) and post-modified $CB_2$ homology model (bottom).

Within a year from the $CB_2$ antagonist crystal structure being published, the $CB_2$ cryo-EM structure with agonist WIN 55,212-2 bound was published (PDB ID: 6PT0) [42]. It was of interest to see how the $CB_2$ homology model created during this study would compare to the X-ray crystal structure. The PDB, 6PT0, was downloaded and prepared using protein preparation in Schrodinger. The prepared protein, 6PT0, and the pre-modified $CB_2$ homology model were superimposed and a protein structure alignment was done. The protein structure alignment produced an alignment score of 0.233 and a RMSD of 2.307 angstroms. Again, it is hypothesized

that the scoring was high due to the amino acids that are present in the crystal structure that were not present in the homology model.

The prepared protein, 6PT0, and the post-modified $CB_2$ homology model were superimposed and a protein structure alignment was done. The protein structure alignment produced an alignment score of 0.206 and an RMSD of 2.154 angstroms. The post-modified $CB_2$ homology model has better alignment with the $CB_2$ agonist crystal structure than with the $CB_2$ antagonist crystal structure, which was expected. The aligned post-modified $CB_2$ homology model and the $CB_2$ agonist crystal structure, a zoomed in view of the binding pockets, and the orientation of TRP 258 is shown in Figure 36. The binding pocket seems to be similar with minor shifts in a few of the amino acids. When investigating the orientation of the toggle switch, the $CB_2$ homology model and the published $CB_2$ crystal structure, have TRP 258 in the same orientation.

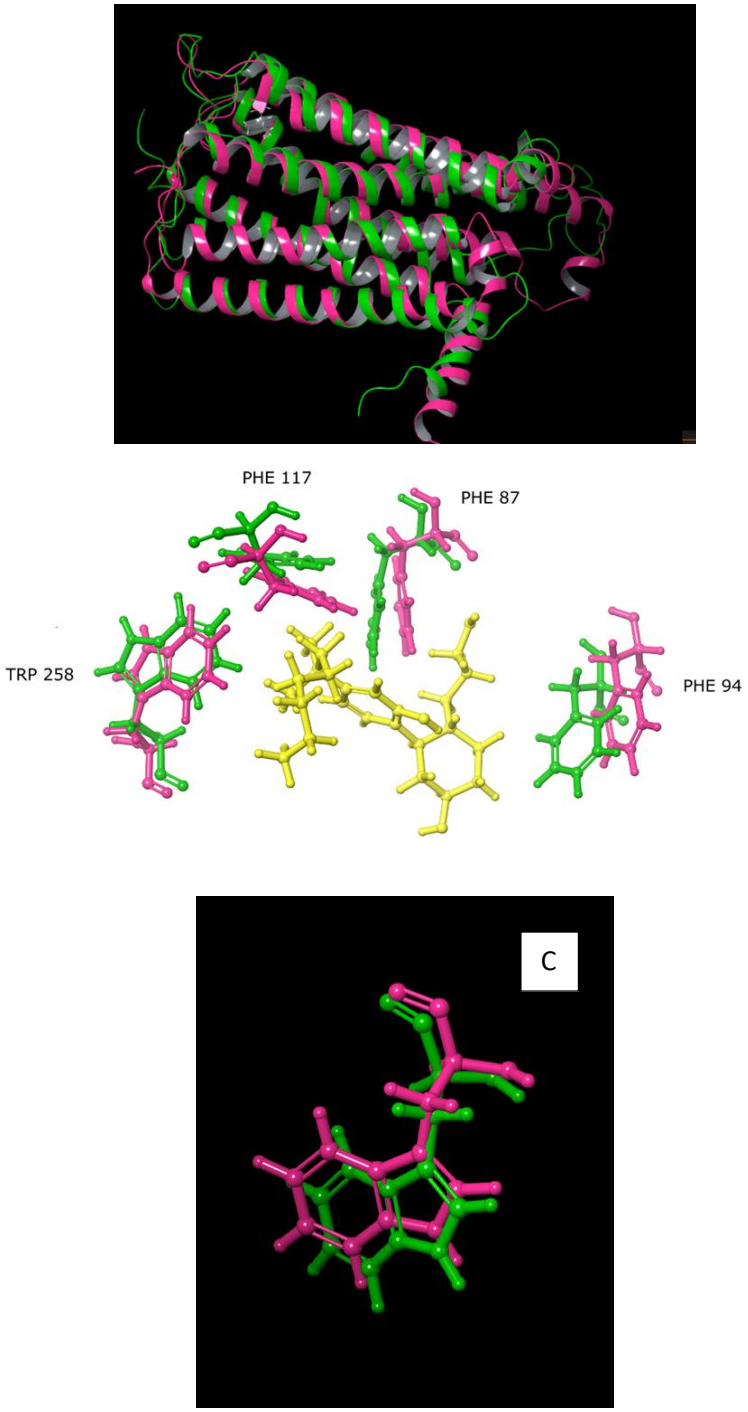


**Figure 36.** A.) protein structural alignment of post-modified $CB_2$ homology model (green) and $CB_2$ crystal structure (pink). B.) Up close view of key amino acids that make up the active site (green: post-modified homology model, pink: $CB_2$ crystal structure, yellow: WIN 55212). C.) The amino acid TRP 258 (green: post-modified homology model, pink: $CB_2$ crystal structure).

An enrichment study was done on 6PT0 using the DUD-E decoy database, which was done in order to compare to the $CB_2$ homology models (pre- and post-modified). The enrichment scores are shown in Table 7 and the percent screen plot is shown in Figure 37. The ROC and AUAC scores were similar between all models, however the BEDROC and RIE scores are higher in the post-modified homology model. In analyzing the percent screen plot, at 10% screened, the pre-modified homology model found approximately 20% actives, the post-modified homology model found approximately 35% actives and the crystal structure found less than 10%. However, at 20% and 30% screened, both the post-modified homology model and crystal structure found approximately the same percent of actives. At 40% screen and higher is when the crystal structure found a higher percent of actives than the post-modified homology model. Based on these results, the modified $CB_2$ homology model is a better predictor than the actual cyro-EM structure of $CB_2$.

| | BEDROC 1 | BEDROC 2 | BEDROC 3 | ROC | RIE | AUAC |
|---|---|---|---|---|---|---|
| 6PT0 | 0.198 | 0.124 | 0.275 | 0.74 | 2.05 | 0.74 |
| Pre-Modified $CB_2$ homology | 0.037 | 0.121 | 0.258 | 0.71 | 2.01 | 0.71 |
| Post-Modified $CB_2$ homology | 0.294 | 0.321 | 0.432 | 0.74 | 5.32 | 0.73 |

**Table 7.** The enrichment scores for 6PT0 and $CB_2$ homology model (pre- and post-modified) using the DUD-E decoy database.

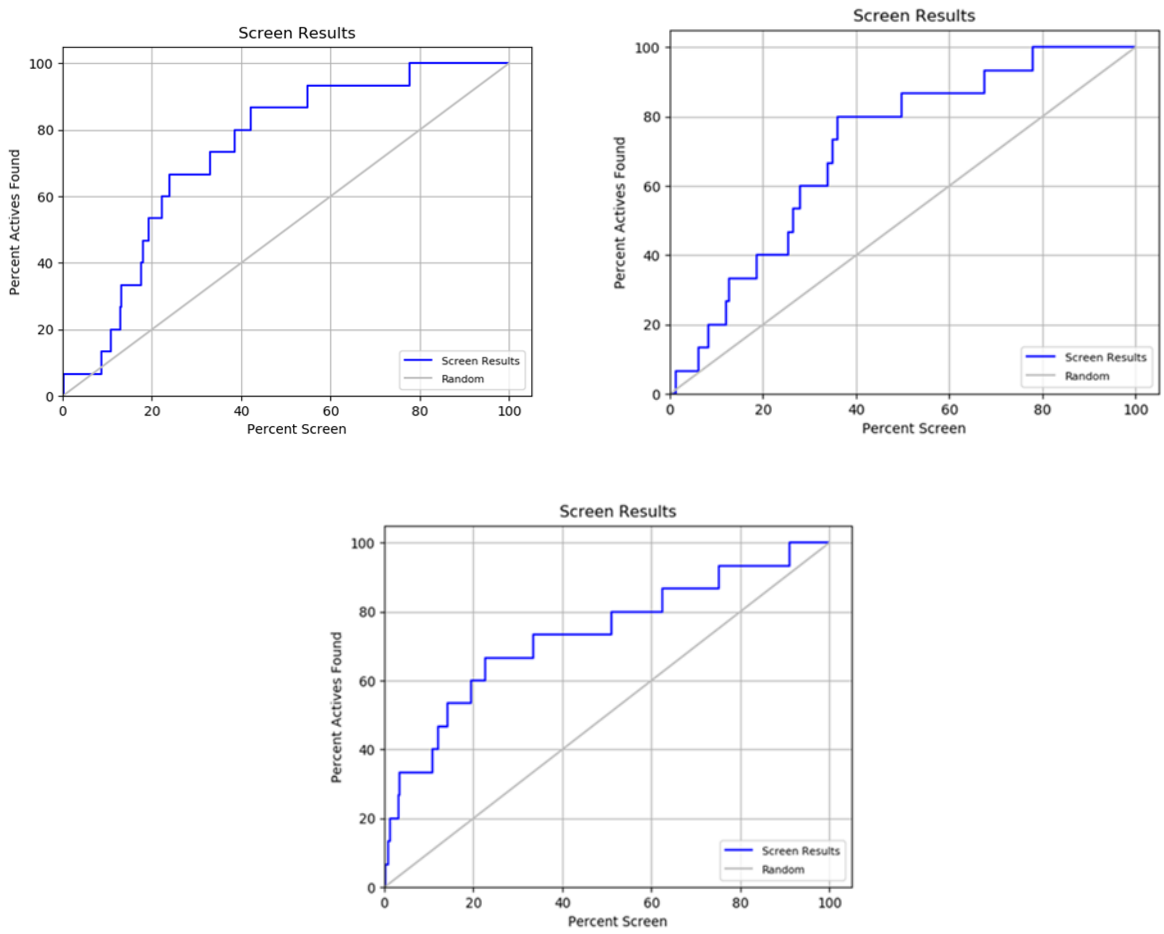


**Figure 37.** The percent screen plot of 6PT0 (top left), pre-modified $CB_2$ homology (top right) and post-modified $CB_2$ homology (bottom).

*3.1.9) Fragment Based Approach*

The next set of proposed compounds were designed utilizing the $CB_2$ crystal structure bound to WIN 55,212-2 (PDB ID: 6PT0) and a computational modeling technique known as fragment based drug design (FBDD). FBDD is a highly recognized and popular technique that uses fragments to design highly potent compounds [91]. Many drugs in clinical trials have been developed by this technique, including the FDA approved drug vemurafenib [92]. The fragments that are identified as top binders usually represent binding motifs as desirable starting points for

further optimization. The first step of FBDD is ligand docking of a database of fragments, followed by further optimization of linking the fragments together in order to design a potential drug candidate. In this study, the database of fragments that were used are from Schrodinger's website [93]. This database consisted of 667 unique fragments, which are derived from molecules found in the medicinal chemistry literature and have a molecular weight range from 32 to 226. This database of fragments was docked into 6PT0 using SP Glide ligand docking. Once the fragments were docked, the combine fragments tool was utilized in order to combine a set of pre-positioned fragments to each other. The parameters used were direct joining, meaning that the fragments were directly joined to each other or with an option to use one or two methylene linkers. The number of rounds was set to 3, which meant that multiple fragments were joined. Once the fragments had been combined, they were redocked into 6PT0. Figure 38, shows four compounds, **81-84**, that produced some of the highest docking scores ranging from -14.671 to -10.533. All these compounds have three main groups, starting with the central tricyclic core with two additional arms attached. One arm consists of a methylsulfonyl-piperadine substituent and the other arm is a xanthine derivative. The tool, core hopping, was used to modify the central ring and discover the additional pi bonding interaction. In order to make the compound synthetically tractable but still maintain the pi-pi interactions, the tricyclic core will be converted into a diphenyl ether. The target compound, **85**, that was designed is shown in Figure 39. However, instead of synthesizing the complete compound initially, it would be of value to synthesize this compound in fragments and then send the fragments for evaluation of binding at $CB_2$. Then further optimization can be done to the compounds based upon the biological results. The four fragments, **86-89**, that will be synthesized based upon the target compound **85**, are shown in Figure 40.

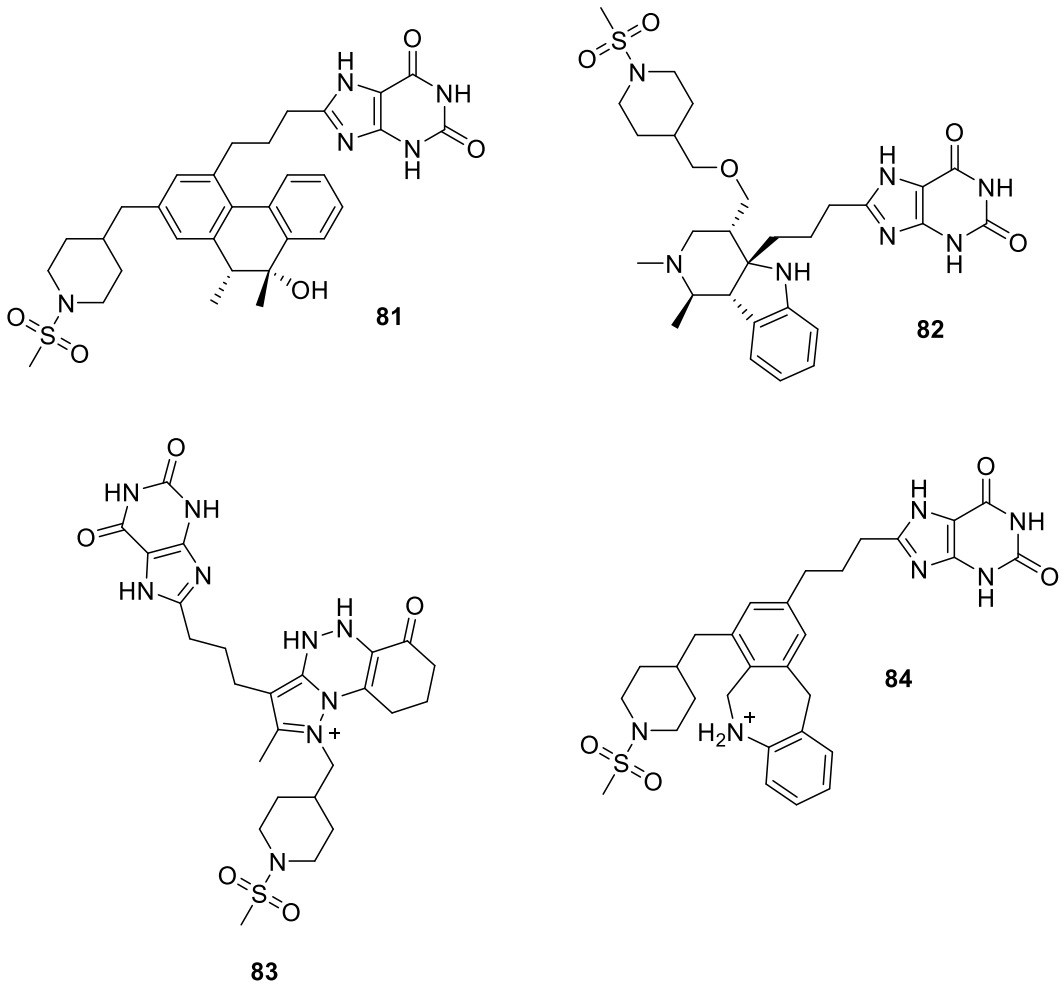


**Figure 38.** The top four compounds produced from fragment-based design.

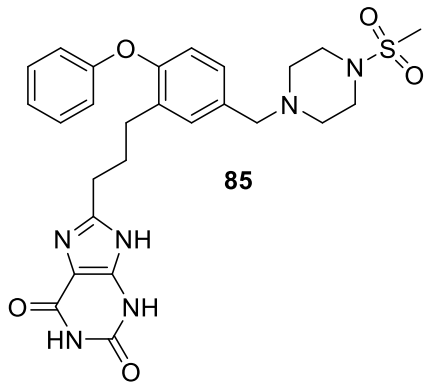


**Figure 39.** The target compound, **85**.

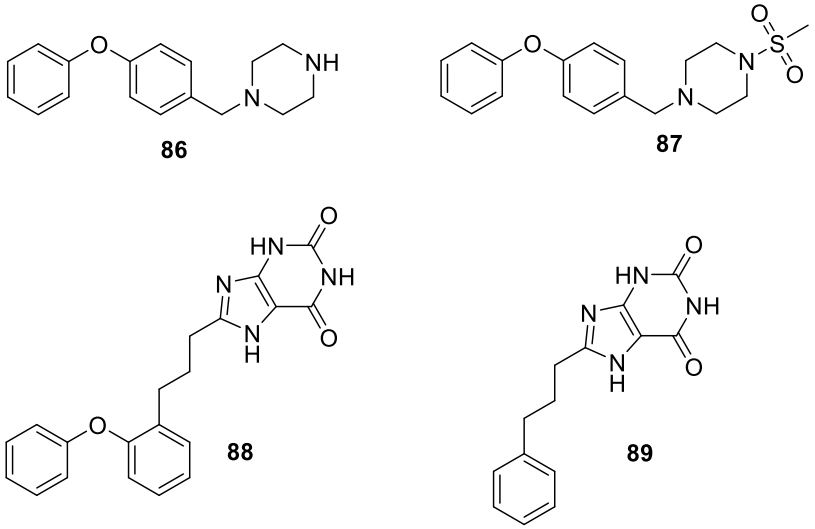


**Figure 40.** The four fragments based on target compound **85**.

In conclusion, a combination of molecular modeling tools was used to design and validate a $CB_2$ homology model based off of the $CB_1$ agonist crystal structure. Two minor modifications were done in order to improve the accuracy of the homology model. These modifications include the shifting of two amino acids in order to correctly orient the amino acid PHE 197 and patching of the disulfide bond CYS 174-CYS179. This modified model in combination of JWH-018 was used in order to develop potential $CB_2$ selective agonist

aminoalkylindole compounds, **77-80**. However, during this study the cryo-EM agonist structure of $CB_2$ was published. The modified homology model was compared to the published cryo-EM structure and the enrichment results indicate that the modified homology model is a better predictor than the actual cryo-EM structure of $CB_2$. In combination with the modified homology model, cryo-EM structure, fragment-based design and core hopping, the target compound **85** was developed. Instead of synthesizing the entire compound**,** it was thought of to synthesize the fragments of compound **85** and receive biological binding information on the fragments. This will determine which group or groups are responsible for binding.

## 3.2 Experimental

All computational modeling methods were carried out using Schrödinger Release 2017-4 to 2020-4.

### *3.2.1 Homology Modeling*

The human $CB_2$ amino acid sequence was downloaded from Uniprot (http://www.uniprot.org). The BLAST search utilizing the NCBI BLAST server was used in order to identify templates with the highest sequence identity. Based on the sequence similarity and crystal structure resolution, the crystal structures of human $CB_1$ receptor 5XR8 (resolution, 2.94 A; cocrystallized ligand, AM841, active conformation), human Beta 2-adrenergic receptor 2RH1 (resolution, 2.40 A; cocrystallized ligand, carazolol, inactive conformation) and human Beta 2-adrenergic receptor 3SN6 (resolution, 3.20 A; active conformation) were downloaded from Protein Data Bank and utilized as templates for the homology model generation. An alignment method using CLUSTAL W was used, followed by a knowledge based model building method.

### *3.2.2 Receptor Grid Generation*

The following amino acids were selected as the active site: F94, S285, W194, V164 and W258. There were not any constraints set. The box size was set for 20 angstroms around the selected residues.

### *3.2.3 Induced Fit Docking*

The protocol was set to standard and the force field was set as OPLS3e. There were not any specific constraints set. The conformational sampling of the ligands was set for an energy window of 2.5 kcal/mol. The glide docking was set for cut off values of 0.5 receptor van der Waals scaling and 0.5 ligand van der Waals scaling. The prime refinement was set to refine

residues within 5.0 angstroms of ligand poses and to optimize the side chains. The glide redocking was set to redock into structures within 30.0 kcal/mol of the best structure and within the top 20 structures overall utilizing standard protocol precision.

### *3.2.4 Molecular Dynamics*

The System Builder tool was used to create the lipid membrane environment around the CB2 homology model/ligand complex. The membrane model was POPC (300K) and the solvent model used was SPC. An addition of 12 sodium ions were added in order to neutralize the model. The model system ensemble class was set for NPT with a temperature of 300 K and a pressure bar of 1.01325. The model was relaxed before simulation and the simulation was set for 100 ns.

### *3.2.5 Desmond Trajectory Clustering*

The backbone of the protein was used for the RMSD calculation. The RMSD was calculated at every $10^{th}$ frame.

### *3.2.6 Glide Ligand Docking*

The standard precision docking was used. The ligand sampling was set to flexible and to sample nitrogen inversions and ring conformations. Epik state penalties were added to docking scores. There were not any specific constraints set. The performance of post-docking minimization was done with a number of poses per ligand set to five.

### *3.2.7 Enrichment Calculator*

The specific 15 active compounds were imported to designate actives versus decoy compounds. The number of decoys was set to 750.

### *3.2.8 Protein Structure Alignment*

The reference residues to align was set to all.

### *3.2.9 Fragment Based Design*

The combine fragments task was utilized and was set to a joining method of direct with a number of three rounds. Before joining, van der Waals clashes were checked. The attachment bonds were set to all hydrogen and halogens. A minimization was done on all atoms plus all hydrogen and halogen atoms. The maximum output was set for 100 structures. The filtering options were set as a minimum fragment centroid distance of 2, maximum bond angle deviation of 15 degrees, maximum atom-atom distance of 1 angstrom and a maximum number of fragment atoms of 200.

## Chapter Four: Synthesis of potential $CB_2$ Selective Agonists for Therapeutic Usage

### 4.1) Synthesis of substituted indoles based upon $CB_2$ homology model

#### 4.1.1) Results and Discussion

In the previous section, four target compounds were designed using molecular modeling of the $CB_2$ homology model. The four substituted amino alkyl indoles to be synthesized are shown in Figure 41. Compounds **77** and **78** are the saturated methyl ester and amide compounds, respectively. Compounds **79** and **80** are the unsaturated methyl ester and amide compounds respectively.

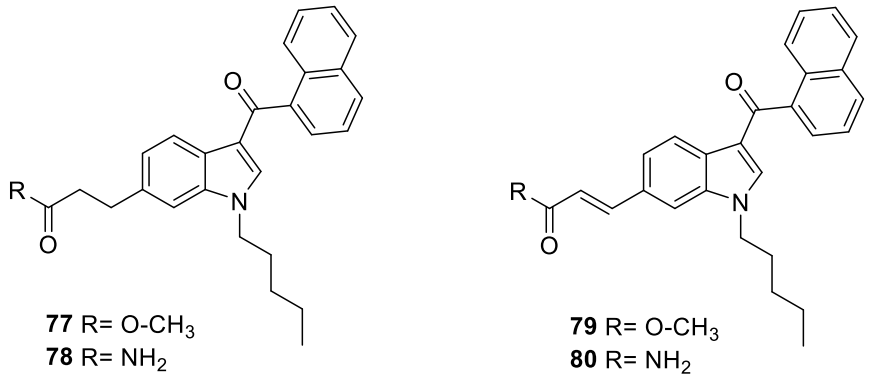


**Figure 41.** The four target compounds (**77-80**) based off the $CB_2$ homology model.

The retrosynthetic plan for the target compounds **77-80** is shown in Scheme 9. Compounds **77** and **78** will be derived from Compounds **79** and **80**, respectively, by a selective hydrogenation of the alkene in the presence of the carbonyls. Compounds **79** and **80** will be synthesized from the aryl halide **90** via a Heck coupling reaction. The aryl halide **90** will be synthesized from the pentylated bromo-indole **91** utilizing a Friedel-Crafts acylation in order to attach the 1-naphthoyl substituent to the 3-position of the indole ring. The pentylated bromo-indole **91** will be derived from 6-bromoindole, **92**, by a simple N-alkylation reaction. The 6-bromo-indole, **92**, will be synthesized from the brominated benzene **93** by a Leimgruber Batcho

indole synthesis. The brominated benzene **93** will be synthesized from the nitroaniline **94** by a Sandmeyer reaction.

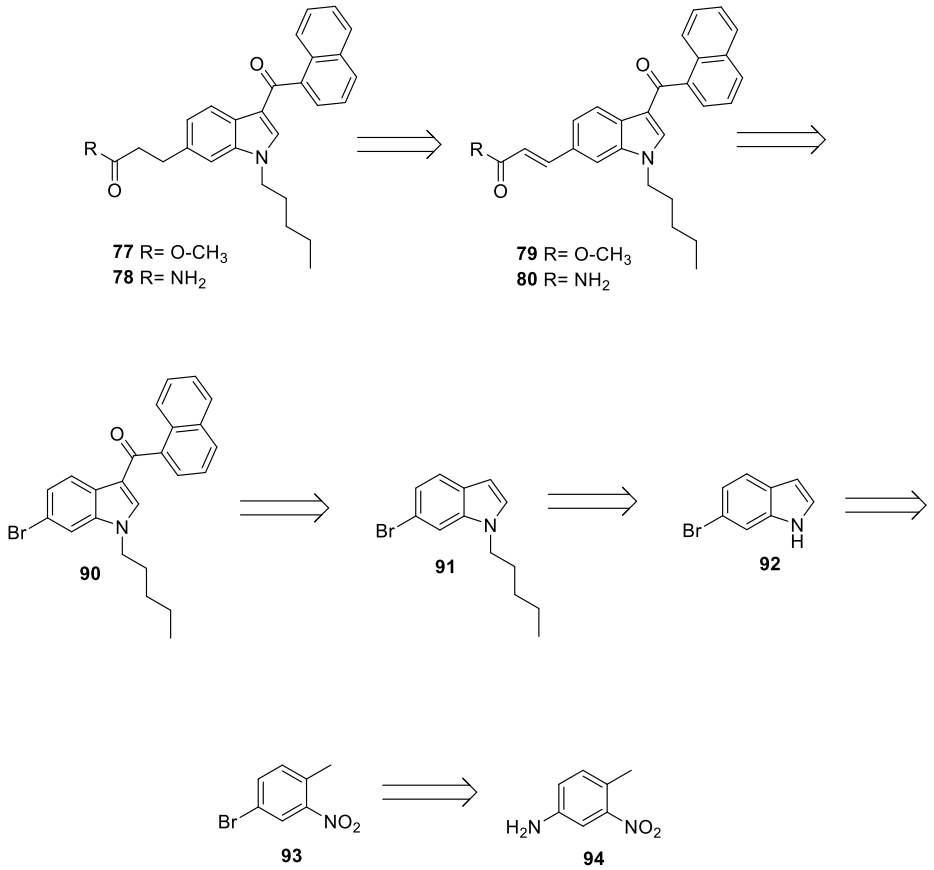


**Scheme 9.** The retrosynthetic plan for target compounds **77**-**80**.

The Sandmeyer reaction was used to convert the nitroaniline **94** to the brominated benzene **93** which is shown in Scheme 10. The Sandmeyer reaction is a versatile reaction involving the aniline that is then converted to a diazonium salt, which then follows a displacement reaction that can result in several different functional groups [94]. The first step of the Sandmeyer reaction was to dissolve 4-methyl-3-nitroaniline, **94**, in water and 48 % aqueous hydrobromic acid [95]. This yielded a dark orange solution that was then cooled to 0°C followed by the addition of sodium nitrite in water. This step resulted in the yellow-brown solution indicating

the formation of the diazo intermediate. The next step was to add the diazo intermediate to a mixture of copper bromide, 48% aqueous hydrobromic acid and water at a temperature of 90°C. After the work up and recrystallization in hot methanol, this yielded 4-bromo-2-nitrotoluene, **93**, as yellow crystals in 89% yield.

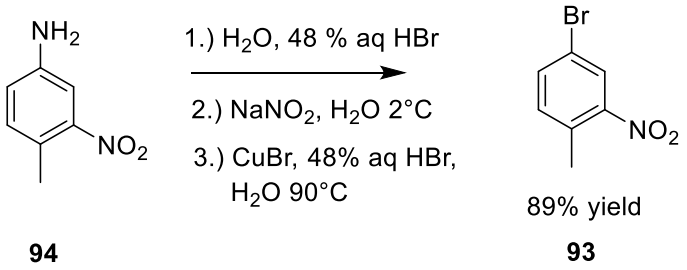


**Scheme 10.** The Sandmeyer reaction converting **94** to **93**.

The next step is the conversion of 4-bromo-2-nitrotoluene, **93**, to 6-bromo-indole, **92**. This reaction was done by using a variation of the Leimgruber Batcho indole synthesis, which is shown in Scheme 11 [96]. The first step was to dissolve 4-bromo-2-nitrotoluene (**93**), dimethyl formamide dimethyl acetal and pyrrolidine in DMF and heat at 110°C for two hours, which yielded the enamine **95**. Upon cooling to 0°C, 4M ammonium acetate, DMF and 15% titanium (III) chloride in 10% hydrochloric acid was added. This solution mixed for 15 minutes and the resulting grey solution was brought to a pH of 9 by utilizing sodium hydroxide. This reaction yielded 6-bromo-indole, **92**. The reaction did not go to completion and the side product, 5-bromo-2-methyl-benzenamine, **96**, was observed. However, dissolving the mixture of **92** and **96** in ethyl acetate and washing with 1 M hydrochloric acid (HCl) three times resulted in a pure solution of 6-bromo-indole, **92**. Upon removal of solvent, **92** was obtained as light brown crystals in 65% yield.

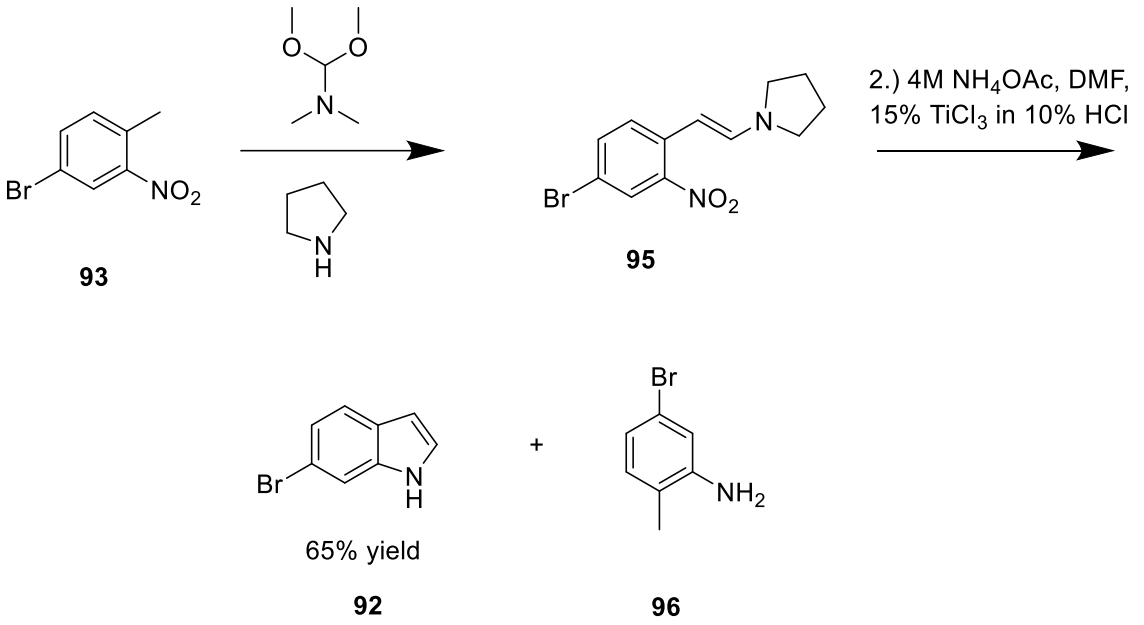


**Scheme 11.** The Leimgruber Batcho indole synthesis of **93** to **92** and side product **96** was observed.

The next step was the alkylation of the nitrogen in the indole ring, which is shown in Scheme 12. 6-Bromo-indole, **92**, was dissolved in a solution of potassium hydroxide/DMF and stirred for 30 minutes. 1-Bromopentane was added and the mixture was stirred for an additional two hours. Upon work up, 1-N-pentyl-6-bromo-indole, **91**, was obtained as a brown oil in 92% yield.

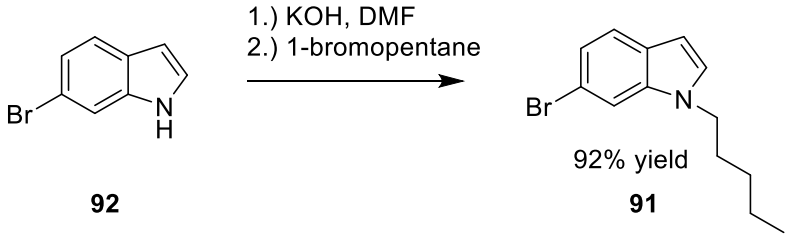


**Scheme 12.** The N-alkylation of **92** to yield **91**.

1-Naphthoyl chloride, **98**, is needed in order to complete the next reaction. The synthesis of the acid chloride **98** is shown in Scheme 13. 1-Naphthoic acid, **97**, was dissolved in benzene, and a couple drops of DMF were added as a catalyst along with thionyl chloride [97]. This solution was refluxed for five hours and the evaporation of the solvent yielded the acid chloride **98** as a yellow oily material.

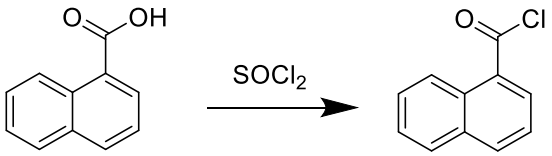


**97** **98**

**Scheme 13.** The synthesis of acid chloride **98**.

The next reaction was the conversion of the pentylated bromo indole **91** to the aryl halide **90** by a known Friedel-Crafts acylation that is shown in Scheme 14. In this case, the Friedel-Crafts acylation reaction involves the Lewis acid, dimethyl aluminum chloride, complexing with the acid chloride **98**, in order to activate it [98]. The chloride from **98** departs and results in a stabilized carbocation, which is referred to as the acylium ion. The electrophile, acylium ion, will react with the most reactive position on the indole ring towards electrophilic substitution which is the carbon at the 3-postion of the indole ring. This resulted in the monoacylated product **90** in 87% yield.

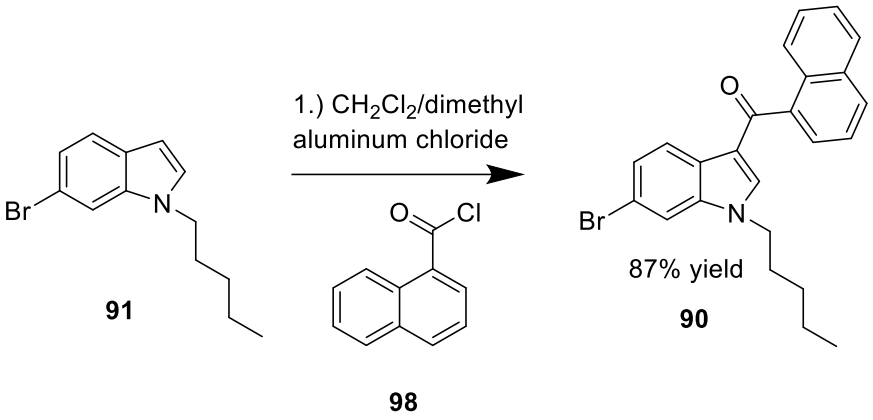


**Scheme 14.** The Friedel-Crafts acylation to yield **90**.

Once this step had been reached, it was determined that the intermediates of the aryl bromide should be synthesized so that structure activity relationships studies could be done. It would be of value to study the relationship between the substituents and the corresponding binding values in order to determine which substituents are responsible for binding. Figure 42 shows the four aryl bromide intermediates (**92**, **91**, **90** and **99**) and the synthetic plan to synthesize the 16 compounds. The synthesis of intermediates **90**, **91** and **92** have been shown previously, but the synthesis of intermediate **99** is shown in Scheme 15. The synthesis utilizes the same Friedel-Crafts acylation protocol that was seen in Scheme 14, but with 6-bromo-indole, **92**, as the starting material. The recrystallization in pure ethyl acetate yielded the final product **99** as crystals in 71% yield.

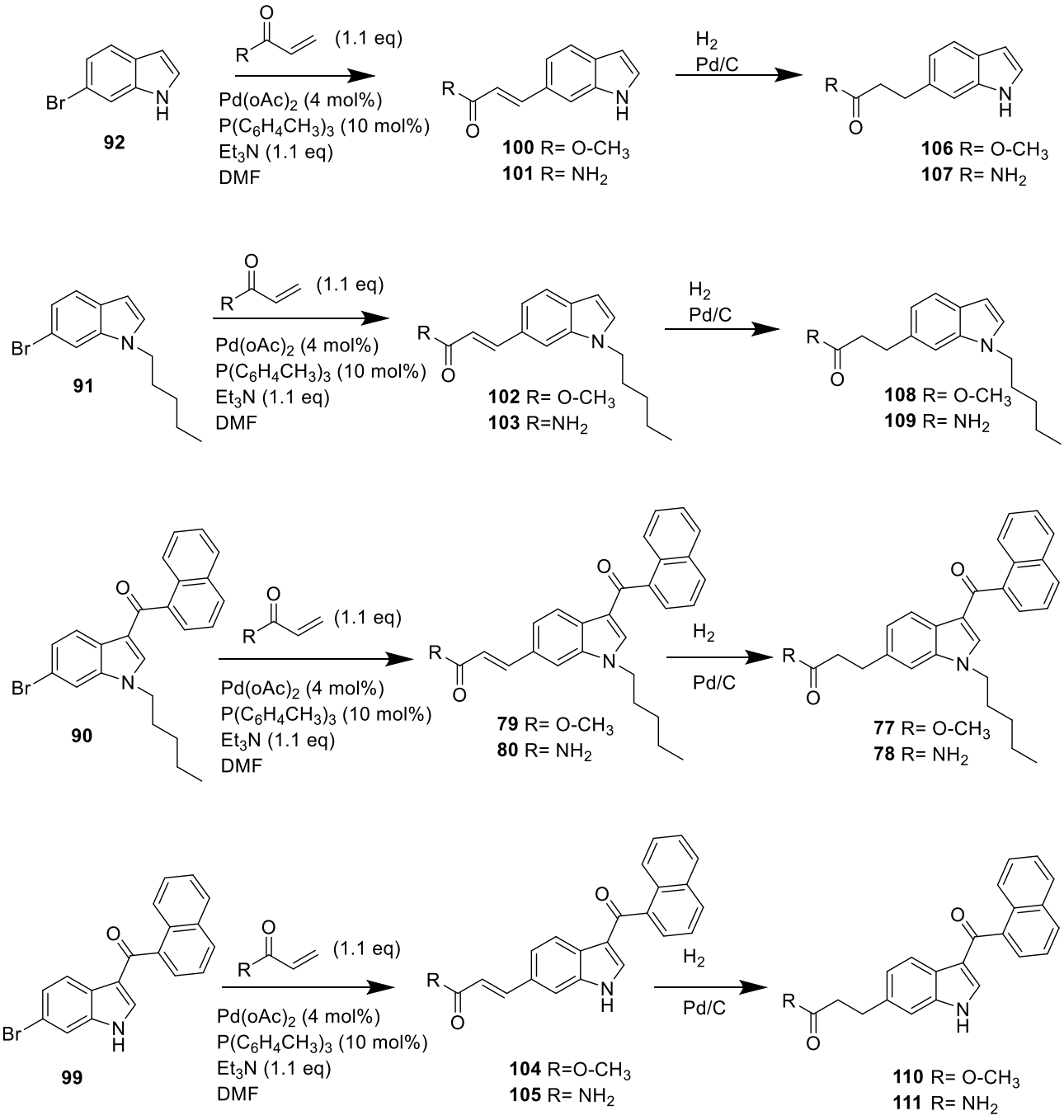


**Figure 42.** The four aryl bromide intermediates and the synthetic plan for 16 compounds.

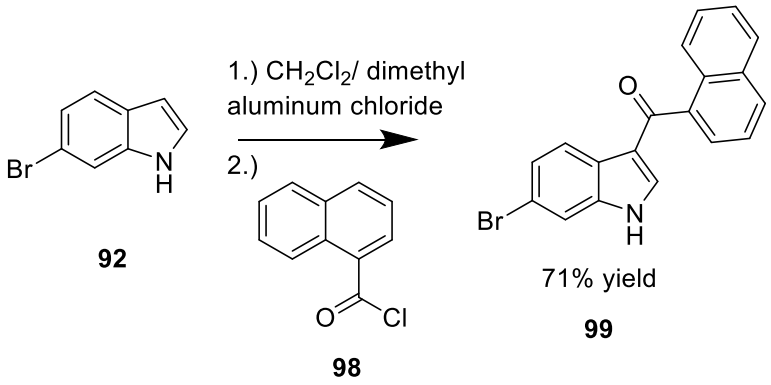


**Scheme 15.** The synthesis of intermediate **99** utilizing the Friedel-Crafts acylation reaction.

Once all the aryl bromide intermediates were synthesized, the next step was the Heck coupling reaction. Mizoroki and Heck established the Heck reaction in 1972, which utilizes a palladium catalyst in order to couple aryl halides and alkenes in the presence of base to yield a trans selective alkene [99]. Scheme 16 illustrates the first attempt of the Heck coupling reaction utilizing the aryl halide **90**, acrylamide, palladium (II) acetate, tris(o-tolyl) phosphine, triethylamine and deoxygenated dimethylformamide [100]. These reagents were added to a dried glass bomb under nitrogen and heated to reflux for approximately 12 hours. After 12 hours, this reaction was monitored by thin layer chromatography (TLC) and the starting material was still present with no additional spots related to the product. There was not any additional evidence of product by GC/MS or by NMR.

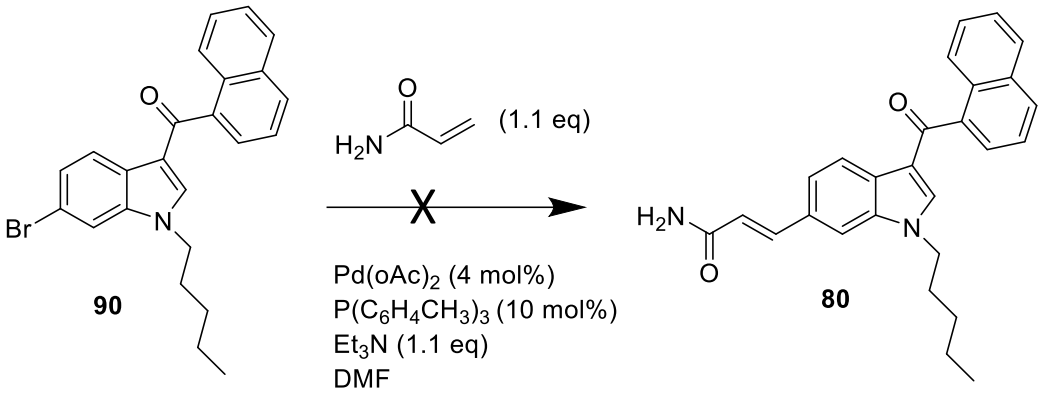


**Scheme 16.** The failed attempt of converting **90** to **80** by the Heck reaction.

While still investigating the Heck Reaction, another synthetic strategy for the synthesis of the target compounds was proposed and shown in Scheme 17. The synthetic strategy consisted of protecting the carbonyl of **90** by utilizing ethylene glycol under a catalytic amount of p-toluenesulfonic acid (TsOH) [101]. Once the acetal had formed, it was then proposed to make a Grignard reagent by adding magnesium turnings to the acetal **112**. Then a Grignard reaction between the newly formed Grignard reagent and acrylamide with the presence of a catalytic amount of copper would produce **113**. The utilization of organocuprates should direct a 1,4 addition at the beta carbon of the alpha beta unsaturated compound [102]. This is due to the "hard" versus "soft" nature of the nucleophiles. The last step would be to deprotect the carbonyl using acidic conditions to yield the desired compound **80**. However, the conversion of the ketone of compound **90** to the acetal **112** failed. The aryl halide **90**, ethylene glycol, a catalytic amount of TsOH and benzene were added to a round bottom flask that was then attached to a Dean-Stark trap and a reflux condenser. The round bottom flask was heated to reflux temperature for two hours. Upon work up, the organic layer was evaluated by GC/MS, but the starting material was not present. There was a peak at 265 m/z was observed, however that was consistent with the

pentylated 6-bromo-indole, **91**, shown in Figure 43. It was hypothesized that the aryl halide **90** is not stable under acidic conditions when heated.

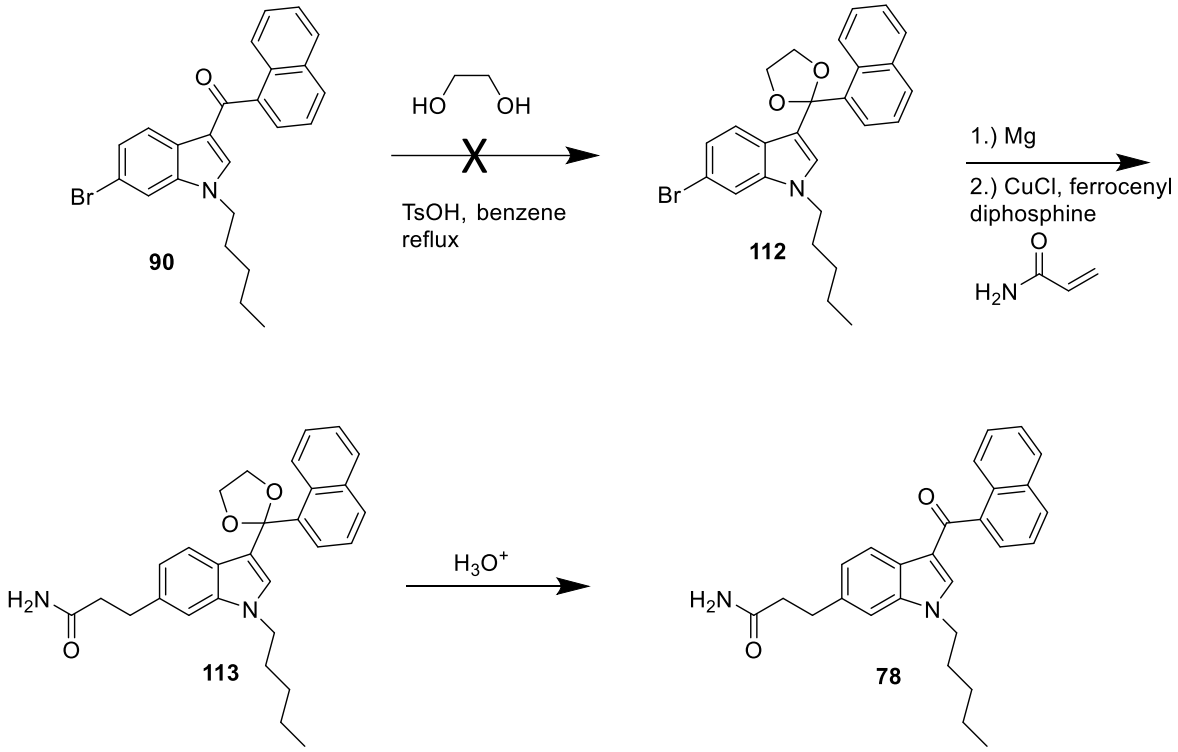


**Scheme 17.** The failed attempt of the ketal protection.

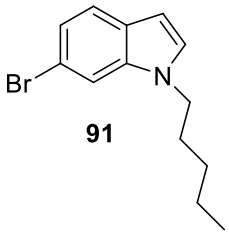


**Figure 43.** The pentylated-bromo-indole (**91**) consistent with m/z 265.

The Heck reaction was attempted again and is shown in Scheme 18. However, the starting material utilized was 6-bromoindole, **92**. The same reaction conditions that were

attempted previously in Scheme 16 were used. After one hour, a GC/MS analysis was done and the major peak was the starting material, but a minor peak of the desired methyl ester **100** had formed. This reaction ran overnight and another GC/MS analysis was done. The results were consistent with the day prior, the major peak being starting material and a minor peak of the desired product **100**, with no evidence that more product had formed.

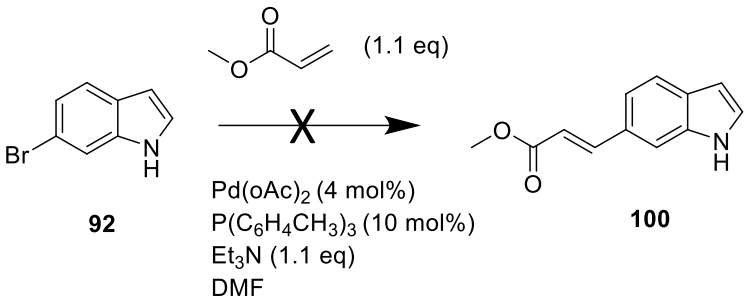


**Scheme 18.** The failed attempt of the Heck reaction to yield compound **100**.

Another alternative approach to synthesize the target compounds is shown in Scheme 19. The first step is the N-alkylation of the 6-carboxaldehyde indole, **114**, to yield the pentylated aldehyde **115** which proceeded in 88% yield. The next step was the generation of the dimethyl malonate anion utilizing piperidine in benzene, followed by the aldol reaction with the aldehyde **115** to yield the diester **116** in 98% yield [103]. The last step is the decarboxylation of the diester **116** to yield the desired product **102** utilizing sodium chloride, water and dimethyl sulfoxide (DMSO) [104]. This step failed and only the diester **116** was seen by GC/MS and by TLC. Another attempt at the decarboxylation of the diester **116** was done using an alternative method, which is shown in Scheme 20. This reaction utilized the diester **116** dissolved in DMSO with sodium

iodide and heated to 190°C. After six hours, this reaction was checked by GC/MS and the desired methyl ester **102** had formed, but there was remaining starting material **116**. This reaction was left over night in order to drive to completion, but it had completely converted back to the aldehyde **115**.

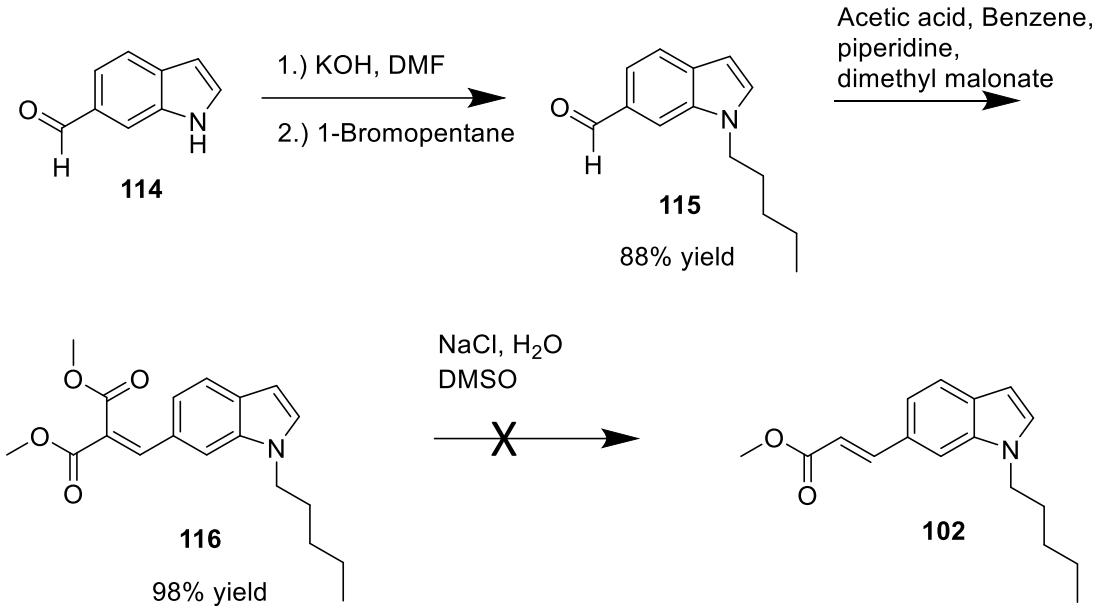


**Scheme 19.** The aldol reaction followed by a failed attempt of decarboxylation.

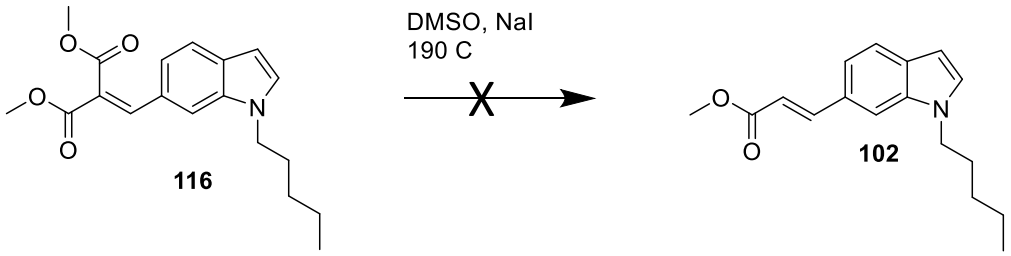


**Scheme 20.** The failed attempt of decarboxylation trial 2.

Another alternative approach in order to synthesize the target compounds is shown in Scheme 21. This approach involves the generation of the ethyl acetate anion so that the need for

a decarboxylation reaction would be avoided. Once the ethyl acetate anion is generated, it will be utilized in an aldol reaction with aldehyde **115** to yield desired product **120**. In order to generate the anion of ethyl acetate, hexamethyldisilazane (**117**) is slowly added to a solution of n-butyl lithium in hexane solvent at 0°C, which ideally will yield lithium bis-(trimethylsilyl)amide, **118** [105]. At a temperature of -78°C, **118** will then be reacted with ethyl acetate to yield the ethyl acetate anion, **119**. A solution of the aldehyde **115** in dry tetrahydrofuran (THF) is added dropwise to the enolate **119**. After 30 minutes, 20% aqueous HCl is used upon work up to yield **120**. However, when analyzing this reaction by GC/MS and TLC, there was not any evidence that desired product **120** had formed, instead only the starting aldehyde **115** was present.

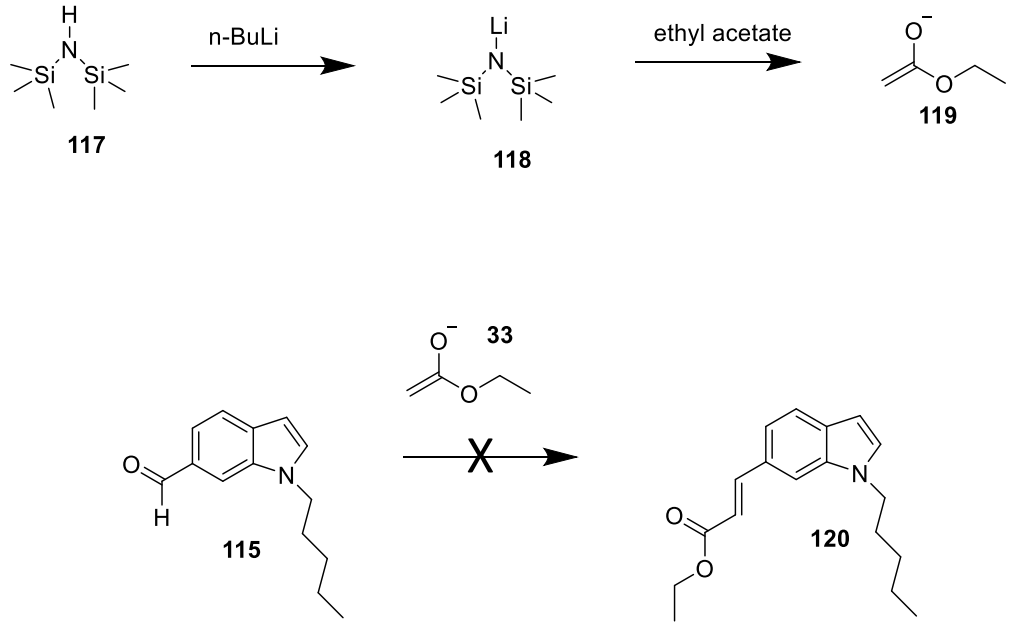


**Scheme 21.** The failed attempt of ethyl acetate anion generation.

The alternative approaches were unsuccessful, so the Heck reaction was reinvestigated, which is shown in Scheme 22. It is evident that the Heck reaction is sensitive to air and moisture, so it could be problematic that the solvent utilized previously, DMF, is hard to dry completely. The Heck reaction was tried again with the 6-bromoindole (**92**), methylacrylate (3 eq), palladium

(II) acetate (0.12 eq), tri(o-tolyl)phosphine (0.2 eq), trimethylamine (1.25 eq) but without DMF [106]. The addition of all reagents occurred in the nitrogen glove box and the reaction was stirred under nitrogen and heated at 120°C for 16 hours. The work up consisted of diluting the reaction in dichloromethane, filtering through celite, washing with water, drying over sodium sulfate and evaporation of the solvent. This yielded the crude material **100** in 76% yield. This suggests that the previous Heck reactions did not work due to the solvent, DMF.

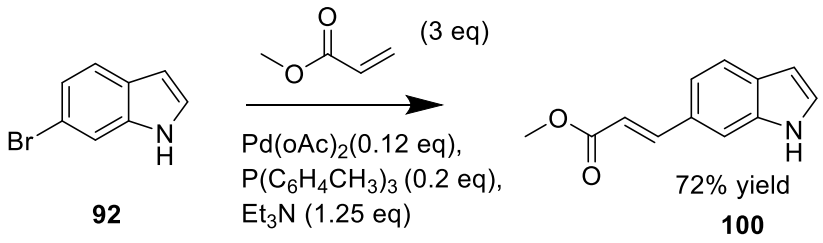


**Scheme 22.** The successful Heck reaction to yield desired product **100**.

Due to the success of the Heck reaction for the desired methyl ester **100** the other aryl bromide intermediates **91**, **99** and **90** were subjected to the Heck reaction using the same protocol. These reactions were successful and are shown in Scheme 23.

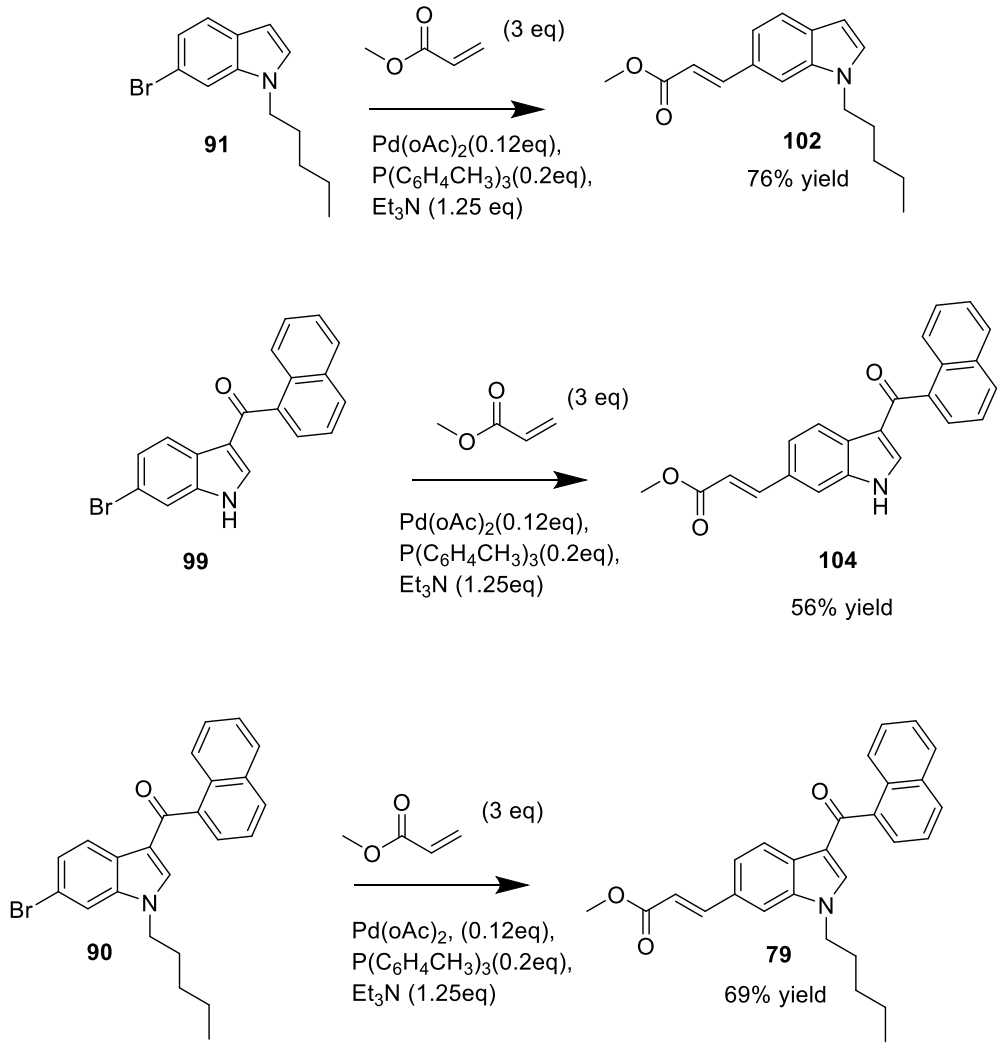


**Scheme 23.** The successful Heck reactions to yield the desired methyl esters.

The next step was the hydrogenation of the alkenes that were produced from the Heck reaction and is shown in Scheme 24. The protocol for the hydrogenation reaction involved dissolving the appropriate alkene in ethyl acetate, adding 10% palladium on carbon, degassing the system using nitrogen and setting up the reaction under hydrogen for 24 hours [107]. The analytical tools, GC/MS and NMR, evaluated the complete conversion to the alkane. For conversion of the alkene **100** to the alkane **106** the NMR data showed the disappearance of the two vinyl hydrogens (6.423 and 7.795 ppm) and the appearance of two aliphatic hydrogens

(2.697 and 3.068 ppm), which confirmed the completion of the reaction. For conversion of the alkene **102** to the alkane **108** the NMR data showed the disappearance of the two vinyl hydrogens (6.471 and 7.827 ppm) and the appearance of the two aliphatic hydrogen (2.681 and 3.048 ppm), which also confirmed the completion of the reaction. However, this protocol failed to convert alkene **79** to alkane **77**. It was hypothesized that this would be the case because **79** also contains a carbonyl that the other alkenes do not possess. When analyzing the reaction by NMR, the proton NMR confirmed that the alkene had been reduced, but the $^{13}C$ NMR also confirmed that the carbonyl peak (191.798 ppm) of the naphthoyl substituent had disappeared. An alternative approach using a selective hydrogenation protocol was explored in order to reduce the alkene intermediate selectively in the presence of the carbonyl.

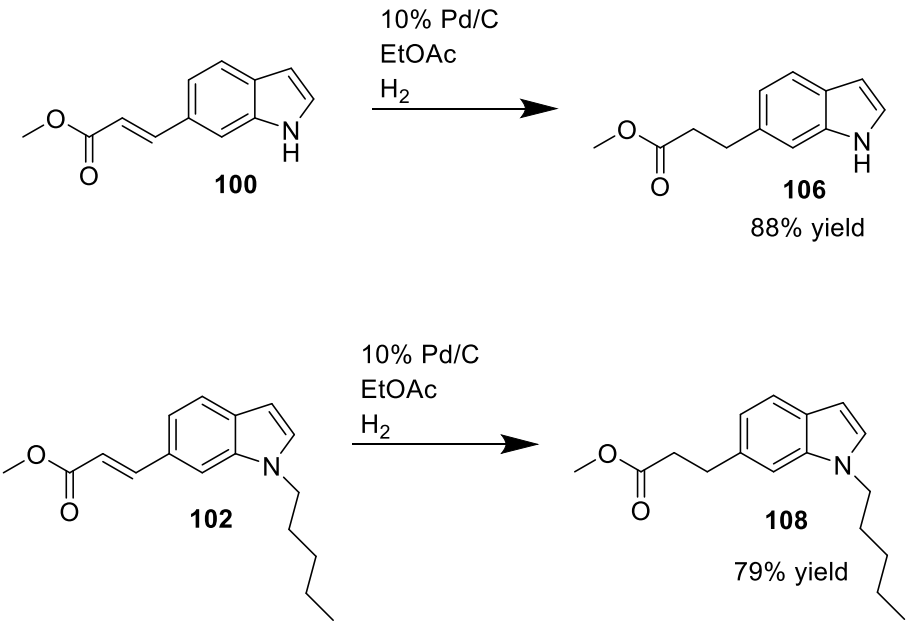

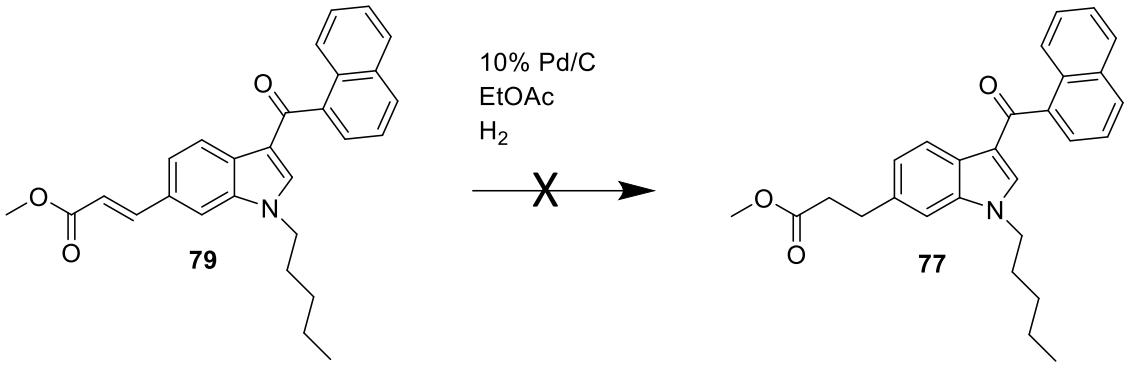


**Scheme 24.** The hydrogenation reactions to yield compounds **106** and **108**.

An alternative to palladium on carbon is Wilkinson's catalyst, which is also known as chloridotris(triphenylphosphine) rhodium(I) and is used in the selective hydrogenation of alkenes [108]. This catalyst was used in order to selectively hydrogenate the alkenes in **104** and **79**, which is shown in Scheme 25. The hydrogenation protocol consists of dissolving the appropriate alkene in 1:1 benzene: ethanol solvent, adding the Wilkinson's catalyst (3 mol %) under nitrogen, degassing the system, and setting up the reaction under hydrogen. After two days, the reaction had proceeded to completion. NMR was used to analyze the complete conversion of alkene **104** to alkane **110** and alkene **79** to alkane **77**. For **110**, the disappearance of the two vinyl hydrogens (6.548 and 7.712 ppm) and the appearance of the two aliphatic hydrogens (2.789 and 3.106 ppm) was confirmed. For **77**, the disappearance of the two vinyl hydrogens (6.536 and 7.640 ppm) and the appearance of the two aliphatic hydrogens (2.727 and 3.110 ppm) was also confirmed. In both cases, the $^{13}$C NMR was also analyzed to ensure that the carbonyl peak of the naphthoyl substituent was still present for both **110** and **77**.

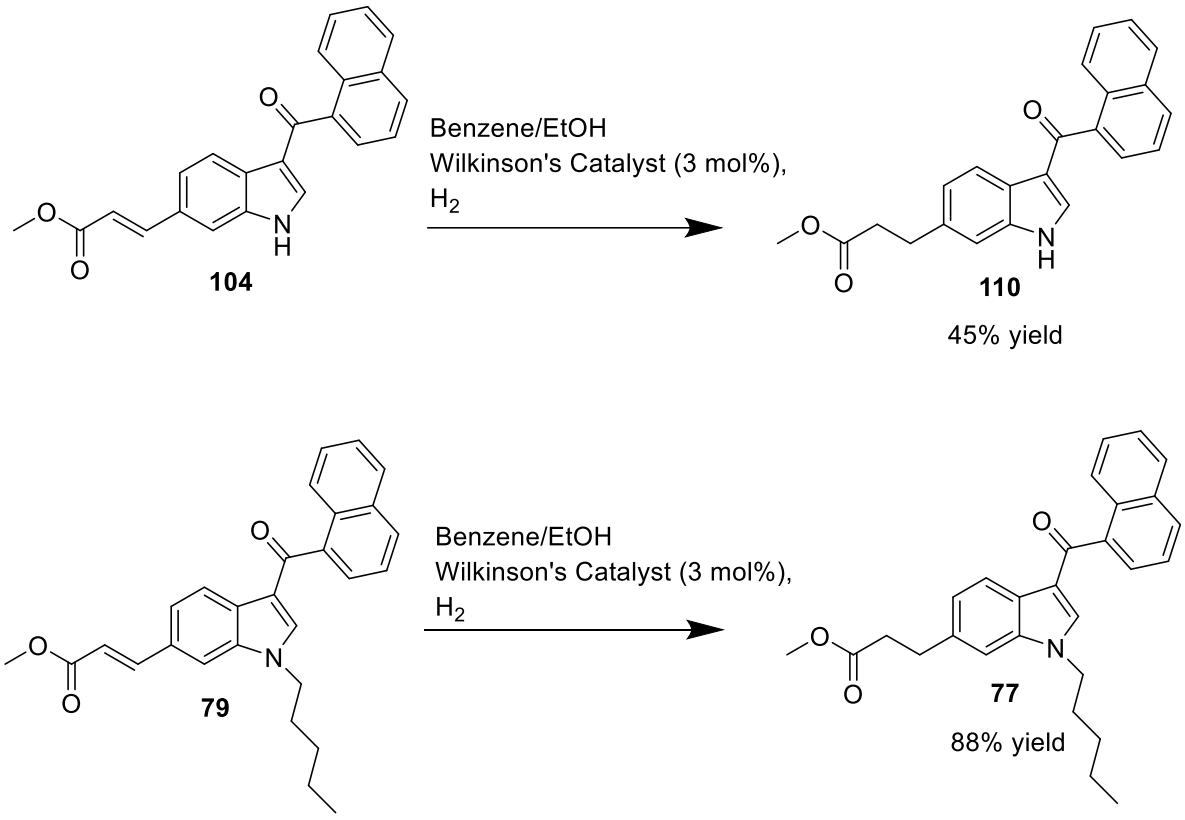


**Scheme 25.** A selective hydrogenation utilizing Wilkinson's catalyst.

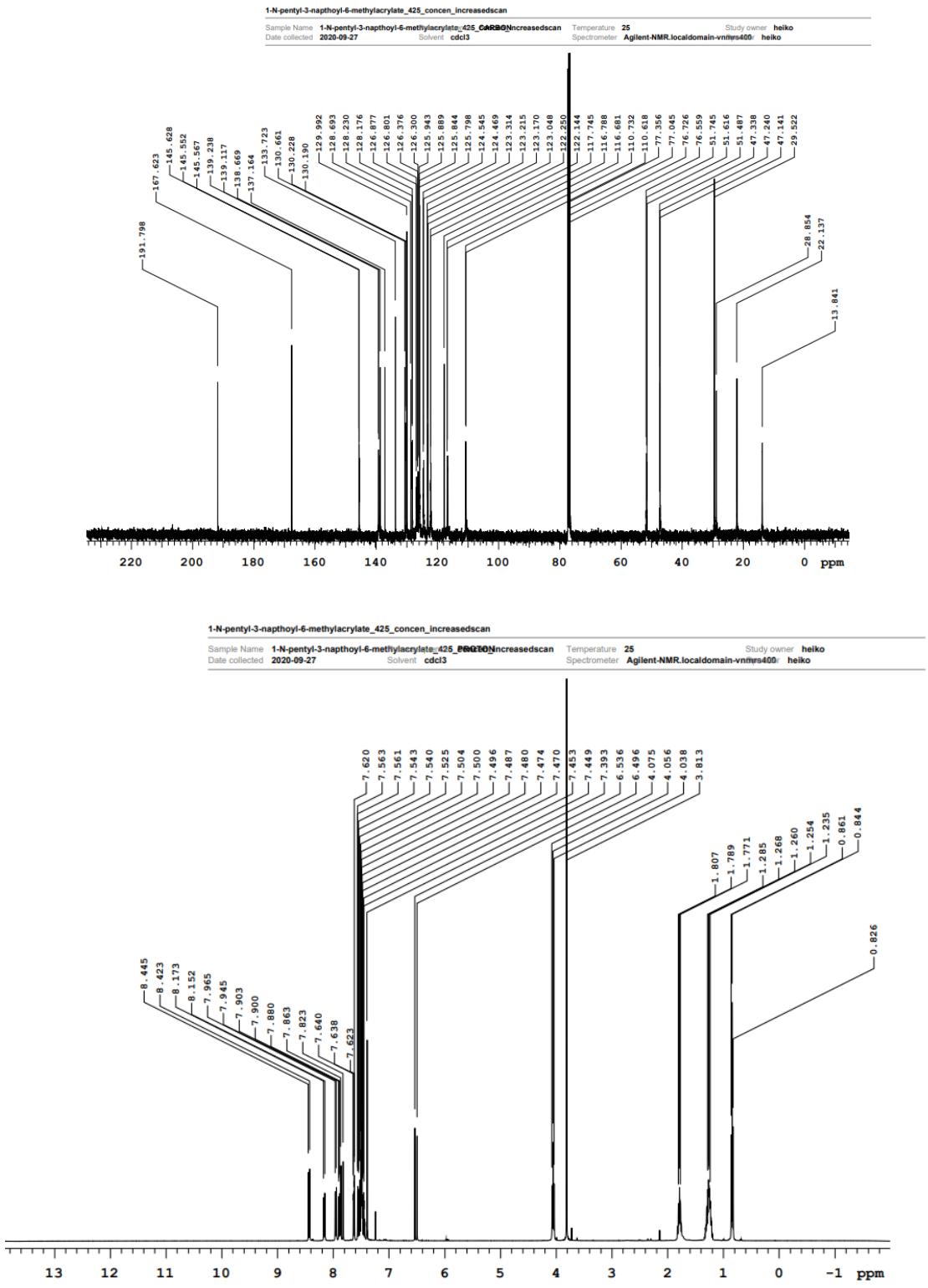


**Figure 44**. $^{1}H$ and $^{13}C$ NMR for compound **79**.

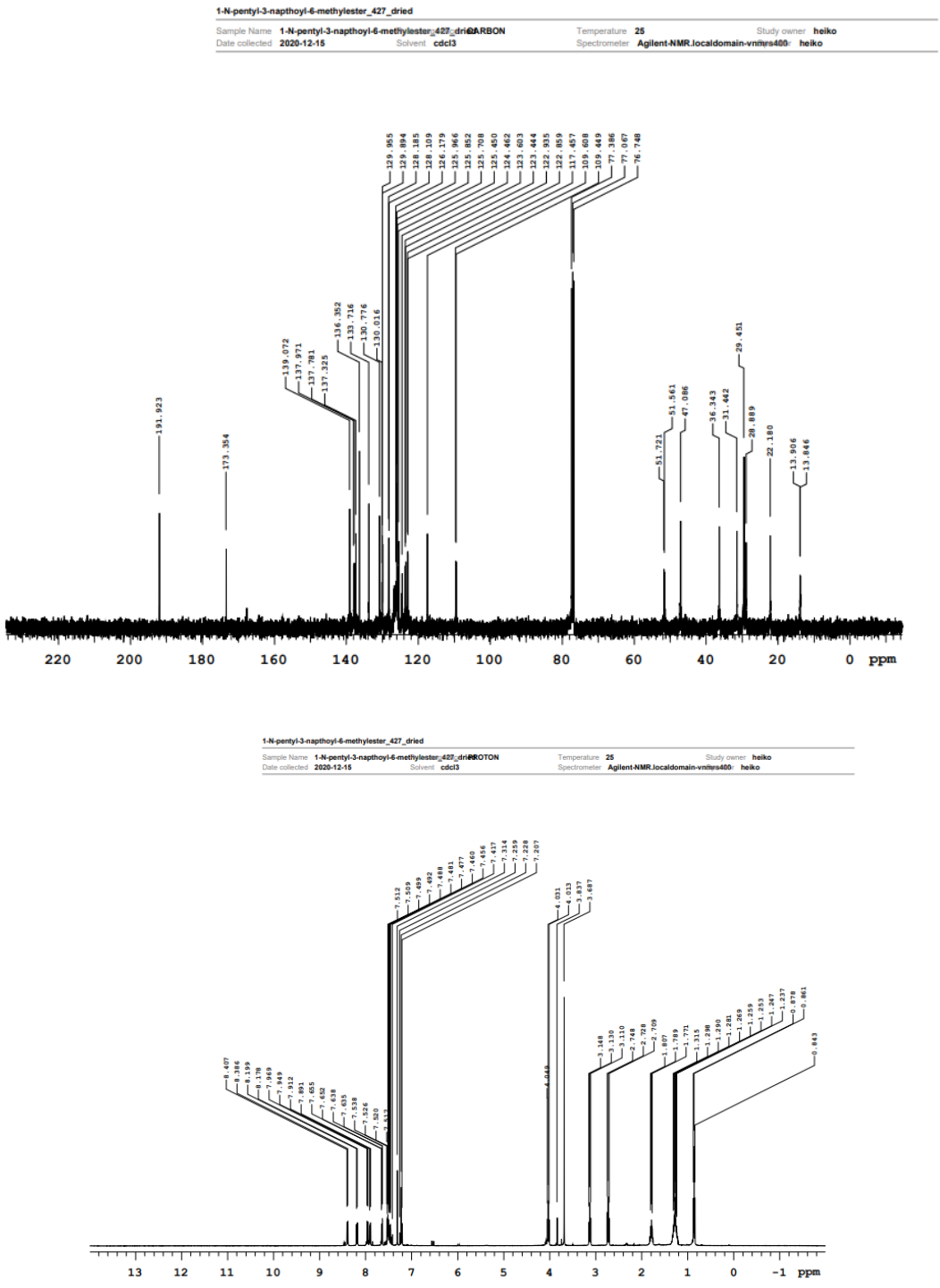


**Figure 45.** $^{1}H$ and $^{13}C$ NMR for compound **77**.

The Heck reaction utilizing the acrylamides were completed as shown in Scheme 26. The previous protocol for the methyl esters was used except for the addition of distilled acetonitrile.

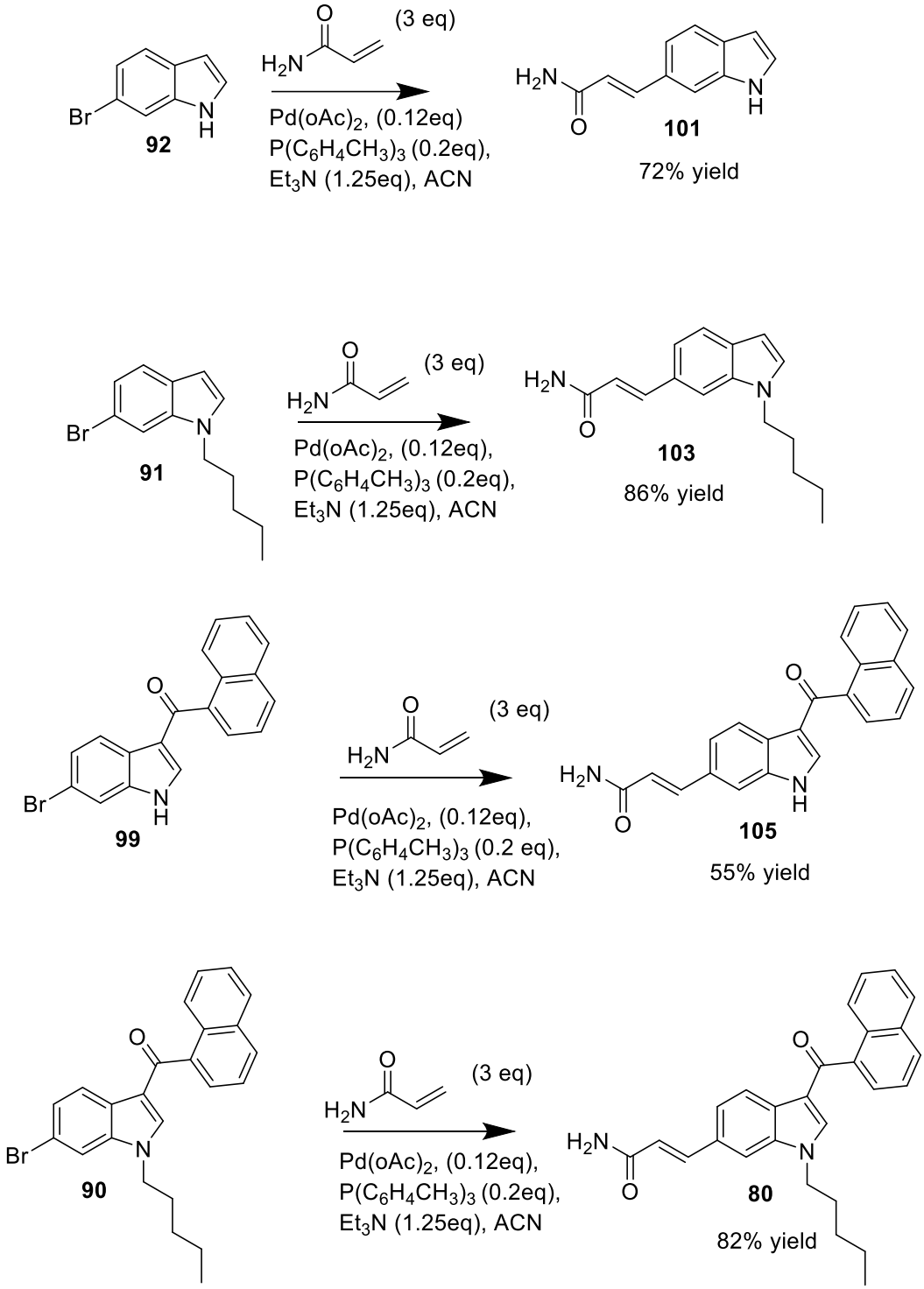


**Scheme 26.** The successful Heck reactions for the amides.

The hydrogenation reactions for conversion of alkene **101** to alkane **107** and alkene **103** to alkane **109** are shown in Scheme 27. These reactions were ran under the same protocol that was shown previously in Scheme 16. The use of Wilkinson's catalyst was not necessary since the carbonyl was not present. These reactions were completed successfully and evaluated by NMR. For the alkane **107** the two vinyl hydrogens (6.423 and 7.542 ppm) had disappeared and the two aliphatic hydrogens (2.339 and 2.837 ppm) were present. Also for alkane **109** the two vinyl hydrogens (6.472 and 7.777 ppm) had disappeared and the two aliphatic hydrogens (2.570 and 3.075 ppm) were present as well.

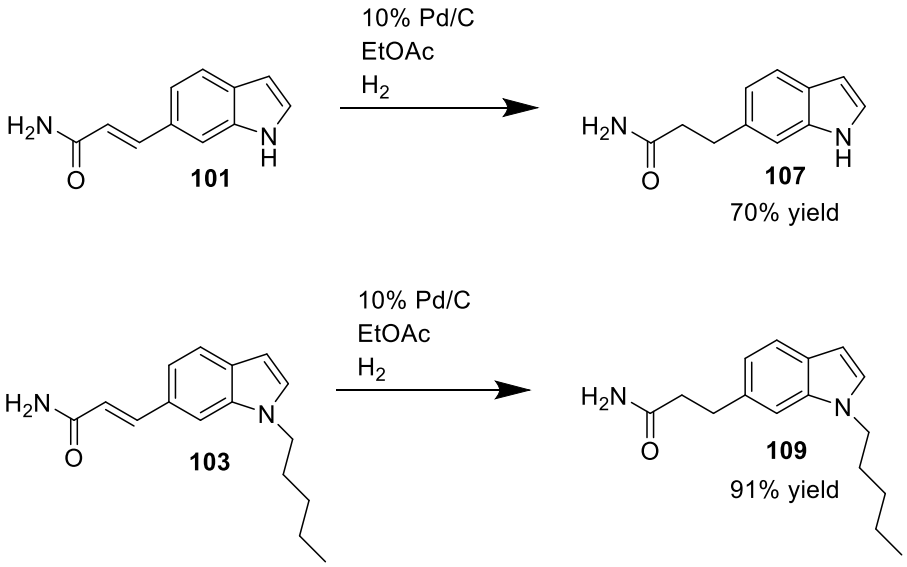


**Scheme 27.** The hydrogenation reactions to yield **107** and **109**.

As indicated before, a chemoselective reducing agents needs to be utilized when other reducible functionalities are present in the compound. In the previous examples, Wilkinson's catalyst had been utilized in order to selectively reduce the alkenes when the carbonyls are

present in the compounds. For alkenes **105** and **80**, Wilkinson's catalyst was utilized again (Scheme 28), but there was no reaction. When analyzing the reaction by NMR, only starting material remained. It is hypothesized that the catalyst had gone bad due to exposure with air. However, when exploring the literature, a more efficient selective hydrogenation approach was found. The use of sulfur-containing catalyst poisons have been studied as chemoselective reducing agents for alkenes when aromatic carbonyls and halogens, benzyl esters, and N-carboxybenzyl (N-Cbz) protective groups are present [109]. In this specific study, the sulfur containing catalyst poison that was used was diphenyl sulfide and this catalyst was used to selectively hydrogenate the alkenes in compounds **105** and **80**. In Scheme 29, the conversion of **105** to **111** and **80** to **78** utilizing diphenyl sulfide are shown. The protocol consists of dissolving the appropriate alkene in 9:1 methanol: ethanol solvent, the addition of 10% palladium on carbon and diphenyl sulfide (0.01eq) under nitrogen, degassing the system and setting up the reaction under 50 psi of hydrogen. After one day, the reaction was evaluated by NMR and found to be complete. By $^{1}$H NMR, the disappearance of the vinyl hydrogens and the appearance of aliphatic hydrogens occurred in both compounds. Also by $^{13}$C NMR, the presence of the carbonyl peak containing the naphthoyl substituent was still present in both compounds.

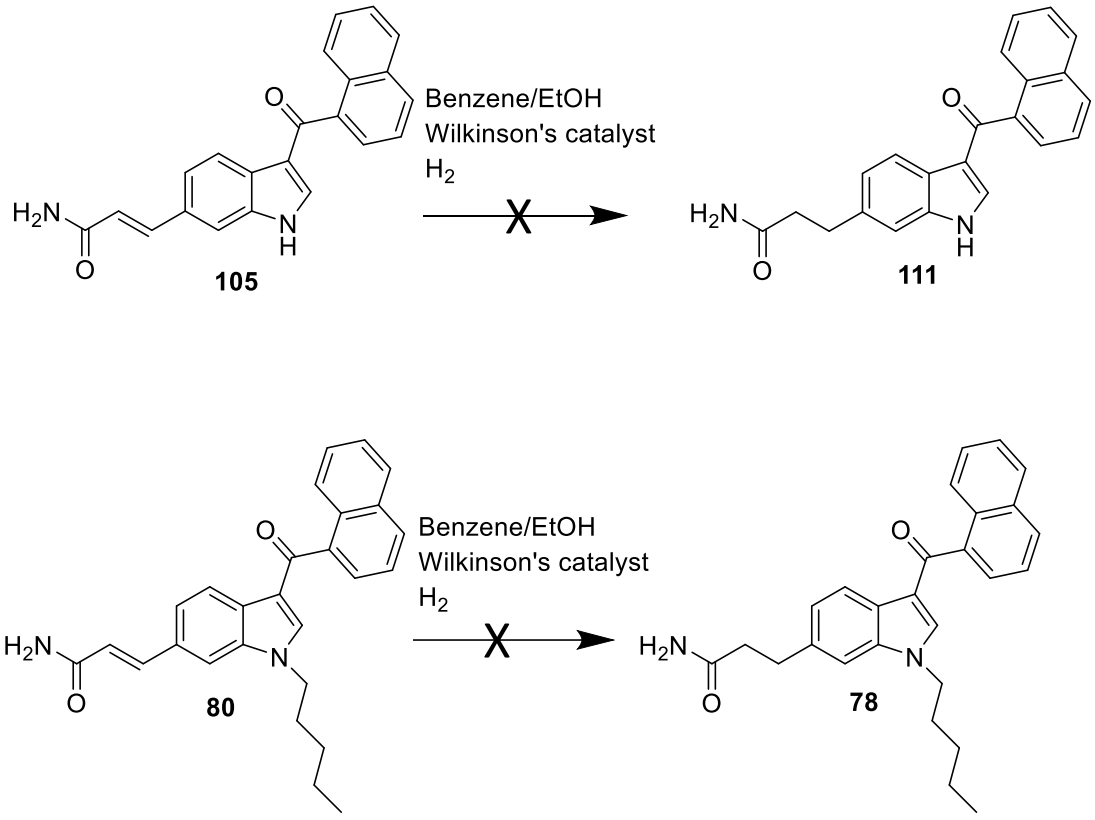


**Scheme 28.** The failed hydrogenation with Wilkinson's catalyst.

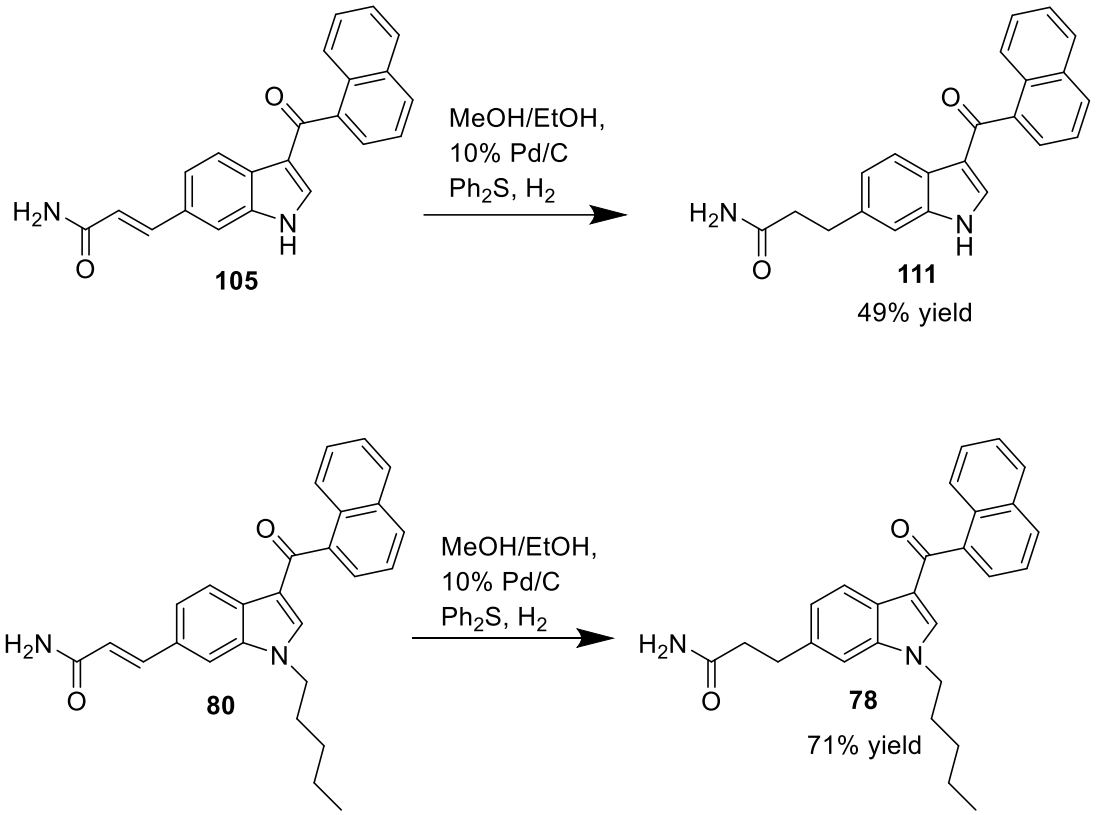


**Scheme 29.** The successful hydrogenation with diphenyl sulfide to yield **111** and **78**.

The compounds **77-80** and **100-111** were sent for biological evaluation using the National Institute of Mental Health's Psychoactive Drug Screening program at the University of North Carolina at Chapel Hill [110]. A functional assay was completed on the compounds at the $CB_1$, $CB_2$, GPR119, and GPR55 receptors and the results are shown in Table 8. The limitation to a functional assay is that is does not provide any quantitative data, only qualitative. The main focus will be the results of the $CB_1$ and $CB_2$ receptor, but the results for GPR119 and GPR55 are also shown for informational purposes. Both GPR119 and GPR55 are g-protein coupled receptors and are cannabinoid receptors. Each compound was tested four times per receptor in order to yield four different percentage results. These percentages were calculated using the following equations:

agonist assay= ((sample- basal average) / (reference agonist average-basal average)) x 100

antagonist assay= 100-((sample-reference antagonist average) / (reference agonist average-reference antagonist average) x 100)

The reference agonist used for $CB_1$ and $CB_2$ was CP 55,950. The reference agonist for GPR119 was APD668 and for GPR55 it was rimonabant. The reference antagonist for $CB_1$ was rimonabant and for $CB_2$ it was SR144528. The reference antagonist for GPR119 and GPR55 was CID16020046. The average of the four results were taken and are shown in Table 8. For the agonist assays, the data represents the percent efficacy (relative to the reference agonist) of the test compound at 10 micromolar. For the antagonist assays, the data represents the percent inhibition of the response to an EC90 of reference agonist by the test compound at 10 micromolar.

When comparing the agonist functional assay for $CB_2$, only eight of the compounds gave a positive average percent. The best average percent was 75.70, which was the unsaturated methyl ester with both the pentyl chain and naphthoyl ring, present (**79**). The second-best average percent was 52.11, which was the unsaturated methyl ester with only the pentyl chain (**102**). Compound **77** gave the third highest percent average of 21.23 and is the saturated methyl ester with both substituents present. The compounds that scored poorly were the methyl esters (alkene and alkane) with no substituents present and the majority of the amides, with exception to **80** and **78**, which are the unsaturated and saturated, respectively, indoles with both substituents present. In most cases, the alkenes gave better average percent results than their respective alkanes. It appears the methyl ester functional group is better than the amide

functionality for $CB_2$ agonism. Also, having both substituents present seems to be an important factor in $CB_2$ agonism.

When comparing the antagonist functional assay for $CB_2$, all of the compounds have a positive average percent. The three highest average percentages were 89.09, 85.47, 76.22 which relate to compounds **80**, **77** and **78** respectively. The similarity between these three compounds is that both substituents, the naphthoyl ring and pentyl chain, are present. The two worst average percentages are 21.08 and 22.57, which correspond to compounds **111** and **106**. Compound **111** is the saturated amide containing only the naphthoyl ring and compound **106** is the saturated methyl ester with no other substituents. Again, in most cases, the alkenes gave a better average percent than their respective alkanes. When comparing the methyl ester functionality with the amide functionality for $CB_2$ antagonism, the results are mixed. Overall, having both substituents, the naphthoyl ring and the pentyl chain, seem to play an important role for $CB_2$ antagonism. It also seems as though these compounds are better antagonists than agonists due to the more positive scores received for the antagonist assay. It is hypothesized that these compounds are better antagonists than agonists due to the large, bulky structural features. In a previous study, it was shown that larger compounds were able to reach further in the $CB_2$ binding pocket and interact with toggle switch TRP 258, which plays a crucial role in determining agonists vs antagonist [42].

Since the goal was to design and synthesize selective $CB_2$ agonists, it is of interest to compare the $CB_1$ vs $CB_2$ results. When evaluating the $CB_1$ agonist assay results, nine of the compounds gave positive average percentages. The top three average percents are 213.38, 120.62, 91.06, which corresponds to indoles **77**, **102**, and **79**. These are the same compounds that have the highest average percent with the $CB_2$ agonist assay. However, the average percent

scores are higher for $CB_1$ than for $CB_2$. The compounds that scored poorly for $CB_1$ agonist assay was compound **104**, which is the unsaturated methyl ester with only the naphthoyl substituent present. Also, the majority of the amides, with exception to **80** and **78**, gave negative average percent results. This was also seen with $CB_2$ agonist assay. In most cases, the average percent results were higher for $CB_1$ than for $CB_2$, except with compounds **104** and **80**. Compound **104** is the unsaturated methyl ester with the naphthoyl substituent present only. For $CB_1$ the percent average was -4.01 and for $CB_2$ it was 17.19. Compound **80** is the amide with both substituents present and gave an average percent of 1.42 and 18.22 for $CB_1$ and $CB_2$, respectively. Overall, it seems that the majority of these compounds synthesized are not selective for $CB_2$ and act more as antagonists than agonists.

When evaluating the $CB_1$ antagonist assay results, all of the compounds gave positive average percentages, which was seen with the $CB_2$ antagonist assay. The top three average percents are 97.57, 85.33 and 83.44 which relate to compounds **80**, **78**, and **104**. The unsaturated (**80**) and saturated (**78**) amides also scored the highest in the $CB_2$ antagonist assay, except the scores are higher for $CB_1$. The two lowest percent averages were 1.54 and 4.78, which related to indoles **111** and **101**. Compound **111** also had the lowest score for the $CB_2$ antagonist assay. In majority of cases, the alkenes had a higher average percent than their respective alkanes, which is a similar pattern seen with the previous assays.

| Compound | Receptor | Functional Assay Type | Average (%) | Std. error |
|---|---|---|---|---|
| 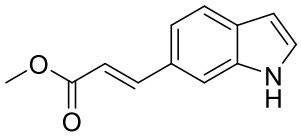 **100** | $CB_1$ | Agonist | 11.80 | 1.50 |
| | $CB_2$ | Agonist | -1.63 | 1.07 |
| | GPR119 | Agonist | 0.07 | 2.55 |
| | GPR55 | Agonist | 2.11 | 4.46 |
| | $CB_1$ | Antagonist | 24.12 | 4.25 |
| | $CB_2$ | Antagonist | 30.10 | 2.12 |
| | GPR119 | Antagonist | -38.29 | 15.01 |
| | GPR55 | Antagonist | -37.60 | 4.24 |
| 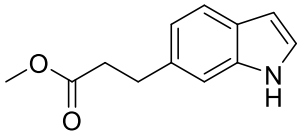 **106** | $CB_1$ | Agonist | 1.27 | 1.15 |
| | $CB_2$ | Agonist | -2.77 | 0.61 |
| | GPR119 | Agonist | -2.33 | 1.40 |
| | GPR55 | Agonist | -1.96 | 1.74 |
| | $CB_1$ | Antagonist | 12.43 | 2.42 |
| | $CB_2$ | Antagonist | 22.57 | 2.30 |
| | GPR119 | Antagonist | -6.76 | 7.90 |
| | GPR55 | Antagonist | -21.45 | 10.31 |
| 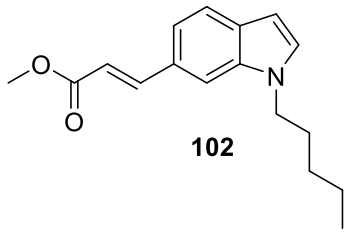 **102** | $CB_1$ | Agonist | 120.62 | 3.80 |
| | $CB_2$ | Agonist | 52.11 | 4.83 |
| | GPR119 | Agonist | -4.53 | 0.77 |
| | GPR55 | Agonist | -6.08 | 2.16 |
| | $CB_1$ | Antagonist | 44.58 | 2.48 |
| | $CB_2$ | Antagonist | 47.64 | 1.39 |
| | GPR119 | Antagonist | -42.01 | 20.42 |
| | GPR55 | Antagonist | 28.72 | 5.94 |
| 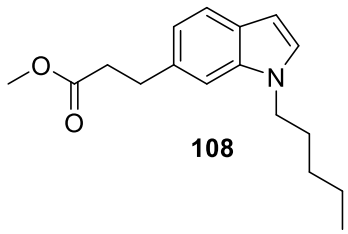 **108** | $CB_1$ | Agonist | 23.37 | 3.15 |
| | $CB_2$ | Agonist | 1.21 | 0.45 |
| | GPR119 | Agonist | -6.05 | 1.47 |
| | GPR55 | Agonist | -1.24 | 2.27 |
| | $CB_1$ | Antagonist | 37.78 | 3.41 |
| | $CB_2$ | Antagonist | 38.61 | 2.27 |
| | GPR119 | Antagonist | -18.27 | 5.75 |
| | GPR55 | Antagonist | 14.25 | 6.54 |
| 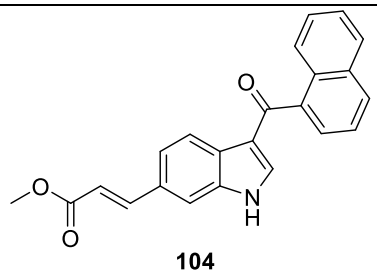 **104** | $CB_1$ | Agonist | -4.01 | 0.24 |
| | $CB_2$ | Agonist | 17.19 | 2.26 |
| | GPR119 | Agonist | -10.72 | 0.34 |
| | GPR55 | Agonist | 2.20 | 2.36 |
| | $CB_1$ | Antagonist | 83.44 | 1.06 |
| | $CB_2$ | Antagonist | 69.67 | 3.39 |
| | GPR119 | Antagonist | 68.72 | 5.73 |
| | GPR55 | Antagonist | 36.22 | 2.03 |

**Table 8.** The functional assay results for compounds **77-80** and **100-111** at $CB_1$, $CB_2$, GPR119 and GPR55 receptors.

| | | | | |
|---|---|---|---|---|
| 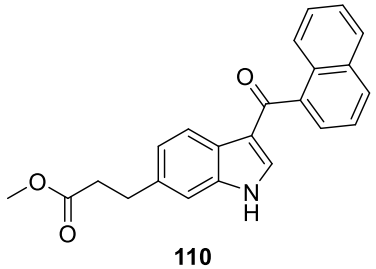 110 | $CB_1$ | Agonist | 22.95 | 0.69 |
| | $CB_2$ | Agonist | 10.33 | 1.38 |
| | GPR119 | Agonist | -5.70 | 0.41 |
| | GPR55 | Agonist | 1.55 | 2.96 |
| | $CB_1$ | Antagonist | 26.54 | 2.46 |
| | $CB_2$ | Antagonist | 34.62 | 3.64 |
| | GPR119 | Antagonist | -30.54 | 12.02 |
| | GPR55 | Antagonist | 4.18 | 3.93 |
| 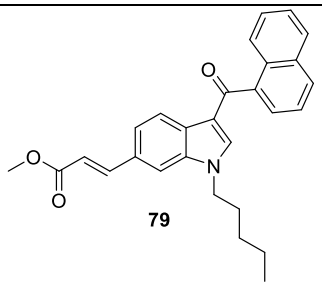 79 | $CB_1$ | Agonist | 91.06 | 3.74 |
| | $CB_2$ | Agonist | 75.70 | 4.51 |
| | GPR119 | Agonist | -3.42 | 1.35 |
| | GPR55 | Agonist | 1.53 | 0.58 |
| | $CB_1$ | Antagonist | 54.29 | 1.32 |
| | $CB_2$ | Antagonist | 53.77 | 3.16 |
| | GPR119 | Antagonist | 1.14 | 8.12 |
| | GPR55 | Antagonist | 14.56 | 8.18 |
| 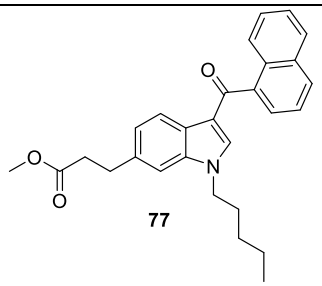 77 | $CB_1$ | Agonist | 213.38 | 20.22 |
| | $CB_2$ | Agonist | 21.23 | 2.81 |
| | GPR119 | Agonist | -3.69 | 0.68 |
| | GPR55 | Agonist | -0.59 | 0.82 |
| | $CB_1$ | Antagonist | 27.55 | 4.20 |
| | $CB_2$ | Antagonist | 85.47 | 0.89 |
| | GPR119 | Antagonist | -36.41 | 6.97 |
| | GPR55 | Antagonist | 3.68 | 4.01 |
| 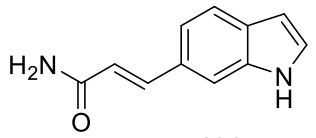 101 | $CB_1$ | Agonist | -0.17 | 0.79 |
| | $CB_2$ | Agonist | -3.74 | 0.64 |
| | GPR119 | Agonist | -0.82 | 1.85 |
| | GPR55 | Agonist | -0.57 | 3.43 |
| | $CB_1$ | Antagonist | 4.78 | 5.73 |
| | $CB_2$ | Antagonist | 30.89 | 2.67 |
| | GPR119 | Antagonist | -55.21 | 15.64 |
| | GPR55 | Antagonist | -31.07 | 8.02 |
| 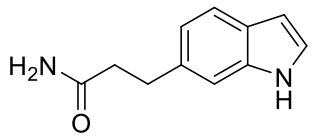 107 | $CB_1$ | Agonist | -1.34 | 0.55 |
| | $CB_2$ | Agonist | -3.70 | -0.53 |
| | GPR119 | Agonist | -4.32 | 0.85 |
| | GPR55 | Agonist | -1.59 | 0.64 |
| | $CB_1$ | Antagonist | 7.17 | 6.71 |
| | $CB_2$ | Antagonist | 28.94 | 3.24 |
| | GPR119 | Antagonist | -28.92 | 7.85 |
| | GPR55 | Antagonist | -11.60 | 3.03 |

**Table 8.** Continued.

| | | | | |
|---|---|---|---|---|
| 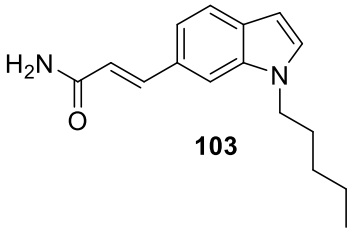 103 | $CB_1$ | Agonist | -1.27 | 0.82 |
| | $CB_2$ | Agonist | -1.94 | -0.95 |
| | GPR119 | Agonist | -5.53 | 1.38 |
| | GPR55 | Agonist | -5.17 | -0.79 |
| | $CB_1$ | Antagonist | 30.48 | 2.64 |
| | $CB_2$ | Antagonist | 34.58 | 2.85 |
| | GPR119 | Antagonist | -11.59 | 7.81 |
| | GPR55 | Antagonist | 21.76 | 4.16 |
| 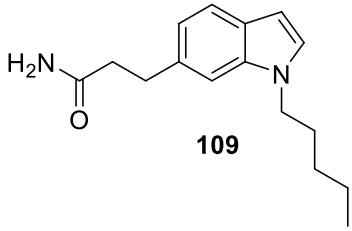 109 | $CB_1$ | Agonist | -3.63 | 0.38 |
| | $CB_2$ | Agonist | -4.70 | 0.26 |
| | GPR119 | Agonist | -7.97 | 0.33 |
| | GPR55 | Agonist | -1.82 | 2.03 |
| | $CB_1$ | Antagonist | 44.74 | 1.85 |
| | $CB_2$ | Antagonist | 36.47 | 3.18 |
| | GPR119 | Antagonist | -14.09 | 9.92 |
| | GPR55 | Antagonist | 6.51 | 6.51 |
| 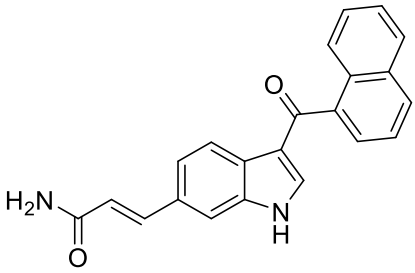 105 | $CB_1$ | Agonist | -2.61 | 0.93 |
| | $CB_2$ | Agonist | -3.67 | 0.54 |
| | GPR119 | Agonist | -10.05 | 0.27 |
| | GPR55 | Agonist | -3.45 | 1.93 |
| | $CB_1$ | Antagonist | 75.96 | 0.35 |
| | $CB_2$ | Antagonist | 50.64 | 3.14 |
| | GPR119 | Antagonist | 14.53 | 16.81 |
| | GPR55 | Antagonist | 59.89 | 4.90 |
| 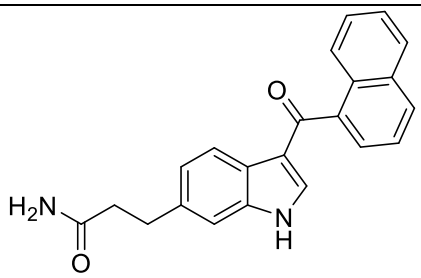 111 | $CB_1$ | Agonist | -0.92 | 0.50 |
| | $CB_2$ | Agonist | -3.48 | 0.48 |
| | GPR119 | Agonist | -3.02 | 1.95 |
| | GPR55 | Agonist | 4.86 | 2.01 |
| | $CB_1$ | Antagonist | 1.54 | 2.41 |
| | $CB_2$ | Antagonist | 21.08 | 5.45 |
| | GPR119 | Antagonist | -68.64 | 3.67 |
| | GPR55 | Antagonist | -20.04 | 8.73 |
| 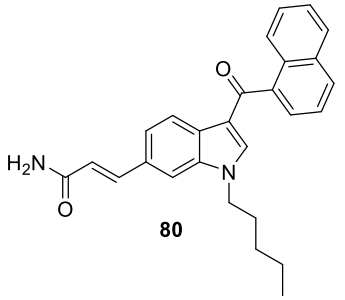 80 | $CB_1$ | Agonist | 1.42 | 0.42 |
| | $CB_2$ | Agonist | 18.22 | 0.32 |
| | GPR119 | Agonist | -11.4 | 0.02 |
| | GPR55 | Agonist | -11.56 | 0.82 |
| | $CB_1$ | Antagonist | 97.57 | 0.35 |
| | $CB_2$ | Antagonist | 89.09 | 1.20 |
| | GPR119 | Antagonist | 102.56 | 2.58 |
| | GPR55 | Antagonist | 98.70 | 0.59 |

**Table 8.** Continued.

| | | | | |
|---|---|---|---|---|
| 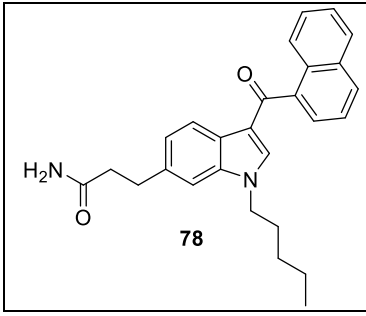 78 | $CB_1$ | Agonist | 24.92 | 1.44 |
| | $CB_2$ | Agonist | 15.88 | 0.94 |
| | GPR119 | Agonist | -8.76 | 0.83 |
| | GPR55 | Agonist | 14.63 | 2.34 |
| | $CB_1$ | Antagonist | 85.33 | 1.61 |
| | $CB_2$ | Antagonist | 76.22 | 1.48 |
| | GPR119 | Antagonist | 16.75 | 9.75 |
| | GPR55 | Antagonist | 49.90 | 3.65 |

**Table 8.** Continued.

The next set of eight compounds to be synthesized are shown in Figure 46 and these were designed upon the publication of the $CB_2$ crystal structure. These compounds contain the same chemical moiety as the previous set of compounds with the exception of one less carbon in the methyl ester or the amide chain. This modification was made because the $CB_2$ crystal structure binding pocket is slightly smaller than the proposed $CB_2$ homology model binding pocket. Even though the crystal structure does suggest there is room for growth around the $6^{th}$ position of the indole, it is limited in size.

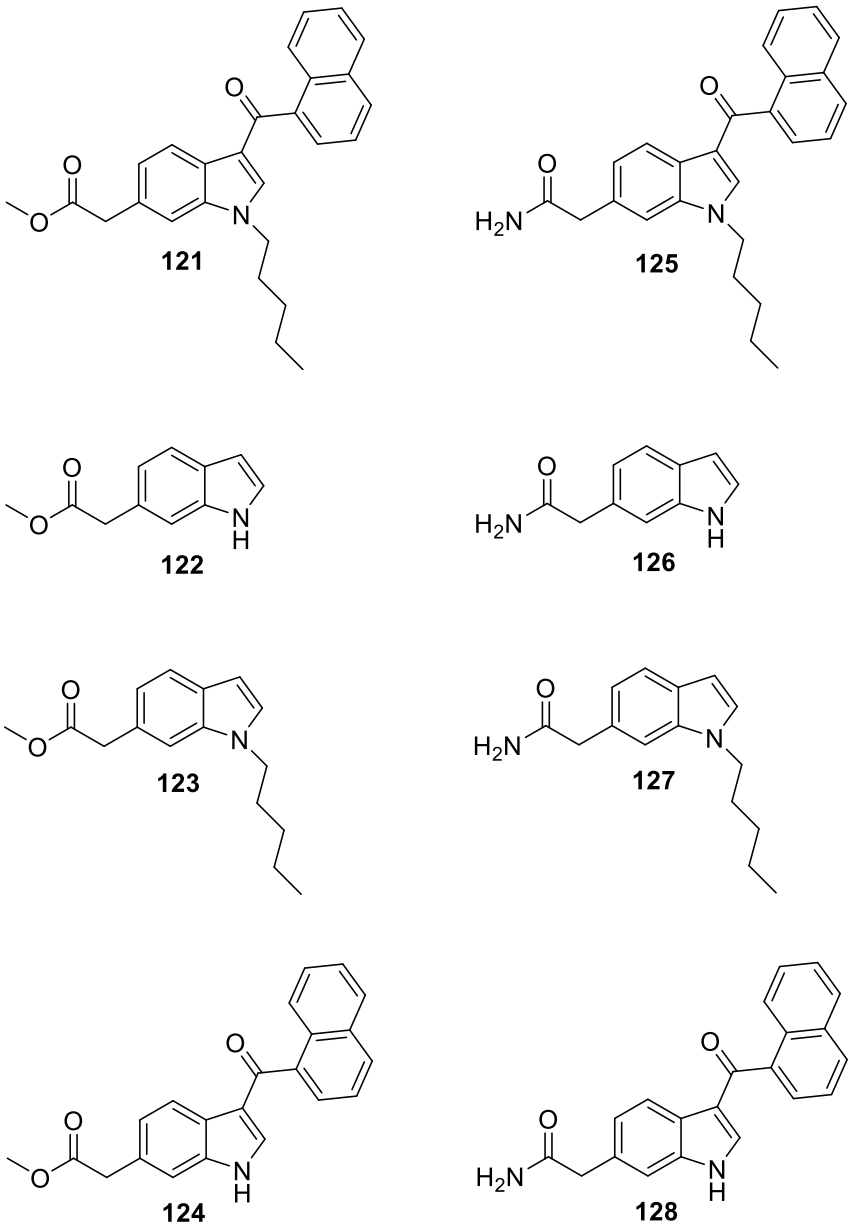


**Figure 46.** The next two target compounds and the intermediates

The synthetic approach for synthesizing the methyl esters **122** and **124** is shown in Scheme 30. The first step is the esterification of 6-acetic acid indole, **129**. This was done by dissolving the acid **129** in DMF and adding 1.3 equivalents of anhydrous potassium carbonate ($K_2CO_3$) [111]. After 30 minutes, methyl iodide was added and mixed for an additional 2 hours. The reaction was quenched with water, extracted with ethyl acetate, washed with water and dried

using sodium sulfate. This yielded the desired methyl ester **122** in 98% yield. The methyl ester **122** was then subjected to the Friedel-Crafts acylation utilizing aluminum chloride as the Lewis acid and the acid chloride **98** as the electrophile. This reaction yielded the monoacylated product **124** in 84% yield.

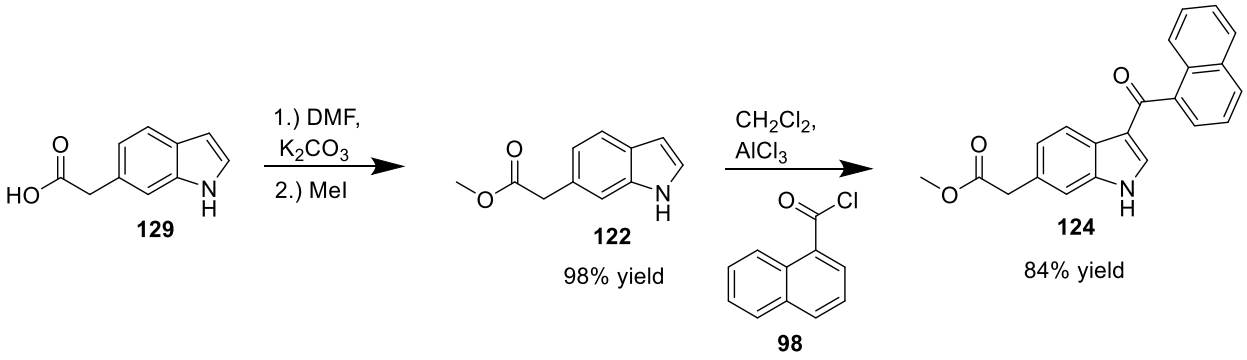


**Scheme 30.** The synthesis of compounds **122** and **124**.

The failed synthesis of the pentylated methyl ester **123** is shown in Scheme 31. The methyl ester **122** was dissolved in a DMF/KOH mixture and mixed for 30 minutes. Then 1-bromopentane was added and mixed for 2 hours. Upon checking the reaction by GC/MS, one peak was seen which corresponds to the dipentylated product **130**. The problem was the acidity of the proton on the methylene carbon. This proton's acidity is similar to that of the proton on the indoles nitrogen, therefore it is hard to selectively deprotonate when using a strong base such as KOH.

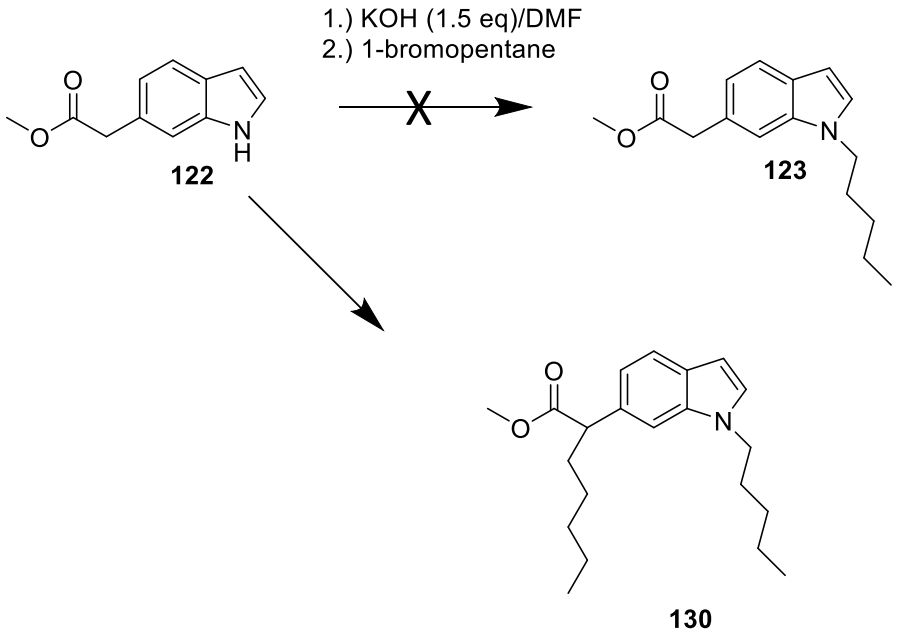


**Scheme 31.** The failed synthesis of compound **123**.

The alternative approach to synthesizing the pentylated methyl ester **123** is shown in Scheme 32. The starting 6-acetic acid indole, **129**, was dissolved in DMF and 2 equivalents of KOH was added, followed by 2 equivalents of 1-bromopentane. Upon work up, this yields the di-pentylated product **131**. However, the hydrolysis of **131** can be achieved by refluxing in NaOH/MeOH overnight and then washing with 1 M HCl to yield the acid **132**. Then the esterification of the carboxylic acid utilizing the same procedure as shown previously yielded the desired pentylated methyl ester **123**. Also, the synthesis of **121** can be accomplished utilizing **123** and the Friedel-Crafts acylation that was used previously.

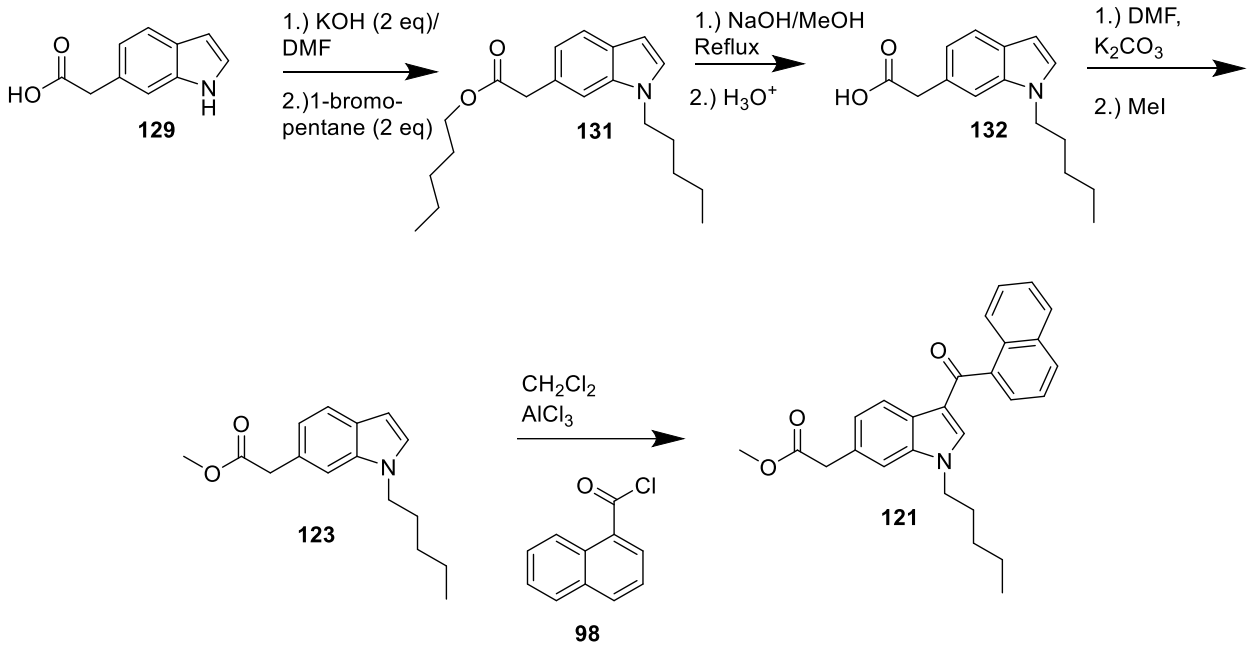


**Scheme 32.** The synthesis of **123** and **121**.

The synthesis of the four amide compounds is shown in Scheme 33. The procedure is to dissolve the methyl esters in a methanol-ammonium hydroxide solution [112]. The reaction was left for 16 hours at room temperature. The methyl esters **122** and **123** had completely converted to the amide compounds **126** and **127**, respectively. The methyl ester **124** was 50% converted to **128** and the methyl ester **121** did not react at all. It was hypothesized that solubility was a factor as to why methyl esters **124** and **121** did not react completely to yield the desired product. Compound **124** did not completely dissolve in the methanol-ammonium hydroxide solution and **121** did not dissolve at all. In order to dissolve compound **121** into solution, the use of heat and the use of a more polar solvent, THF, were attempted but both of these options were not successful.

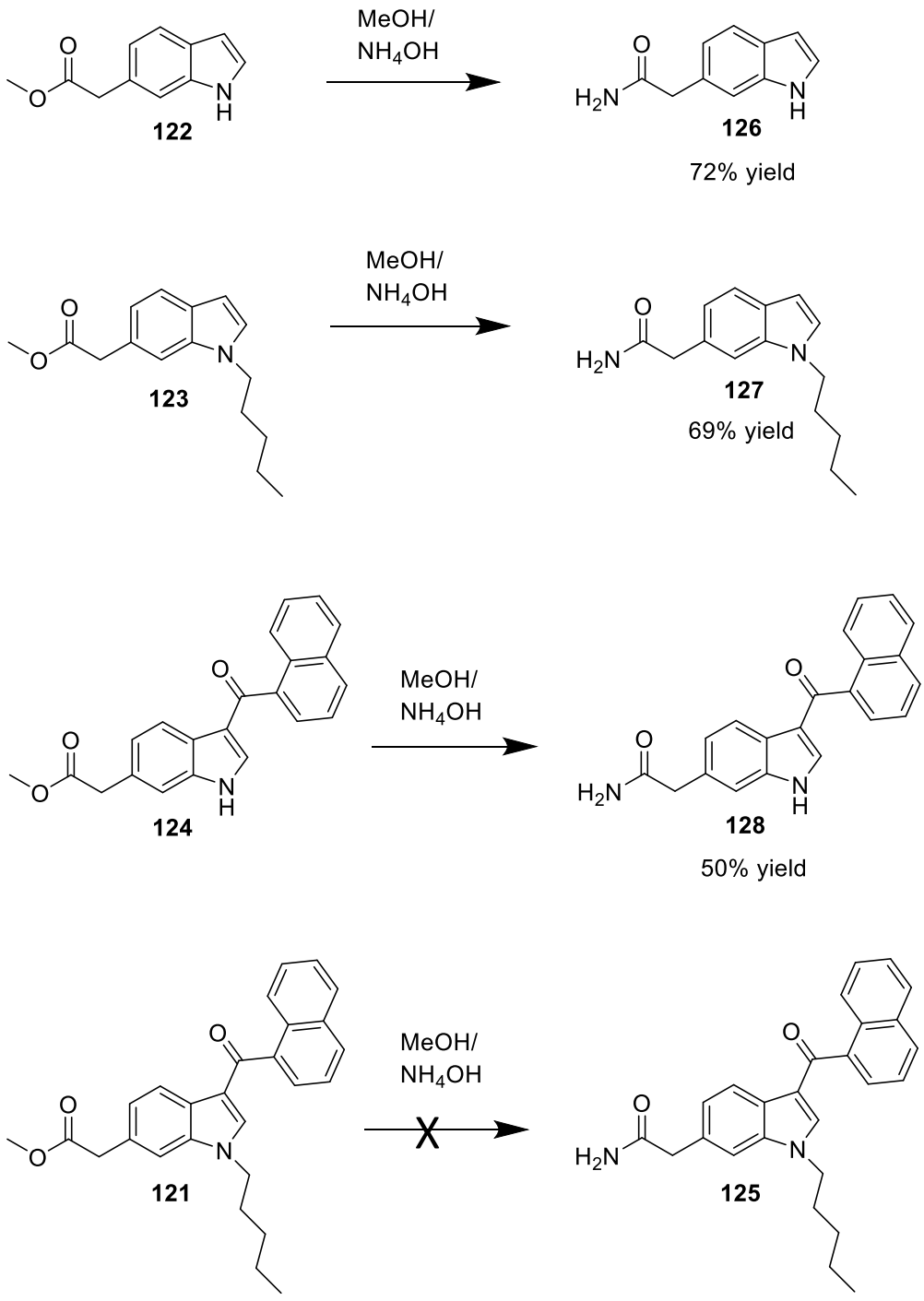


**Scheme 33.** The synthesis of compounds **126-128**.

### 4.2) Synthesis of fragment compounds based upon $CB_2$ crystal structure

#### 4.2.1) Results and Discussion

In the previous section, four fragment compounds were designed using molecular modeling of the $CB_2$ crystal structure. The four fragment compounds are shown in Figure 47 and two of them have been synthesized.

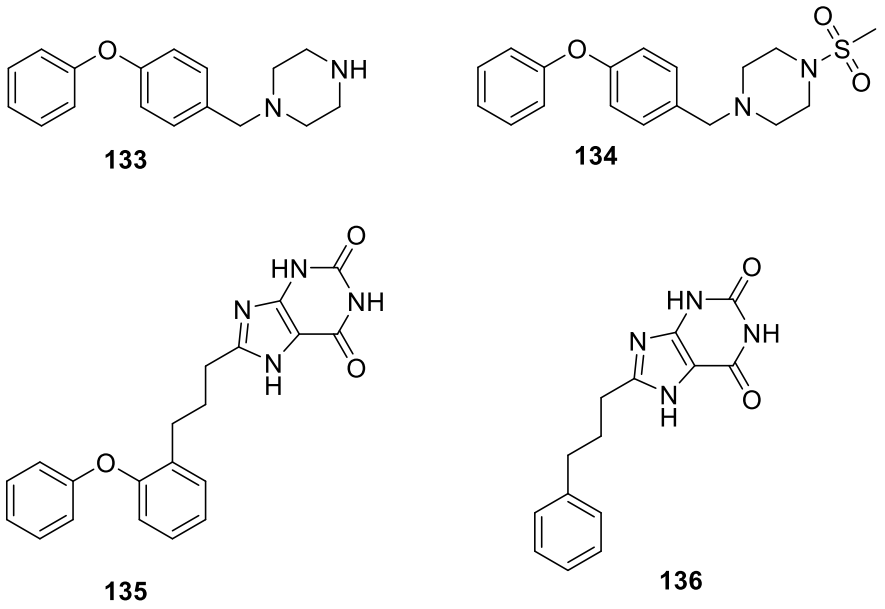


**Figure 47.** The four fragment compounds (**133-136**) based off the $CB_2$ crystal structure.

The synthetic steps for the diphenyl compounds **133** and **134** are shown in Scheme 34. Piperazine was dissolved in dry methylene chloride and cooled by an ice bath to 0°C [113]. The commercially available starting material, 4-phenoxybenzyl bromide (**137**), was added dropwise and then mixed for one hour. Upon work up and recrystallization using 100% methanol the desired fragment **133** was produced in 87% yield. The diphenyl fragment **133** was then dissolved in dry methylene chloride, trimethylamine was added and then cooled in an ice bath [114]. Methane sulfonyl chloride was added dropwise and mixed for one hour. Work up yielded the desired product **134** in 91% yield.

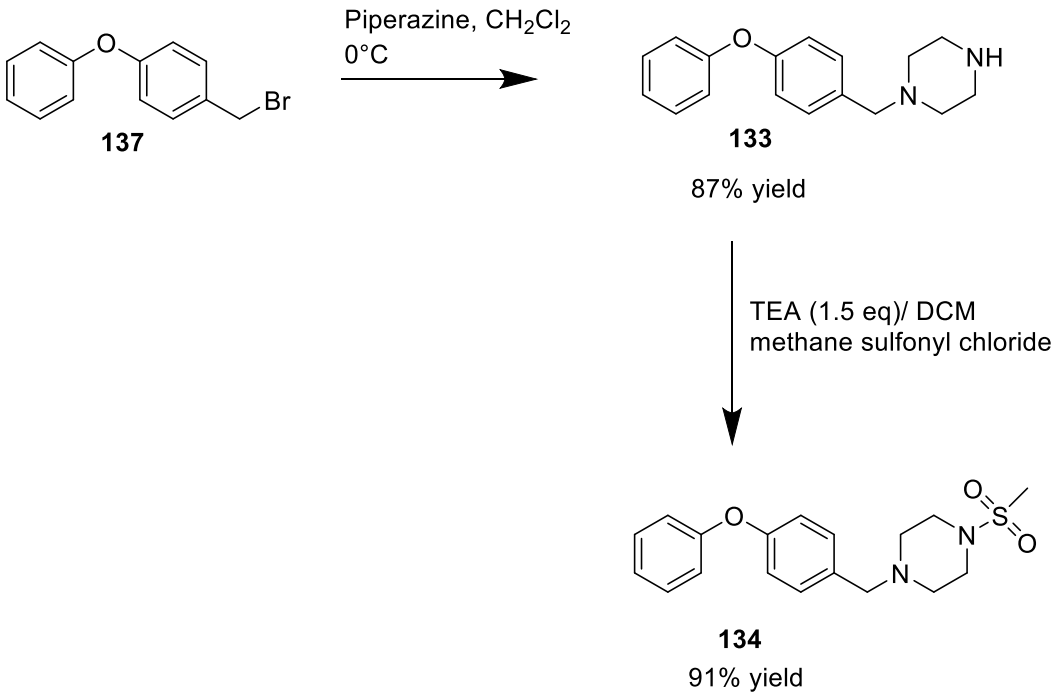


**Scheme 34.** The synthesis of fragments **133** and **134**.

In conclusion, the four target aminoalkylindoles **77-80** that were designed from the $CB_2$ homology model were synthesized. Also, the intermediates of those target compounds were synthesized in order to determine structure activity relationship. The analytical data GC-MS, NMR and CHN analysis was used in order to confirm the synthesis and the purity of the compounds. These compounds were sent for biological evaluation at UNC Chapel Hill in order to receive functional assay data. The results concluded that in most cases, having both the pentyl chain and naphthoyl group gave better results. Also, these compounds did not seem selective to CB2 and they acted more like antagonists than agonists. Once the cryo-EM $CB_2$ structure was published, it was determined that the binding pocket was smaller than what was predicted from the homology model. This led to designing compounds **121-128**, which are similar to compounds

**77-80**, with the exception of one less carbon in the methyl ester or amide side chain. All the compounds except for **125** were synthesized and evaluated by GC-MS, NMR and CHN analysis. In addition, fragment compounds **133** and **134** were synthesized and evaluated by GC-MS, NMR and CHN analysis.

## 4.3 Experimental

### *4.3.1 Instrumentation*

Reactions were monitored by thin-layer chromatography (TLC) using 0.25 mm E. Merck silica gel 60-F254 precoated silica gel plates with visualization by the irradiation with Mineralight UVGL-25 lamp. Column chromatography was performed on Whatman silica gel (average particle size 2-25 µm, 60Å) and elution with the indicated solvent system.

**NMR**

$^{1}H$ and $^{13}C$ NMR spectra were recorded on a Varian MR400. All $^{1}H$ chemical shifts are reported in δ relative to the internal standard tetramethylsilane (TMS, δ 0.00). $^{13}C$ chemical shifts are reported in δ relative to $CDCl_3$ (center of triplet, δ 77.23) or relative to DMSO-$d_6$ (center of septet, δ 39.51). The spin multiplicities are indicated by the symbols s (singlet), d (doublet), t (triplet), q (quartet), m (multiplet), and br (broad).

**GC-MS**

GC-MS was performed with an HP-5890 GC coupled with an HP-5970 mass selective detector (Hewlett Packard, Palo Alto, CA) using Helium (grade 5.0) as carrier gas. The mass spectrometer was operated on the electron impact (EI) mode using ionization voltage of 70 eV and a source temperature of 230°C. Samples were dissolved in HPLC grade acetonitrile (Fisher Scientific, NJ, USA) and manually introduced (1µL) individually.

**Elemental Analysis**

Atlantic Microlabs, Norcross, Georgia, performed elemental analyses.

### *4.3.2 Synthetic Methods*

**4-Bromo-2-nitrotoluene (93):**

4-Methyl-3-nitroaniline (**94**) (5 g), water (50 mL) and 48% aqueous HBr (16.5 mL) were added to a round bottom flask and heated until all the solid was dissolved. The dark orange solution was cooled to 0°C. A solution of $NaNO_2$ (2.7 g) in water (10 mL) was then added dropwise at a rate that maintained the reaction temperature below 2°C. This yellow-brown solution was then stirred for another 45 minutes at 0-2°C and then added to a solution of CuBr (7 g), 48% aqueous HBr (11 mL) and water (32.5 mL) at 90°C. When the addition was complete, the reaction was stirred at 90°C for another 30 minutes, cooled to room temperature, poured into a separatory funnel, and extracted with diethyl ether (3 x 20 mL). The combined organic extracts were then washed with 10% aqueous ammonium hydroxide (3 x 20 mL), saturated sodium bicarbonate, water, dried over sodium sulfate, and concentrated. This crude material was recrystallized from hot methanol, filtered and dried in a vacuum oven to afford a yellow solid. (89% yield). $^{1}$H-NMR ($CDCl_3$): 2.554 (3H, s), 7.259 (1H, dd, J= 8.34, 1.61 Hz), 7.608 (1H, dd, J= 8.34, 0.45 Hz), 8.117 (1H, dd, J=1.61, 0.45 Hz). $^{13}$C-NMR ($CDCl_3$): δ 20.029, 117.867, 127.551, 129.182, 130.741, 134.077, 135.946. GC-MS (EI): 215.0 (molecular ion), 198.0, 170.0, 119.0, 90.1 (100%), 63.1.

**6-Bromo-indole (92):**

4-Bromo-2-nitrotoluene (**93**) (1.55 g), dimethyl formamide dimethyl acetal (1.2 mL) and pyrrolidine (0.72 mL) in DMF (15.5 mL) were heated at 110°C for two hours. After cooling to 0°C, 4M $NH_4OAc$ (31 mL), DMF (62 mL) and 15% $TiCl_3$ in 10% HCl (35.6 mL) were added. After stirring for 15 minutes the resulting grey suspension was brought to pH 9 by adding 4M NaOH. Extraction with diethyl ether (3 x 25 mL), followed by drying with sodium sulfate and

solvent removal gave the crude product. (65 % yield). GC-MS (EI): 195.0 (molecular ion and 100%), 116.1, 89.1.

**1-N-Pentyl-6-bromo-indole (91):**

6-Bromo-indole (**92**) was dissolved in DMF and treated with KOH (1.5 eq). This solution was mixed for 30 minutes. 1-Bromopentane (1 eq) was added to the indole/KOH mixture and the resulting mixture was stirred for 2 hours. This mixture was poured into water and extracted with ethyl acetate (3 x 25 mL). The combined ethyl acetate extracts were washed with water (3 x 25 mL), dried over sodium sulfate and evaporated to yield the desired intermediate. No further purification was done. GC-MS (EI): 265.1 (molecular ion), 210.0, 129.1, 102.1.

**1-Naphthoyl chloride (98):**

1-Naphthoic acid (**97**) (5 g), benzene (50 mL), and thionyl chloride (4.1 mL) with a couple drops of DMF was added to a dry round bottom flask. The reaction was refluxed for five hours. The solvent was evaporated, and then benzene (25 mL) was added to the round bottom flask and evaporated again to yield the desired yellow oily compound. (90 % yield)

**1-N-Pentyl-3-(1-naphthoyl)-6-bromo-indole (90):**

1-N-Pentyl-6-bromo-indole (**91**) (0.55g) was dissolved in dry methylene chloride (7 mL) and added to a dry round bottom flask under nitrogen. The reaction mixture was cooled and 0.9 M dimethyl aluminum chloride (3.22 mL) was added via septum/syringe. Compound 12 (0.39 mL) in dry methylene chloride (2 mL) was added over a period of five minutes and stirred over an ice bath for one hour. The reaction mixture was quenched with 1 N HCl (15 mL) and extracted with

methylene chloride (25 mL). The organic extract was washed with water (3 x 20 mL), saturated sodium bicarbonate (2 x 20 mL) and dried with magnesium sulfate. Evaporation of the solvent and recrystallization using 100% diethyl ether yielded the desired compound. (87% yield). GC-MS (EI): 421.1 (molecular ion and 100%), 362.1, 292.1, 269.1, 224.0, 155.1, 127.1.

**1-NH-3-(1-Naphthoyl)-6-bromo-indole (99):**

6-Bromo-indole (**92**) (0.5 g) was dissolved in methylene chloride (10 mL) and added to a dry round bottom flask under nitrogen. The reaction mixture was cooled and 0.9 M dimethyl aluminum chloride (4 mL) was added via septum/syringe. Compound 12 ( 0.5 mL) in dry methylene chloride (2 mL) was added over a period of five minutes and stirred in an ice bath for one hour. The reaction mixture was quenched with 1 N HCl (15 mL) and extracted with methylene chloride (25 mL). The organic extract was washed with water (3 x 20 mL), saturated sodium bicarbonate (2 x 20 mL) and dried with magnesium sulfate. Evaporation of the solvent and recrystallization using 100% ethyl acetate yielded the desired compound. (71% yield). GC-MS (EI): 349.1 (molecular ion), 155.1 (100%), 127.1.

**1-N-Pentyl-6-carboxaldehyde-indole (115):**

6-Carboxaldehyde-indole (**114**) was dissolved in DMF and treated with KOH (1.5 eq). This solution was mixed for 30 minutes. 1-Bromopentane (1 eq) was added to the indole/KOH mixture and the resulting mixture was stirred for 2 hours. This mixture was poured into water and extracted with ethyl acetate (3 x 25 mL). The combined ethyl acetate extracts were washed with water (3 x 25 mL), dried over sodium sulfate and evaporated to yield the desired

intermediate. No further purification was done. (88% yield). GC-MS (EI): 215.2 (molecular ion), 186.2, 158.1, 130.1.

**1-N-Pentyl-6-(2-methylene-dimethyl-malonate)-indole (116):**

1-N-Pentyl-6-carboxaldehyde-indole (**115**) (0.44 g), dimethyl malonate (0.23 mL), piperidine (0.02 mL) and acetic acid (0.023 mL) in benzene (7 mL) was refluxed with a Dean-Stark trap for three hours. The reaction mixture was washed with 5% aqueous HCl (3 x 10 mL) and 5% aqueous sodium bicarbonate (3 x 10 mL). The organic layer was dried over magnesium sulfate and evaporated to yield the desired intermediate. No further purification was done. (98% yield). GC-MS (EI): 329.2 (molecular ion and 100%), 298.1, 272.1, 196.1, 154.1.

**General Heck Reaction for methyl esters:**

Aryl halide, methyl acrylate (3 eq), trimethylamine (1.25 eq), palladium (II) acetate (0.12 eq), tri(o-toly)phosphine (0.2 eq) was added to a heavy walled pressure tube inside the nitrogen glove box and sealed. This reaction was heated to 120°C for 12 hours. The work up consisted of cooling the reaction to room temperature, diluting with dichloromethane and filtering through celite. The organic layers were washed with water (3 x 20 mL), dried with magnesium sulfate and evaporation of solvent to yield crude material.

**1-NH-6-Methylacrylate-indole (100):**

This was purified by column chromatography (silica gel) with 20:80 ethyl acetate- petroleum ether as the mobile phase. (72% yield). $^{1}$H-NMR ($CDCl_3$): 3.803 (3H, s), 6.423 (1H, d, J= 16.3 Hz), 6.560 (1H, ddt, J= 2.24, 1.10, 0.44 Hz), 7.281 (1H, ddd, J= 8.59, 1.75, 0.44 Hz), 7.347 (1H,

dt, J= 2.24, 0.46 Hz), 7.626 (1H, d, J= 16.30 Hz), 7.795 (1H, ddt, J= 8.59, 1.10, 0.46 Hz), 7.834 (1H, dq, J=1.75, 0.44 Hz). $^{13}$C-NMR ($CDCl_3$): δ 51.654, 103.150, 112.176, 115.329, 119.462, 121.103, 126.505, 128.389, 129.817, 135.812, 146.502, 168.033. GC-MS (EI): 201.1 (molecular ion and 100%), 170.1, 142.1, 115.1, 70.7. Anal. Calcd. for $C_{12}H_{11}NO_2$ 0.1 molecule $H_2O$ C: 70.99, H: 5.56, N: 6.90. Found C: 70.93, 5.51, 6.87.

**1-N-Pentyl-6-methylacrylate-indole (102):**

This was purified by column chromatography (silica gel) with 20:80 ethyl acetate-petroleum ether as the mobile phase. (76% yield). $^1$H-NMR ($CDCl_3$): δ 0.898 (3H, t, J= 6.5 Hz), 1.274 (2H, h, J=6.5 Hz), 1.304 (2H, tt, J= 7.0, 6.5 Hz), 1.829 (2H, tt, J=7.0, 6.29 Hz), 3.804 (3H, s), 4.107 (2H, t, J= 6.29 Hz), 6.473 (1H, d, 16.27 Hz), 7.158 (1H, ddt, 6.55, 2.17, 0.45 Hz), 7.332 (1H, ddd, 8.39, 1.9, 0.45 Hz), 7.461 (1H, dt, J=6.55, 0.52 Hz), 7.580 (1H, dq, 1.9, 0.48 Hz), 7.601 (1H, d, J=16.27 Hz), 7.867 (1H, ddt, J=8.39, 2.17, 0.49 Hz). $^{13}$C-NMR ($CDCl_3$): δ 13.902, 22.289, 29.074, 29.978, 46.495, 51.593, 101.501, 110.687, 115.093, 118.740, 121.293, 127.766, 130.114, 130.471, 135.933, 146.714, 167.965. GC-MS (EI): 271.1 (molecular ion), 256.1, 240.2, 214.2 (100%), 182.1, 170.1, 154.1, 115.1, 77.3. Anal. Calcd. for $C_{17}H_{21}NO_2$ 0.1 molecule $H_2O$ C: 74.75, H: 7.82, N: 5.13. Found C: 74.50, H: 7.76, N: 5.12.

**1-NH-3-(1-Naphthoyl)-6-methylacrylate-indole (104):**

This was purified by column chromatography (silica gel) with 40:60 ethyl acetate-petroleum ether as the mobile phase. (56% yield). $^1$H-NMR (DMSO): δ 3.727 (3H, s), 6.616 (1H, d, J=16.6 Hz), 7.490 (1H, dd, J= 6.37, 1.89 Hz), 7.527 (1H, ddd, J= 7.59, 2.67, 0.44 Hz), 7.542 (1H, dddd, J= 7.9, 6.98, 1.54, 0.5 Hz), 7.580 (1H, ddd, J= 8.4, 7.59, 0.45 Hz), 7.609 (1H, dddt, J= 8.4, 2.67,

1.81, 0.5 Hz), 7.628 (1H, ddd, J= 8.32, 6.98, 2.28 Hz), 7.688 (1H, d, J= 16.69 Hz), 7.706 (1H, dt, J= 1.89, 0.44 Hz), 7.783 (1H, dt, J= 6.37, 0.49 Hz), 7.812 (1H, dddt, J= 7.9, 2.28, 1.81, 0.5 Hz), 8.004 (1H, ddq, J= 8.32, 1.54, 0.46 Hz), 8.230 (1H, t, 0.49). $^{13}$C-NMR (DMSO): δ 51.000, 114.144, 117.814, 122.190, 122.289, 125.343, 125.617, 126.225, 126.703, 128.041, 128.801, 129.682, 130.343, 130.411, 132.037, 133.739, 137.523, 138.655, 138.799, 138.929, 146.048, 167.345, 191.727. Anal. Calcd. For $C_{23}H_{17}NO_3$ 0.1 molecule $H_2O$ C: 77.34, H: 4.85, N: 3.92. Found C: 77.11, H: 4.88, N: 3.91.

**1-N-Pentyl-3-(1-naphthoyl)-6-methylacrylate-indole (79):**

This was purified by column chromatography (silica gel) with 20:80 ethyl acetate-petroleum ether as the mobile phase. (69% yield). $^{1}$H-NMR ($CDCl_3$): δ 0.826 (3H, t, J=6.5 Hz), 1.235 (2H, h, J=6.5 Hz), 1.285 (2H, tt, J= 7.23, 6.50 Hz), 1.807 (2H, tt, J=7.23, 6.28 Hz), 3.813 (3H, s), 4.038 (2H, t, J=6.28 Hz), 6.496 (1H, d, J=16.55 Hz), 7.449 (1H, dt, J=1.90, 0.52 Hz), 7.480 (1H, dd, J=6.05, 1.90 Hz), 7.500 (1H, dddd, J=7.90, 6.98, 1.54, 0.45 Hz), 7.620 (1H, ddd, J=8.40, 7.55, 0.45 Hz), 7.638 (1H, dddt, J=8.40, 2.56, 1.88, 0.46 Hz), 7.823 (1H, ddd, J=8.32, 6.98, 1.96 Hz), 7.903 (1H, d, J=16.55 Hz), 7.945 (1H, dt, J=6.05, 0.47 Hz), 8.152 (1H, ddd, J=7.55, 2.56, 0.44 Hz), 8.173 (1H, dtt, J=7.90, 1.92, 0.47 Hz), 8.423 (1H, ddq, J=8.32, 1.54, 0.46 Hz), 8.445 (1H, t, J=0.51 Hz). $^{13}$C-NMR ($CDCl_3$): δ 13.841, 22.137, 28.854, 29.522, 47.338, 51.745, 110.732, 116.788, 117.745, 122.250, 123.170, 123.314, 124.545, 125.889, 126.376, 126.877, 128.230, 128.693, 129.992, 130.228, 130.661, 133.723, 137.164, 138.669, 139.238, 145.628, 167.623, 191.798. Anal. Calcd. for $C_{28}H_{27}NO_3$ 0.2 molecules $H_2O$ C: 78.37, H: 6.44, N: 3.26. Found C: 78.11, H: 6.35, N: 3.28.

**1-NH-6-Propanoic-acid-methyl-ester-indole (106):**

To a Parr flask was added 1-NH-6-Methylacrylate-indole (**100**) (0.3 g) in ethyl acetate (15 mL) and 10% Pd/C (30 mg). This solution was placed in a nitrogen glove box and degassed for 15 minutes. The mixture was hydrogenated at 50 psi overnight. The mixture was filtered through celite and evaporated to yield the crude material which was purified by column chromatography (silica gel) with 20:80 ethyl acetate-petroleum ether as the mobile phase. (88% yield). $^{1}$H-NMR ($CDCl_3$): δ 2.675 (2H, t, J= 7.40 Hz), 3.047 (2H, t, J=7.40 Hz), 3.676 (3H, s), 6.502 (1H, ddt, J= 2.65, 1.24, 0.53 Hz), 6.963 (1H, ddd, J= 7.89, 1.54, 0.52 Hz), 7.121 (1H, dq, J= 1.54, 0.5 Hz), 7.198 (1H, dt, J= 2.65, 0.51 Hz), 7.556 (1H, ddt, J=7.89, 1.24, 0.48 Hz). $^{13}$C-NMR ($CDCl_3$): δ 31.300, 36.512, 51.798, 102.352, 110.542, 120.693, 123.975, 124.081, 126.300, 134.414, 136.093, 173.731. GC-MS (EI): 203.1 (molecular ion), 172.1, 143.1, 130.1, 115.1, 103.1, 77.1. Anal Calcd. for $C_{12}H_{13}NO_2$ C: 70.92, H: 6.45, N: 6.89. Found C: 70.79, H: 6.43, N: 6.91.

**1-N-Pentyl-6-propanoic-acid-methyl-ester-indole (108):**

To a Parr flask was added 1-N-Pentyl-6-methylacrylate-indole (**102**) (0.26 g) in ethyl acetate (15 mL) and 10% Pd/C (26 mg). This solution was placed in a nitrogen glove box and degassed for 15 minutes. The mixture was hydrogenated at 50 psi overnight. The mixture was filtered through celite and evaporated to yield the crude material which was purified by column chromatography (silica gel) with 20:80 ethyl acetate-petroleum ether as the mobile phase. (79% yield). $^{1}$H-NMR ($CDCl_3$): δ 0.858 (3H, t, J=6.50 Hz), 1.228 (2H, h, J=6.50 Hz), 1.293 (2H, tt, J= 6.63, 6.50 Hz), 1.791 (2H, tt, J= 7.43, 6.63 Hz), 2.662 (2H, t, J= 7.40 Hz), 3.069 (2H, t, J=7.40 Hz), 3.661 (3H, s), 4.044 (2H, t, J= 7.43 Hz), 6.413 (1H, ddt, J=3.80, 1.61, 0.51 Hz), 6.916 (1H, ddd, J= 7.92, 1.45, 0.48 Hz), 6.941 (1H, ddt, J= 1.45, 0.55, 0.45 Hz), 7.037 (1H, dt, J=3.80, 0.5 Hz), 7.243

(1H, dddd, J=7.92, 1.61, 0.55, 0.45 Hz). $^{13}$C-NMR ($CDCl_3$): δ 13.947, 22.320, 29.120, 29.894, 31.558, 36.603, 46.305, 51.601, 100.658, 108.833, 119.941, 120.898, 126.976, 127.675, 133.821, 136.146, 173.594. GC-MS (EI): 273.1 (molecular ion), 242.2, 216.1, 200.2 (100%), 156.1, 143.1, 130.1, 115.1, 77.1. Anal. Calcd. for $C_{17}H_{23}NO_2$ 0.1 molecule $H_2O$ C: 74.20, H: 8.50, N: 5.09. Found C: 74.06, H: 8.44, N: 4.99.

**1-NH-3-(1-Naphthoyl)-6-propanoic-acid-methyl-ester-indole (110):**

To a Parr flask was added 1-NH-3-(1-Naphthoyl)-6-methylacrylate-indole (**104**) (0.3 g) in 1:1 benzene (5 mL): ethanol (5 mL) and then Chloridotris-(triphenylphosphine)-rhodium I (3 mol %, 24 mg). The solution was placed in a nitrogen glove box and degassed for 15 minutes. The mixture was hydrogenated at 50 psi overnight. The mixture was filtered through celite and evaporated to yield the crude material which was purified by column chromatography (silica gel) with 40:60 ethyl acetate-petroleum ether as the mobile phase. (45% yield). $^{1}$H-NMR ($CDCl_3$): δ 2.475 (2H, t, J=7.40 Hz), 3.117 (2H, t, J=7.40 Hz), 3.465 (3H, s), 6.549 (1H, dd, J=8.17, 1.80 Hz), 6.870 (1H, dt, J=1.80, 0.45 Hz), 7.139 (1H, dddd, J= 7.90, 6.98, 1.54, 0.45 Hz), 7.281 (1H, t, J= 0.50 Hz), 7.350 (1H, ddd, J=8.40, 7.55, 0.45 Hz), 7.472 (1H, dddt, J= 8.40, 2.57, 1.89, 0.46 Hz), 7.579 (1H, ddd, J=8.32, 6.98, 2.28 Hz), 7.684 (1H, ddd, J=8.17, 0.54, 0.44 Hz), 7.803 (1H, ddd, J=7.55, 2.57, 0.44 Hz), 7.889 (1H, dddt, J= 7.90, 2.28, 1.89, 0.47 Hz), 7.927 (1H, ddq, J= 8.32, 1.54, 0.46 Hz). $^{13}$C-NMR ($CDCl_3$): δ Anal. Calcd. for $C_{23}H_{19}NO_3$ 0.8 molecules EtOAc/ 0.3 molecules EtOH C: 72.87, H: 6.21, N: 3.17. Found C: 72.71, H: 6.33, N: 3.28.

**1-N-Pentyl-3-(1-naphthoyl)-6-propanoic-acid-methyl-ester-indole (77):**

To a Parr flask was added 1-N-Pentyl-3-(1-naphthoyl)-6-methylacrylate-indole (**79**) (0.3 g) in 1:1 benzene (5 mL): ethanol (5 mL) and then Chloridotris-(triphenylphosphine)-rhodium I (3 mol %, 20 mg). The solution was placed in a nitrogen glove box and degassed for 15 minutes. The mixture was hydrogenated at 50 psi overnight. The mixture was filtered through celite and evaporated to yield the crude material which was purified by column chromatography (silica gel) with 20:80 ethyl acetate-petroleum ether as the mobile phase. (88% yield). $^{1}$H-NMR ($CDCl_3$): δ 0.843 (3H, t, J=6.50 Hz), 1.237 (2H, h, J=6.50 Hz), 1.298 (2H, tt, J=7.00, 6.50 Hz), 1.807 (2H, tt, J=7.43, 7.00 Hz), 2.709 (2H, t, J=7.40 Hz), 3.110 (2H, t, J=7.40 Hz), 3.687 (3H, s), 4.031 (2H, t, J=7.43 Hz), 7.207 (1H, dd, J=8.32, 1.81 Hz), 7.314 (1H, dt, J=1.81, 0.45 Hz), 7.417 (1H, dddd, J= 7.90, 6.98, 1.54, 0.45 Hz), 7.481 (1H, dt, J=8.32, 0.45 Hz), 7.509 (1H, ddd, J=8.40, 7.55, 0.45 Hz), 7.538 (1H, dddt, J=8.40, 2.56, 1.89, 0.46 Hz), 7.655 (1H, ddd, J=8.32, 6.98, 2.28 Hz), 7.891 (1H, ddd, J= 7.55, 2.56, 0.44 Hz), 7.949 (1H, dddt, J=7.90, 2.28, 1.89, 0.47 Hz), 8.178 (1H, ddq, J=8.32, 1.54, 0.46 Hz), 8.407 (1H, t, J=0.45 Hz). $^{13}$C-NMR ($CDCl_3$): δ 13.906, 22.180, 28.889, 29.451, 31.442, 36.343, 47.086, 51.721, 109.608, 117.457, 122.935, 123.603, 124.462, 125.450, 125.708, 125.966, 126.179, 128.185, 129.955, 130.016, 130.776, 133.716, 136.352, 137.325, 137.781, 139.072, 173.354, 191.923. Anal. Calcd. For $C_{28}H_{29}NO_3$ 0.1 molecule $H_2O$ C: 78.33, H: 6.86, N: 3.26. Found C: 78.06, H: 6.96, N: 3.25.

**General Heck Reaction for amides:**

Aryl halide, acrylamide (2 eq), trimethylamine (1.25 eq), palladium acetate (0.12 eq), tri(o-toly)phosphine (0.2 eq) and distilled acetonitrile were added to a heavy walled pressure tube inside a nitrogen glove box and sealed. This mixture was heated to 100°C for 12 hours. Then

cooled to room temperature, diluted with acetonitrile and filtered through celite. Water (10 mL) was added and the product was extracted with ethyl acetate (3 x 15 mL). The organic layer was dried by sodium sulfate and evaporated to yield the crude product.

**1-NH-6-(2-Propenamide)-indole (101):**

This was purified by column chromatography (silica gel) with 5:95 ethanol-ethyl acetate as the mobile phase. (72% yield). $^{1}$H-NMR (DMSO): δ 6.423 (1H, d, J= 16.13 Hz), 6.552 (1H, ddt, J= 2.26, 1.17, 0.44 Hz), 7.226 (1H, ddd, J= 8.59, 1.90, 0.44 Hz), 7.402 (1H, d, J= 16.13 Hz), 7.465 (1H, dt, J= 2.26, 0.46 Hz), 7.504 (1H, ddt, J= 8.59, 1.17, 0.46 Hz), 7.542 (1H, dq, J= 1.90, 0.44 Hz). $^{13}$C-NMR (DMSO): δ 101.950, 112.222, 118.528, 119.705, 120.845, 127.736, 128.268, 129.286, 136.412, 141.404, 167.585. GC-MS (EI): 186.1 (molecular ion and 100%), 170.1, 141.1, 115.1, 70.6. Anal. Calcd. For $C_{11}H_{10}N_2O$ 0.3 molecules $H_2O$ C: 68.95, H: 5.58, N: 14.62. Found C: 68.70, H: 5.34, N: 14.47.

**1-N-Pentyl-6-(2-propenamide)-indole (103):**

This was purified by column chromatography (silica gel) with 100% ethyl acetate as the mobile phase. (86% yield). $^{1}$H-NMR ($CDCl_3$): δ 0.864 (3H, t, J= 6.50 Hz), 1.259 (2H, h, J= 6.50 Hz), 1.349 (2H, tt, J= 7.00, 6.50 Hz), 1.823 (2H, tt, J= 7.00, 6.29 Hz), 4.111 (2H, t, J= 6.29 Hz), 6.472 (1H, d, J= 16.09 Hz), 6.516 (1H, ddt, J= 5.91, 2.21, 0.45 Hz), 7.144 (1H, ddd, J= 8.19, 1.91, 0.46 Hz), 7.259 (1H, d, J= 16.09 Hz), 7.334 (1H, dt, 5.91, 0.52 Hz), 7.571 (1H, dq, J= 1.91, 0.48 Hz), 7.777 (1H, ddt, J= 8.19, 2.21, 0.47 Hz). $^{13}$C-NMR ($CDCl_3$): δ 13.937, 22.294, 29.087, 29.968, 46.478, 101.448, 110.862, 117.039, 118.346, 121.256, 127.889, 129.910, 130.175, 135.973, 144.231, 168.651. GC-MS (EI): 256.1 (molecular ion), 199.1 (100%), 170.1, 154.1, 115.1, 77.2.

Anal. Calcd. For $C_{16}H_{20}N_2O$ 0.1 molecule EtOAc C: 74.29, H: 7.91, N: 10.56. Found C: 74.12, H: 7.73, N: 10.24.

**1-NH-3-(1-Naphthoyl)-6-(2-propenamide)-indole (105):**

This was purified by column chromatography (silica gel) with 5:95 ethanol-ethyl acetate as the mobile phase. (55% yield). $^{1}$H-NMR (DMSO): δ 6.616 (1H, d, J= 16.23 Hz), 6.656 (1H, d, J= 16.23 Hz), 7.491 (1H, dd, J= 6.33, 1.90 Hz), 7.512 (1H, dddd, J= 7.90, 6.98, 1.54, 0.45 Hz), 7.587 (1H, ddd, J= 8.40, 7.55, 0.45 Hz), 7.606 (1H, dddt, J= 8.40, 2.56, 1.88, 0.46 Hz), 7.685 (1H, ddd, J= 8.32, 6.98, 2.28 Hz), 7.707 (1H, dt, J= 1.90, 0.49 Hz), 7.740 (1H, ddd, J= 7.55, 2.56, 0.44 Hz), 7.985 (1H, dt, J= 6.33, 0.49 Hz), 8.029 (1H, dddt, J= 7.90, 2.28, 1.88, 0.47 Hz), 8.091 (1H, ddq, J= 8.32, 1.54, 0.46 Hz), 8.258 (1H, t, J=0.49 Hz). $^{13}$C-NMR (DMSO): δ 112.837, 117.791, 121.347, 121.864, 122.152, 125.328, 125.419, 125.685, 126.194, 126.681, 127.296, 128.747, 130.267, 130.624, 133.747, 137.705, 138.435, 138.556, 138.762, 140.539, 167.315, 191.689. Anal. Calcd. For $C_{22}H_{16}N_2O_2$ 0.8 molecules EtOAc C: 74.48, H: 5.00, N: 7.90. Found C: 74.44, H: 4.78, N: 7.99.

**1-N-Pentyl-3-(1-naphthoyl)-6-(2-propenamide)-indole (80):**

This was purified by column chromatography (silica gel) with 5:95 ethanol-ethyl acetate as the mobile phase. (82% yield). $^{1}$H-NMR (DMSO): δ 0.780 (3H, t, J= 6.50 Hz), 1.136 (2H, h, J= 6.50 Hz), 1.243 (2H, tt, J= 7.23, 6.50 Hz), 1.728 (2H, tt, J= 7.23, 6.28 Hz), 4.212 (2H, t, J= 6.28 Hz), 6.665 (1H, d, J= 16.20 Hz), 7.499 (1H, dt, J= 1.90, 0.51 Hz), 7.524 (1H, d, J= 16.20 Hz), 7.576 (1H, dd, J= 6.03, 1.90 Hz), 7.611 (1H, dddd, J= 7.90, 6.98, 1.54, 0.45 Hz), 7.673 (1H, ddd, J=

8.40, 7.55, 0.45 Hz), 7.690 (1H, dddt, J= 8.40, 2.56, 1.88, 0.46 Hz), 7.824 (1H, ddd, J= 8.32, 6.98, 1.96 Hz), 7.855 (1H, ddd, J= 7.55, 2.56, 0.44 Hz), 7.978 (1H, dtt, J= 7.90, 1.92, 0.47 Hz), 7.999 (1H, ddq, J= 8.32, 1.54, 0.46 Hz), 8.096 (1H, dt, J=6.03, 0.47 Hz), 8.299 (1H, t, J=0.50 Hz). $^{13}$C-NMR (DMSO): δ 14.283, 22.064, 28.674, 29.601, 46.636, 111.865, 116.727, 121.696, 121.879, 122.426, 125.457, 125.701, 126.316, 127.182, 127.729, 128.778, 130.290, 130.472, 130.768, 133.770, 137.553, 138.731, 140.509, 140.965, 141.056, 167.330, 191.241. Anal. Calcd. for $C_{27}H_{26}N_2O_2$ 0.3 molecules $H_2O$ C: 77.30, H:6.49, N: 6.68. Found C: 77.39, H: 6.39, N: 6.77.

**1-NH-6-Propanamide-indole (107):**

To a Parr flask was added 1-NH-6-(2-Propenamide)-indole (**101**) (0.32 g) in ethyl acetate (15 mL) and 10% Pd/C (32 mg). This solution was placed in a nitrogen glove box and degassed for 15 minutes. The mixture was hydrogenated at 50 psi overnight. The mixture was filtered through celite and evaporated to yield the crude material which was purified by column chromatography (silica gel) with 5:95 ethanol-ethyl acetate as the mobile phase. (70% yield). $^{1}$H-NMR (DMSO): δ 2.339 (2H, t, J= 6.88 Hz), 2.837 (2H, t, J= 6.88 Hz), 6.325 (1H, ddt, J= 2.65, 1.24, 0.53 Hz), 6.825 (1H, ddd, J= 7.80, 1.54, 0.52 Hz), 7.182 (1H, dq, J= 1.54, 0.50 Hz), 7.224 (1H, dt, J= 2.65, 0.51 Hz), 7.390 (1H, ddt, J= 7.80, 1.24, 0.48 Hz). $^{13}$C-NMR (DMSO): δ 31.812, 38.080, 101.250, 111.052, 120.093, 120.207, 125.199, 126.278, 134.643, 136.581, 174.145. GC-MS (EI): 188.1 (molecular ion), 143.1, 130.1, 117.1, 77.1. Anal. Calcd. for $C_{11}H_{12}N_2O$ 0.1 molecules EtOAc/ 0.1 molecules $H_2O$ C: 68.86, H: 6.59, N: 14.09. Found C: 68.66, H: 6.38, N: 13.97.

**1-N-Pentyl-6-propanamide-indole (109):**

To a Parr flask was added 1-N-Pentyl-6-(2-propenamide)-indole (**103**) (0.29 g) in ethyl acetate (15 mL) and 10 % Pd/C (29 mg). This solution was placed in a nitrogen glove box and degassed for 15 minutes. The mixture was hydrogenated at 50 psi overnight. The mixture was filtered through celite and evaporated to yield the crude material which was purified by column chromatography (silica gel) with 5:95 ethanol-ethyl acetate as the mobile phase. (91% yield). $^{1}$H-NMR ($CDCl_3$): δ 0.894 (3H, t, J= 6.50 Hz), 1.298, (2H, h, J= 6.50 Hz), 1.344 (2H, tt, J= 6.63, 6.50 Hz), 1.822 (2H, tt, J= 7.43, 6.63 Hz), 2.590 (2H, t, J= 6.88 Hz), 3.095 (2H, t, J= 6.88 Hz), 4.074 (2H, t, J= 7.43 Hz), 6.445 (1H, ddt, J= 3.80, 1.61, 0.51 Hz), 6.944 (1H, ddd, J= 7.92, 1.70, 0.48 Hz), 7.053 (1H, ddt, J= 1.70, 0.55, 0.45 Hz), 7.182 (1H, ddd, J= 3.80, 0.55, 0.44 Hz), 7.259 (1H, ddt, J= 7.92, 1.61, 0.50 Hz). $^{13}$C-NMR ($CDCl_3$): δ 13.967, 22.340, 29.132, 29.923, 32.118, 38.508, 46.326, 100.688, 109.008, 119.850, 121.013, 127.038, 127.767, 133.891, 136.208, 174.987. GC-MS (EI): 258.1 (molecular ion), 200.1 (100%), 156.1, 143.1, 130.1, 115.1, 77.1. Anal Calcd. for $C_{16}H_{22}N_2O$ 0.1 molecules EtOAc C: 73.73, H: 8.60, N: 10.49. Found C: 73.79, H: 8.68, N: 10.34.

**1-NH-3-(1-Naphthoyl)-6-propanamide-indole (111):**

To a Parr flask was added 1-NH-3-(1-Naphthoyl)-6-(2-propenamide)-indole (**105**) (0.34 g) in 9:1 MeOH (9 mL): EtOH (1 mL), $Ph_2S$ (0.01 eq, 1.67 uL) and 10% Pd/C (34 mg). This solution was placed in a nitrogen glove box and degassed for 15 minutes. The mixture was hydrogenated at 50 psi overnight. The mixture was filtered through celite and evaporated to yield the crude material which was purified by column chromatography (silica gel) with an ethanol-ethyl acetate as the mobile phase. (49% yield). $^{1}$H-NMR ($CDCl_3$): δ 2.749 (2H, t, J= 6.86 Hz), 3.031 (2H, t, J=6.86

Hz), 6.655 (1H, dd, J= 8.17, 1.81 Hz), 7.230 (1H, dt, J= 1.81, 0.45 Hz), 7.582 (1H, dddd, J= 7.90, 6.98, 1.54, 0.45 Hz), 7.659 (1H, t, J= 0.50 Hz), 7.711 (1H, ddd, J= 8.40, 7.55, 0.45 Hz), 7.894 (1H, dddt, J= 8.40, 2.57, 1.89, 0.46 Hz), 7.901 (1H, ddd, J= 8.32, 6.98, 2.28 Hz), 7.998 (1H, dt, J= 8.17, 0.50 Hz), 8.005 (1H, ddd, J= 7.55, 2.57, 0.44 Hz), 8.176 (1H, dddt, J= 7.90, 2.28, 1.89, 0.47 Hz), 8.259 (1H, ddq, J= 8.32, 1.54, 0.46 Hz). $^{13}$C-NMR ($CDCl_3$): δ 32.407, 34.598, 112.087, 115.609, 121.648, 123.987, 125.006, 125.893, 125.924, 126.832, 127.103, 127.943, 129.208, 130.343, 131.129, 133.125, 134.021, 138.213, 137.562, 138.292, 174.054, 191.083. Anal Calcd. for $C_{22}H_{18}N_2O_2$ 0.2 molecules $H_2O$ C: 76.37, H: 5.36, N: 8.10. Found C: 76.41, H: 5.42, N: 8.12.

**1-N-Pentyl-3-(1-naphthoyl)-6-propanamide-indole (78):**

To a Parr flask was added 1-N-Pentyl-3-(1-naphthoyl)-6-(2-propenamide)-indole (**80**) (0.27 g) in 9:1 MeOH (9 mL): EtOH (1 mL), $Ph_2S$ (0.01 eq, 1.1 uL) and 10% Pd/C (27 mg). This solution was placed in a nitrogen glove box and degassed for 15 minutes. The mixture was hydrogenated at 50 psi overnight. The mixture was filtered through celite and evaporated to yield the crude material which was purified by column chromatography (silica gel) with a ethanol-ethyl acetate as the mobile phase. (71% yield). $^1$H-NMR ($CDCl_3$): δ 0.846 (3H, t, J= 6.50 Hz), 1.307 (2H, h, J= 6.50 Hz), 1.482 (2H, tt, J= 7.00, 6.50 Hz), 2.007 (2H, tt, J= 7.43, 7.00 Hz), 2.639 (2H, t, J= 6.86 Hz), 3.019 (2H, t, J= 6.86 Hz), 4.287 (2H, t, J= 7.43 Hz), 6.559 (1H, dd, J= 8.32, 2.00 Hz), 6.940 (1H, dt, J= 2.00, 0.46 Hz), 7.382 (1H, dddd, J= 7.90, 6.98, 1.54, 0.45 Hz), 7.472 (1H, dt, J= 8.32, 0.45 Hz), 7.612 (1H, ddd, J= 8.40, 7.55, 0.45 Hz), 7.743 (1H, dddt, J= 8.40, 2.56, 1.89, 0.46 Hz), 7.823 (1H, ddd, J= 8.32, 6.98, 2.28 Hz), 7.974 (1H, ddd, J= 7.55, 2.56, 0.44 Hz), 8.046 (1H, dddt, J= 7.90, 2.28, 1.89, 0.47 Hz), 8.075 (1H, ddq, J= 8.32, 1.54, 0.46 Hz), 8.188 (1H, t, J=

0.46 Hz). $^{13}$C-NMR ($CDCl_3$): δ 14.311, 23.829, 27.361, 29.042, 31.879, 33.157, 50.462, 115.293, 118.882, 121.062, 124.749, 125.283, 125.896, 126.234, 126.571, 126.958, 127.884, 127.981, 128.603, 129.042, 130.672, 131.111, 132.982, 134.558, 136.607, 174.082, 191.201. Anal Calcd. for $C_{27}H_{28}N_2O_2$ 0.2 molecules EtOH C: 78.03, H: 6.98, N: 6.64. Found C: 78.18, H: 7.12, N: 6.72.

**1-NH-6-Acetic-acid-methyl-ester-indole (122):**

6-Acetic acid indole (**129**) (0.5 g) was dissolved in DMF (7 mL) and cooled by an ice bath. Anhydrous potassium carbonate (1.3 eq, 0.51 g) was added and mixed for 30 minutes. Methyl iodide (0.2 mL) was added and then the mixture was stirred at room temperature for 2 hours. Water was added to quench the reaction and the product extracted with ethyl acetate (3 x 10 mL). The organic layers were combined and washed with water (3 x 20 mL), dried with sodium sulfate and evaporated to yield the desired compound. No further purification was done. (98% yield). $^1$H-NMR ($CDCl_3$): δ 3.725 (3H, s), 3.756 (2H, s), 6.510 (1H, ddt, J= 3.13, 1.24, 0.54 Hz), 7.054 (1H, ddd, J= 7.89, 1.64, 0.53 Hz), 7.229 (1H, dq, J= 1.64, 0.50 Hz), 7.606 (1H, dt, J= 3.13, 0.51 Hz), 7.626 (1H, ddt, J= 7.89, 1.24, 0.49 Hz). $^{13}$C-NMR ($CDCl_3$): δ 41.701, 52.423, 102.252, 111.940, 120.815, 121.294, 124.820, 126.970, 127.441, 136.035, 173.115. GC-MS (EI): 189.1 (molecular ion), 130.1 (100%), 103.1, 77.1. Anal. Calcd. for $C_{11}H_{11}NO_2$ C: 69.83, H: 5.86, N: 7.40. Found C: 69.95, H: 5.79, N: 7.39.

**1-NH-3-(1-Naphthoyl)-6-acetic-acid-methyl-ester-indole (124):**

To a stirred suspension of aluminum chloride (2.6 eq, 0.46 g) and 1-naphthoyl chloride (0.25 mL) in dry dichloromethane (10 mL), 1-NH-6-Acetic-acid-methyl-ester-indole (**122**) (0.25 g)

was added. The mixture was stirred for 1 hour at 20°C. The resulting mixture was poured into ice and extracted with ethyl acetate (20 mL). The organic layer was washed with aqueous sodium bicarbonate (3 x 25 mL) then dried with sodium sulfate. Upon evaporation, tan crystals appeared. This was purified by column chromatography with 50:50 ethyl acetate-petroleum ether as the mobile phase. (84% yield). $^{1}$H-NMR ($CDCl_3$): δ 3.582 (3H, s), 3.761 (2H, s), 7.113 (1H, dd, J= 8.27, 1.79 Hz), 7.385 (1H, dt, J= 1.79, 0.48 Hz), 7.449 (dddd, J= 7.90, 6.98, 1.54, 0.45 Hz), 7.505 (ddd, J= 8.40, 7.55, 0.45 Hz), 7.616 (1H, t, J= 0.48 Hz), 7.652 (1H, dddt, J= 8.40, 2.57, 1.89, 0.46 Hz), 7.941 (1H, ddd, J= 8.32, 6.98, 2.28 Hz), 7.996 (1H, dt, J= 8.27, 0.52 Hz), 8.033 (1H, ddd, J= 7.55, 2.57, 0.44 Hz), 8.143 (1H, dddt, J= 7.90, 2.28, 1.89, 0.47 Hz), 8.163 (1H, ddq, J= 8.32, 1.54, 0.46 Hz). $^{13}$C-NMR ($CDCl_3$): δ 52.188, 113.567, 117.503, 121.629, 124.159, 124.349, 125.078, 125.261, 125.732, 125.952, 128.680, 128.741, 129.888, 130.093, 130.458, 133.703, 137.190, 137.395, 137.540, 138.961, 172.363, 191.670. Anal. Calcd. for $C_{22}H_{17}NO_3$ C: 76.95, H: 4.99, N: 4.08. Found C: 76.66, H: 4.85, N: 4.13.

**Compound 131:**

6-Acetic acid indole (**129**) (0.4 g) was dissolved in DMF (10 mL) at room temperature and KOH (2.2 eq, 0.3 g) was added and mixed for 30 minutes. 1-Bromopentane (2 eq, 0.57 mL) was added and mixed for two hours. Water was added to quench the reaction and the product extracted with ethyl acetate (20 mL). The organic layers were combined and washed with water (3 x 25 mL), dried with sodium sulfate and evaporated. No further purification was done. (98% yield).

**1-N-Pentyl-6-acetic-acid-indole (132):**

Compound **131** (0.37 g) was dissolved in 1M NaOH/MeOH solution and refluxed overnight. The methanol was evaporated off, washed residue in 1 M HCl and extracted with ethyl acetate (3 x 20 mL). The organic layers were combined, dried with sodium sulfate and evaporated. No further purification was done. (89% yield)

**1-N-Pentyl-6-acetic-acid-methyl-ester-indole (123):**

1-N-Pentyl-6-acetic-acid-indole (**132**) (0.3 g) was dissolved in DMF (10 mL) and anhydrous potassium carbonate 1.3 eq, 0.22 g). After 30 minutes, methyl iodide (0.08 mL) was added and mixed for an additional two hours at room temperature. Water was added to quench the reaction and the product extracted with ethyl acetate (3 x 10 mL). The organic layers were combined and washed with water (3x 20 mL), dried with sodium sulfate and evaporated to yield the crude material. This was purified by column chromatography (silica gel) with 50:50 ethyl acetate-petroleum ether as the mobile phase. (88% yield). $^{1}$H-NMR ($CDCl_3$): δ 0.984 (3H, t, J= 6.50 Hz), 1.359 (2H, h, J= 6.50 Hz), 1.434 (2H, tt, J= 6.63, 6.50 Hz), 1.898 ( 2H, tt, J= 7.43, 6.63 Hz), 3.757 (3H, s), 3.841 (2H, s), 4.111 (2H, t, J= 7.43 Hz), 6.536 (1H, ddt, J= 3.81, 1.67, 0.51 Hz), 7.117 (1H, ddd, J= 7.92, 1.60, 0.50 Hz), 7.133 (1H, dq, J= 1.60, 0.51 Hz), 7.361 (1H, dt, J= 3.81, 0.55 Hz), 7.651 (1H, ddt, J= 7.92, 1.67, 0.50 Hz). $^{13}$C-NMR ($CDCl_3$): δ 14.127, 22.424, 29.194, 30.000, 41.975, 46.329, 52.073, 100.938, 110.185, 120.663, 121.104, 127.137, 127.996, 128.262, 136.240, 172.697. GC-MS (EI): 259.1 (molecular ion), 200.2 (100%), 143.1, 130.1, 103.1, 77.1. Anal. Calcd. for $C_{16}H_{21}NO_2$ C: 74.10, H: 8.16, N: 5.40. Found C: 74.31, H: 8.23, N: 5.54.

**1-N-Pentyl-3-(1-naphthoyl)-6-acetic-acid-methyl-ester-indole (121):**

To a stirred suspension of aluminum chloride (2.6 eq, 0.2 g) and 1-Naphthoyl chloride (0.11 mL) in dry dichloromethane (7 mL), 1-N-Pentyl-6-acetic-acid-methyl-ester-indole (**123**) (0.15 g) was added. The mixture was stirred for 1 hour at 20°C. The resulting mixture was poured into ice and extracted with ethyl acetate (20 mL). The organic layer was washed with aqueous sodium bicarbonate (3 x 10 mL) then dried with sodium sulfate. Upon evaporation, tan crystals appeared. This was purified by column chromatography (silica gel) with 50:50 ethyl acetate-petroleum ether as the mobile phase. (92% yield) $^{1}$H-NMR ($CDCl_3$): δ 0.821 (3H, t, J= 6.50 Hz), 1.238 (2H, h, J=6.50 Hz), 1.272 (2H, tt, J= 7.00, 6.50 Hz), 1.762 (2H, tt, J= 7.43, 7.00 Hz), 3.695 (3H, s), 3.778 (2H, s), 4.022 (2H, t, J= 7.43 Hz), 7.236 (1H, dd, J= 8.28, 1.79 Hz), 7.317 (1H, dt, J= 1.79, 0.46 Hz), 7.437 (1H, dt, J= 8.28, 0.45 Hz), 7.486 (1H, dddd, J= 7.90, 6.98, 1.54, 0.45 Hz), 7.513 (1H, ddd, J= 8.40, 7.55, 0.45 Hz), 7.614 (1H, dddt, J= 8.40, 2.56, 1.89, 0.46 Hz), 7.635 (1H, ddd, J= 8.32, 6.98, 2.28 Hz), 7.868 (1H, ddd, J= 7.55, 2.56, 0.44 Hz), 7.923 (1H, dddt, J= 7.90, 2.28, 1.89, 0.47 Hz), 8.160 (1H, ddq, J= 8.32, 1.54, 0.46 Hz), 8.409 (1H, t, J= 0.46 Hz). $^{13}$C-NMR ($CDCl_3$): δ 13.922, 22.151, 28.868, 29.430, 41.542, 47.073, 52.195, 110.763, 118.000, 122.981, 124.455, 125.906, 126.149, 126.605, 126.856, 128.216, 129.515, 129.918, 130.009, 130.746, 133.710, 137.266, 137.972, 138.253, 138.998, 172.256, 191.883. Anal. Calcd for $C_{27}H_{27}NO_3$ 0.2 molecules EtOAc C: 77.45, H: 6.69, N: 3.25. Found C: 77.55, H: 6.55, N: 3.39.

**1-NH-6-Acetamide-indole (126):**

1-NH-6-Acetic-acid-methyl-ester-indole (**122**) (0.1 g) was dissolved in methanol (3 mL) and ammonium hydroxide (3 mL) was added. This was allowed to stir overnight at room temperature. The methanol was evaporated, water added and the product extracted with ethyl

acetate (3 x 10 mL). The organic layers were combined, dried with magnesium sulfate and evaporated. The product was recrystallized (ethyl acetate) to give white crystals. (72% yield). $^{1}$H-NMR ($CDCl_3$): δ 3.361 (2H, s), 6.317 (1H, ddt, J= 3.13, 1.24, 0.54 Hz), 6.857 (1H, ddd, J= 7.89, 1.63, 0.53 Hz), 7.232 (1H, dq, J= 1.63, 0.50 Hz), 7.329 (1H, dt, J= 3.13, 0.52 Hz), 7.388 (1H, ddt, J= 7.89, 1.24, 0.49 Hz). $^{13}$C-NMR ($CDCl_3$): δ 43.123, 101.258, 112.131, 120.041, 120.846, 125.489, 126.530, 129.501, 136.446, 173.373. GC-MS (EI): 174.1 (molecular ion), 130.1 (100%), 103.0, 77.0. Anal. Calcd. for $C_{10}H_{10}N_2O$ C: 68.95, H: 5.79, N: 16.08. Found C: 68.74, H: 5.64, N: 15.88.

**1-N-Pentyl-6-acetamide-indole (127):**

1-N-Pentyl-6-acetic-acid-methyl-ester-indole (**123**) (0.1 g) was dissolved in methanol (3 mL) and ammonium hydroxide (3 mL) was added. This was allowed to stir overnight at room temperature. The methanol was evaporated, water added and the product extracted with ethyl acetate (3 x 10 mL). The organic layers were combined, dried with magnesium sulfate and evaporated. The product was recrystallized (ethyl acetate) to give white crystals. (69% yield). $^{1}$H-NMR ($CDCl_3$): δ 0.812 (3H, t, J= 6.50 Hz), 1.187 (2H, h, J= 6.50 Hz), 1.264 (2H, tt, J= 6.63, 6.50 Hz), 1.715 (2H, tt, J= 7.43, 6.63 Hz), 3.408 (2H, s), 4.082 (2H, t, J= 7.43 Hz), 6.325 (1H, ddt, J= 3.81, 1.66, 0.51 Hz), 6.789 (1H, ddd, J= 7.92, 1.57, 0.49 Hz), 6.881 (1H, dq, J= 1.57, 0.50 Hz), 7.265 (1H, dt, J= 3.81, 0.54 Hz), 7.289 (1H, ddt, J= 7.92, 1.66, 0.50 Hz). $^{13}$C-NMR ($CDCl_3$): δ 14.394, 22.197, 28.922, 29.879, 43.313, 45.843, 100.642, 110.543, 120.542, 120.899, 127.054, 129.014, 129.675, 136.157, 173.290. GC-MS (EI): 244.2 (molecular ion), 200.2 (100%), 187.1, 143.1, 130.1, 77.1. Anal. Calcd. for $C_{15}H_{20}N_2O$ C: 73.74, H: 8.25, N: 11.47. Found C: 73.48, H: 8.18, N: 11.24.

**1-NH-3-(1-Naphthoyl)-6-acetamide (128):**

1-NH-3-(1-Naphthoyl)-6-acetic-acid-methyl-ester-indole (**124**) (0.1 g) was dissolved in methanol (3 mL) and ammonium hydroxide (3 mL) was added. This was allowed to stir overnight at room temperature. The methanol was evaporated, water added and the product extracted with ethyl acetate (3 x 10 mL). The organic layers were combined, dried with magnesium sulfate and evaporated. The product was recrystallized (ethyl acetate) to give white crystals. (50% yield). $^{1}$H-NMR ($CDCl_3$): δ 3.456 (2H, s), 7.135 (1H, dd, J= 8.26, 1.78 Hz), 7.391 (1H, dt, J= 1.78, 0.48 Hz), 7.475 (1H, dddd, J= 7.90, 6.98, 1.54, 0.45 Hz), 7.496 (1H, ddd, J= 8.40, 7.55, 0.45 Hz), 7.535 (1H, t, J= 0.49 Hz), 7.613 (1H, dddt, J= 8.40, 2.57, 1.89, 0.46 Hz), 7.656 (1H, ddd, J= 8.32, 6.98, 2.28 Hz), 7.948 (1H, dt, J= 8.26, 0.52 Hz), 8.005 (1H, ddd, J= 7.55, 2.57, 0.44 Hz), 8.062 (1H, dddt, J= 7.90, 2.28, 1.89, 0.47 Hz), 8.146 (1H, ddq, J= 8.32, 1.54, 0.46 Hz). $^{13}$C-NMR ($CDCl_3$): δ 42.933, 112.929, 117.526, 121.393, 124.737, 125.177, 125.686, 125.869, 126.249, 127.160, 128.741, 130. 048, 130.496, 131.659, 132.160, 133.718, 137.600, 138.224, 139.044, 172.978, 191.662. Anal. Calcd for $C_{21}H_{16}N_2O_2$ 0.3 molecules $H_2O$ C: 75.57, H: 5.01, N: 8.39. Found C: 75.57, H: 5.16, N: 8.29.

**1-(4-Phenoxybenzyl)-piperazine (133):**

Piperazine (5eq, 0.23 g) in dry dichloromethane (8 mL) was cooled to 0°C. 4-Phenoxybenzyl bromide (**137**) (0.1 mL) was added dropwise and the mixture was stirred for one hour. The solution was washed with saturated aqueous sodium bicarbonate and dried with sodium sulfate and evaporated. The product was recrystallized (methanol) to give tan crystals. (82 % yield). $^{1}$H-NMR ($CDCl_3$): δ 2.489 (4H, ddd, J= 7.20, 6.68, 2.50 Hz), 2.957 (4H, ddd, J= 9.49, 6.68, 2.50

Hz), 3.465 (2H, s), 6.926 (2H, ddd, J= 8.18, 1.33, 0.55 Hz), 7.076 (2H, dddd, J= 8.11, 1.50, 1.35, 0.51 Hz), 7.236 (1H, tt, J= 7.59, 1.35 Hz), 7.308 (2H, ddd, J= 8.18, 1.14, 0.55 Hz), 7.330 (2H, dddd, J= 8.11, 7.59, 1.47, 0.51 Hz). $^{13}$C-NMR ($CDCl_3$): δ 45.341 (2eq C), 53.395 (2 eq C), 62.673, 115.116 (2 eq C), 119.334 (2 eq C), 123.345, 129.880 (2 eq C), 130.693 (2 eq C), 132.479, 156.345, 157.226. GC-MS (EI): 268.1 (molecular ion), 226.1, 212.1, 183.1 (100%), 153.1, 107.0, 85.1, 56.1. Anal. Calcd for $C_{17}H_{20}N_2O$ 0.1 molecule $CH_2Cl_2$/$H_2O$/EtOAc C: 73.12, H: 7.43, N: 9.75. Found C: 73.33, H: 7.32, N: 9.48.

**1-(4-Phenoxybenzyl)-piperazine-methylsulfonyl (134):**

1-(4-Phenoxybenzyl)-piperazine (**133**), trimethylamine (1.5 eq) and dry dichloromethane were added to a round bottom flask and cooled in an ice bath. Methanesulfonyl chloride (1.1 eq) was added dropwise and the solution was mixed for one hour, evaporated, extracted with dichloromethane and washed with aqueous 1M NaOH solution. The organic layer was washed with saturated aqueous ammonium chloride solution then dried with sodium sulfate and evaporated. The product was recrystallized (8:2 petroleum ether: ethyl acetate) to give yellow crystals. (87% yield). $^{1}$H-NMR ($CDCl_3$): δ 2.548 (4H, ddd, J= 13.32, 6.70, 2.82 Hz), 2.759 (3H, s), 3.234 (4H, ddd, J= 14.40, 6.73, 2.79 Hz), 3.506 (2H, s), 6.937 (2H, ddd, J= 8.18, 1.47, 0.55 Hz), 6.984 (2H, dddd, J=8.11, 1.50, 1.35, 0.51 Hz), 7.002 (1H, tt, J= 7.59, 1.35 Hz), 7.233 (2H, ddd, J= 8.18, 1.14, 0.55 Hz), 7.319 (2H, dddd, J= 8.11, 7.59, 1.47, 0.51 Hz). $^{13}$C-NMR ($CDCl_3$): δ 34.331, 45.880 (2 eq C), 52.521(2 eq C), 61.936, 118.817 (2 eq C), 119.402 (2 eq C), 123.475, 129.477 (2 eq C), 130.610 (2 eq C), 132.167, 156.558, 157.120. GC-MS (EI): 346.2 (molecular ion), 267.1, 183.1 (100%), 155.1, 107.0, 77.0. Anal. Calcd for $C_{18}H_{22}N_2O_3S$ 0.2 molecules $H_2O$/EtOAc C: 61.42, H: 6.58, N: 7.62, S: 8.72. Found C: 61.22, H: 6.20, N: 7.62, S: 8.69.

## References


[1] Mechoulam, R. and Parker, L.A. The endocannabinoid system and the brain. Annu. Rev. Psychol. (2013) 64:21-47.

[2] Russo, E. B. Taming THC: potential cannabis synergy and phytocannabinoid-terpenoid entourage effects. Brj. Pharmacol. (2011) 163 1344-1364.

[3] Marzo, V. D. and Piscitelli, F. The endocannabinoid system and its modulation by phytocannabinoids. Neurotherapeutics. (2015). 12: 692-698.

[4] Lu, H.C. and Mackie, K. Review of the endocannabinoid system. Biological Psychiatry. (2021) 6:607-615

[5] Battista, N., Tommaso, M.D., Bari, M., Maccarrone, M. The endocannabinoid system: an overview. Frontiers in Behavioral Neuroscience. (2012). 6: 1-7. doi: 10.3389/fnbeh.2012.00009

[6] Fakhoury, M. Role of the Endocannabinoid system in the pathophysiology of schizophrenia. Mol Neurobiol. (2017) 54: 768-778.

[7] Khan, M.I., Sobocinska, A.A., Czarnecka, A.M., Krol, M., Botta, B., Szczylik, C. The therapeutic aspects of the endocannabinoid syste, (ECS) for cancer and their development: from nature to laboratory. Current Pharmaceutical Design (2016) 22: 1756-1766.

[8] Mechoulam, R., Fride, E., Marzo, V.D. Endocannabinoids. European Journal of Pharmacology. (1998) 359: 1-18.

[9] Mackie, K. Cannabinoid receptors as therapeutic targets. Annu. Rev. Pharmacol. Toxicol. (2006) 46: 101-122.

[10] Herkenham, M., Lynn, A.B., Little, M.D., Johnson, M.R., Melvin, L.S., DE Costa, B.R., Rice, K.C. Cannabinoid receptor localization in brain. Proc. Natl. Acad. Sci. (1990). 87: 1932-1936.

[11] Pertwee, R.G. Pharmacology of cannabinoid CB1 and CB2 receptors. Pharmacol. Ther. (1997). 74: 129-180.

[12] Guindon, J. and Hohmann, A.G. Cannabinoid CB2 receptors: a therapeutic target for the treatment of inflammatory and neuropathic pain. British Journal of Pharmacology. (2008) 153: 319-334.

[13] Lu, H.C., and Mackie, K. An introduction to the endogenous cannabinoid system. Biol Psychiatry. (2016) 79: 516-525.

[14] Fowler, C.J. Transport of endocannabinoids across the plasma membrane and within the cell. FEBS Journal. (2013). 280: 1895-1904.

[15] CBD Source. 3 Classes of cannabinoids. Nov. 10, 2020. URL: 3 Classes of Cannabinoids | CBD Source (cbd4x.com). Accessed: September 16, 2021.

[16] Lambert, D.M. and Fowler, C.J. The endocannabinoid system: drug targets, lead compounds, and potential therapeutic applications. Journal of Medicinal Chemistry. (2005). 48: 5059-5087.

[17] Niesink, R.J.M. and van Laar, M.W. Does cannabidiol protect against adverse psychological effects of THC? Front. Psychiatry (2013). 130: 1-8. https://doi.org/10.3389/fpsyt.2013.00130

[18] Hoffmann, D.E. and Weber, E. Medical marijuana and the law. N Engl J Med. (2010). 362: 1453-1457.

[19] Pisanti, S., Malfitano, A.M., Ciaglia, E., Lamberti, A., Ranieri, R., Cuomo, G., Abate, M., Faggiana, G., Proto, M.C., Fiore, D., Laezza, C., Bifulco, M. Cannabidiol: state of the art and new challenges for therapeutic applications. Pharmacology and Therapeutics (2017). 175: 133-150.

[20] Le Boisselier, R., Alexandre, J., Lelong-Boulouard, V., Debruyne. D. Focus on cannabinoids and synthetic cannabinoids. Clinical Pharmacology and Therapeutics. (2017). 101: 220-229.

[21] Lemberger L. (1999) Nabilone. In: Nahas G.G., Sutin K.M., Harvey D., Agurell S., Pace N., Cancro R. (eds) Marihuana and Medicine. Humana Press, Totowa, NJ. https://doi.org/10.1007/978-1-59259-710-9_54

[22] Lumitos. Chemeurope.com. CP 55,940. https://www.chemeurope.com/en/encyclopedia/CP_55%2C940.html. Accessed September 18, 2021.

[23] Kuster, J.E., Stevenson, J.I., Ward, S.J., D'ambra, T.E., Haycock, D.A. Aminoalkylindole binding in rat cerebellum: selective displacement by natural and synthetic cannabinoids. J Pharmacol Exp Ther. (1993). 264(3):1352-1363.

[24] Hudson, S. and Ramsey, J. The emergence and analysis of synthetic cannabinoids. Drug Test. Analysis. (2011). 3: 466-478.

[25] S. Every-Palmer. Synthetic cannabinoid JWH-018 and psychosis: an explorative study. Drug Alcohol Depend. (2011). 117: 152-157.

[26] Mills, B., Yepes, A., Nugent, K. Synthetic cannabinoids. The American Journal of the Medical Sciences. (2015). 350: 59-62.

[27] NIDA. 2018, February 5. Synthetic Cannabinoids (K2/Spice) DrugFacts. Retrieved from https://www.drugabuse.gov/publications/drugfacts/synthetic-cannabinoids-k2spice on 2021, October 18

[28] Simmons, J., Cookman, L., Kang, C., Skinner, C. Three cases of "spice" exposure. Clinical Toxicology (2011). 49: 431-433.

[29] Federal Register Volume 76, Number 40, 2011, pp.11075-11078.

[30] Lindigkeit, R., Boehme, A., Eiserloh, I., Luebbecke, M., Wiggermann, M., Ernst, L., Beuerle, T. Spice: A never ending story? Forensic Science International. (2009). 191: 58-63.

[31] Congress.gov. H.R. 5484- Anti-Drug Abuse Act of 1986. https://www.congress.gov/bill/99th-congress/house-bill/5484. Accessed August 10, 2021

[32] Kusano, M., Yamanaka, M., Zaitsu, K., Nakayama, H., Nakajima, J., Moriyasu, T., Tsuchihasi, H., Ishii, A. Regioisomeric differentiation of the alkyl-substituted synthesis cannabinoids JWH-122 and JWH-210 by GC-EI-MS/MS. Forensic Toxicol. (2016). 34: 304-315.

[33] Montero, C., Campillo, N. E., Goya, P., Paez, J. A. Homology models of the cannabinoid CB1 and CB2 receptors. A docking analysis study. European Journal of Medicinal Chemistry. (2005). 40: 75-83.

[34] Atwood, B. K., Straiker, A., Mackie, K. CB2: Therapeutic target-in-waiting. Progress in Neuro-Psychopharmacology & Biological Psychiatry. (2012). 38: 16-20.

[35] Henness, S., Robinson, D. M., Lyseng-Williamson, K.A. Rimonabant. Drugs. (2006). 66: 2109-2119.

[36] Proietto, J., Rissanen, A., Harp, J. B., Erondu, N., Yu, Q., Suryawanshi, S., et. al. clinical trial assessing the safety and efficacy of the CB1R inverse agonist taranbant in obese and overweight patients: low-dose study. Int J Obes. (2010). 34: 1243-1254.

[37] Addy, C., Wright, H., Laere, K. V., Gantz, I., Erondu, N., Musser, B. J., et. al. The acyclic CB1R inverse agonist taranabant mediates weight loss by increasing energy expenditure and decreasing caloric intake. Cell Metabolism. (2008). 7: 68-78.

[38] Dhopeshwarkar, A., and Mackie, K. CB2 cannabinoid receptors as a therapeutic target-What does the future hold? Mol Pharmacol. (2014). 86: 430-437.

[39] Magham, S.V., Krishnamurthy, P.T., Shaji, N., Mani, L., Balasubramanian, S. Cannabinoid receptor 2 selective agonists and Alzheimer's disease: An insight into the therapeutic potentials. J Neurosci Res. (2021). 1-18.

[40] Hashiesh, H. M., Sharma, C., Goyal, S. N., Jha, N. K., Ojha, S. Pharmacological properties, therapeutic potential and molecular mechanisms of JWH-133, a CB2 receptor-selective agonist. Front. Pharmacol. (2021). 12: 702675.

[41] Hashiesh, H.M., Jha, N.K., Sharma, C., Gupta, P.K., Jha, S.K., Patil, C.R., et. al. Pharmacological potential of JWH133, a cannabinoid type 2 receptor agonist in neurodegenerative, neurodevelopmental and neuropsychiatric diseases. European Journal of Pharmacology. (2021). 909: 174398.

[42] Xing, C., Zhuang, Y., Xu, T. H., Feng, Z., Zhou, X. E., Chen, M., et. al. Cryo-EM structure of the human cannabinoid receptor CB2-Gi signaling complex. Cell. (2020). 180: 645-654.

[43] Kalita, J. M., Saha, A., Nath, D., Patangia, U. Advances in computer aided drug design. Universal J Pharm Sci Res (UJPSR). (2015). 2: 17-22.

[44] Yu, W., and MacKerell Jr, A. D. Computer-aided drug design methods. Methods in Mol Biol. (2017). 1520: 85-106.

[45] Sabe, V. T., Ntombela, T., Jhamba, L. A., Maguire, G. E. M., Govender, T., Naicker, T. et. al. Current trends in computer aided drug design and a highlight of drugs discovered via computional techniques: A review. European Journal of Medicinal Chemistry. (2021). 224: 113705.

[46] Abiedalla, Y., Smith, L. W., Abdel-Hay, K. M., Neel, L., Belal, T. S., Thaxton-Weissenfluh, A. et. al. Spectroscopic differentiation and chromatographic separation of regioisomeric indole aldehydes: synthetic cannabinoids precursors. Forensic Chemistry. (2019). 12. 78-90.

[47] Jang, M., Yang, W., Shin, I., Choi, H., Chang, H., Kim, E. Determination of Am-2201 metabolites in urine and comparison with JWH-018 abuse. Int J Legal Med. (2014). 128: 285-294.

[48] DeRuiter, J., Smith, F., Abiedalla, Y., Neel, L., Clark, C. R. GC-MS and GC-IR analysis of regioisomeric cannabinoids related to 1-(5-fluoropentyl)-3-(1-naphthoyl)-indole. Forensic Chemistry. (2018). 10: 48-57.

[49] Thaxton, A., Belal, T. S., Smith, F., DeRuiter, J., Abdel-Hay, K. M., Clark, C.R. GC-MS studies on the six naphthoyl-substituted 1-n-pentyl-indoles: JWH-018 and five regioisomeric equivalents. Forensic Sci Int. (2015). 252:107-113.

[50] Thaxton-Weissenfluh, A., Alsegiani, A.S., Abiedalla, Y., DeRuiter, J., Smith, F., Clark, C.R. Analytical studies on the 2-naphthoyl substituted-1-n-pentylindoles: regioisomeric synthetic cannabinoids. J Chromatogr. B. (2018). 1077-1078: 77-84.

[51] Thaxton, A., Belal, T.S., Smith, F., DeRuiter, J., Abdel-Hay, K.M., Clark, C.R. Mass spectral studies on 1-n-pentyl-3-(1-naphthoyl)-indole (JWH-018), three deuterium labeled analogues and the inverse isomer 1-naphthoyl-3-n-pentylindole. Rapid Commun Mass Spectrom. (2015). 29: 871-877.

[52] Abdel-Hay, K. M., DeRuiter, J., Smith, F., Alsegiani, A.S., Thaxton-Weissenfluh, A., Clark, C.R. GC-MS differentiation of the six regioisomeric dimethoxybenzoyl-1-pentylindoles: isomeric cannabinoid substances. J Pharm Biomed Anal. (2016). 125: 360-368.

[53] Smith, F.T., DeRuiter, J., Abdel-Hay, K.M., Clark, C.R. GC-MS and FTIR evaluation of the six benzoyl-substituted-1-pentylindoles: isomeric synthetic cannabinoids. Talanta. (2014). 129: 171-182.

[54] Shevyrin, V., Melkozerov, V., Nevero, A., Eltson, O., Morzherin, Y., Shafran, Y. Identification and analytical properties of new synthetic cannabimimetics bearing 2,2,3,3-tetramethylcyclopropanecarbonyl moiety. Forensic Sci Int. (2013). 226: 62-73.

[55] Aung, M.M., Griffin, G., Huffman, J.W., Wu, M.J., Keel, C., Yang, B., et. al. Influence of the N-1 alkyl chain length of cannabimimetic indoles upon CB1 and CB2 receptor binding. Drug Alcohol Depend. (2000). 60: 133-140.

[56] Huffman, J.W., Zengin, G., Wu, M.J., Lu. J., Hynd, G., Bushell, K., et. al. Structure-activity relationships for 1-alkyl-3-(1-naphthoyl)indoles at the cannabinoid CB1 and CB2 receptors: steric and electronic effects on naphthoyl substituents. New highly selective CB2 receptor agonists. Bioorg Med Chem. (2005). 13: 89-112.

[57] Uchiyama, N., Matsuda, S., Kawamura, M., Kikura-Hanajiri, R., Goda, Y. Two new-type cannabimimetic quinolinyl carboxylates, QUPIC and QUCHIC, two new cannabimimetic carboxamide derivatives, ADB-FUBINACA and ADBICA, and five synthetic cannabinoids detected with a thiophene derivative a-PVT and an opioid receptor agonist AH-7921 identified in illegal products. Forensic Toxicol. (2013). 31: 223-240.

[58] Carroll, F.I., Lewin, A.H., Mascarella, S.W., Seltzman, H.H., Reddy, P.A. Designer drugs: a medicinal chemistry perspective. Annals of the New York Academy of Sciences. (2012). 1248: 18-38.

[59] Shulgin, A. PiHKAL: a chemical love story. Transform Press, Berkley, CA. (1991).

[60] Bauer, C.T., Banks, M.L., Blough, B.E., Negus, S.S., Use of intracranial self-stimulation to evaluate abuse-related and abuse-limiting effects if monoamine releasers in rats. British Journal of Pharmacology. (2013). 168: 850-862.

[61] DeRuiter, J., Clark, C.R., Noggle, F.T. GC-MS and HPLC analysis of bromination products of the regioisomeric dimethoxyphenethylamines: Differentiation of nexus from five positional isomers. Journal of Chromatographic Science. (1998). 36: 23-28.

[62] Thaxton-Weissenfluh, A., Belal, T.S., DeRuiter, J., Smith, F., Abiedalla, Y, Neel, L. et. al. GC-MS and GC-IR analyses of the methoxy-1-n-pentyl-3-(1-naphthoyl)-indoles: regioisomeric designer cannabinoids. Journal of Chromatographic Science. (2018). 56: 779-788.

[63] Pan, W., Dong, D., Wang, K., Zhang, J., Wu, R., Xiang, D., et. al. Efficient one-pot synthesis of highly substituted pyridine-2-(1H)-ones via the Vilsmeier-Haack reaction of 1-Acetyl,1-carbamoyl cyclopropanes. Org Lett. (2007). 9:2421-2423.

[64] Organic Chemistry Portal. Dess-Martin Oxidation. https://www.organic-chemistry.org/namedreactions/dess-martin-oxidation.shtm. Accessed July 29, 2021.

[65] Abdel-Hay, K.M., DeRuiter, J., Smith, F., Belal, T.S., Clark, C.R. GC-MS analysis of the regioisomeric methoxy- and methyl-benzoyl-1-pentylindoles: Isomeric synthetic cannabinoids. Science and Justice. (2015). 55: 291-298

[66] Nakajima, J., Takahashi, M., Nonaka, R., Seto, T., Suzuki, J., Yoshida, M., et. al. Identification and quantification of a benzoylindole (2-methoxyphenyl) (1-pentyl-1H-indol-3-yl)methanone and a naphthoylindole 1-(5-fluoropentyl-1H-indol-3-yl)-(naphthalene-1-yl)methanone (AM-2201) found in illegal products obtained via the internet and their cannabimimetic effects evaluated by in vitro [35S] GTPcS binding assays. Forensic Toxicology. (2011). 29: 132-141.

[67] Jabeen, A., Mohamedali, A., Ranganathan, S. Protocol for protein structure modeling. Encyclopedia of Bioinformatics and Computational Biology. (2019). 3: 252-272.

[68] Ramachandran, G.N., Ramakrishnan, C., Sasisekharan, V. Stereochemistry of polypeptide chain configurations. J Mol Biol. (1963). 7:95-99.

[69] Ho, B.K. and Brasseur, R. The Ramachandran plots of glycine and pre-proline. BMC Struct Biol. (2005). 5:14.

[70] Hu, J., Feng, Z., Ma, S., Zhang, Y., Tong, Q., Alqarni, M.H., et. al. Difference and influence of inactive and active states of cannabinoid receptor subtype CB2: From conformation to drug discovery. J Chem Inf Model. (2016). 56:1152-1163.

[71] Chiba, T., Ueno, S., Obara, Y., Nakahata, N. A synthetic cannabinoid, CP55940, inhibits lipopolysaccharide-induced cytokine mRNA expression cannabinoid receptor-independent mechanism in rat cerebellar granule cells. Journal of Pharmacy and Pharmacology. (2011). 63: 636-647.

[72] Niederhoffer, N. and Szabo, B. Effect of the cannabinoid receptor agonist WIN55212-2 on sympathetic cardiovascular regulation. British Journal of Pharmacology. (1999). 126: 457-466.

[73] Han, S., Thatte, J., Buzard, D.J., Jones, R.M. Therapeutic utility of cannabinoid receptor type 2 (CB2) selective agonists. J Med Chem. (2013). 56: 8224-8256.

[74] Schrodinger. Docking and Scoring. https://www.schrodinger.com/science-articles/docking-and-scoring. Retrieved September 17, 2021.

[75] Warren, G.L.; Andrews, C.W.; Capelli, A.-M.; Clarke, B.; LaLonde, J.; Lambert, M.H.; Lindvall, M.; Nevins, N.;Semus, S.F.; Senger, S.; et al. A critical assessment of docking programs and scoring functions. J. Med. Chem.2006, 49, 5912–5931.

[76] Ferrara, P.; Gohlke, H.; Price, D.J.; Klebe, G.; Brooks, C.L. Assessing scoring functions for protein-ligand interactions. J. Med. Chem. 2004, 47, 3032–3047.

[77] Kontoyianni, M.; McClellan, L.M.; Sokol, G.S. Evaluation of docking performance: Comparative data on docking algorithms. J. Med. Chem. 2004, 47, 558–565.

[78] Perola, E.; Walters, W.P.; Charifson, P.S. A detailed comparison of current docking and scoring methods on systems of pharmaceutical relevance. Proteins 2004, 56, 235–249.

[79] Bender, A. and Glen, R.C. A discussion of measures of enrichment in virtual screening: comparing the information content of descriptors with increasing levels of sophistication. J Chem Inf Model. (2005). 45: 1369-1375.

[80] Friesner, R. A.; Banks, J. L.; Murphy, R. B.; Halgren, T. A.; Klicic, J. J.; Mainz, D. T.; Repasky, M. P.; Knoll, E. H.; Shaw, D. E.; Shelley, M.; Perry, J. K.; Francis, P.; Shenkin, P. S, "Glide: A New Approach for Rapid, Accurate Docking and Scoring. 1. Method and Assessment of Docking Accuracy". *J. Med. Chem.* (**2004**). *47*: 1739-1749.

[81] Halgren, T. A.; Murphy, R. B.; Friesner, R. A.; Beard, H. S.; Frye, L. L.; Pollard, W. T.; Banks, J. L., "Glide: A New Approach for Rapid, Accurate Docking and Scoring. 2. Enrichment Factors in Database Screening". *J. Med. Chem.* (**2004**). *47*: 1750-1759.

[82] Ahmed, L., Alogheli, H., McShane, S.A., Alvarsson, J., Berg, A., Larsson, A. Predicting target profiles with confidence as a service using docking scores. J. Cheminform. (2020). 12: 62.

[83] Truchon, J.F. and Bayly, C.I. Evaluating virtual screening methods: good and bad metrics for the “early recognition" problem. J. Chem. Inf. Model. (2007). 47: 488-508.

[84] Pharmacelera Science. Measuring virtual screening accuracy. https://new.pharmacelera.com/science/measuring-virtual-screening-accuracy/. Accessed October 25, 2021.

[85] Gouldson, P., Calandra, B., Legoux, P., Kerneis, A., Rinaldi-Carmona, M., Barth, F., et. al. Mutational analysis and molecular modelling of the antagonist SR 144528 binding site on the human cannabinoid CB2 receptor. European Journal of Pharmacology. (2000). 401: 17-25.

[86] Shahbazi, F., Grandi, V., Banerjee, A., Trant, J.F. Cannabinoids and cannabinoid receptors: the story so far. iScience. (2020). 23: 101301.

[87] Sobolevsky, T., Prasolov, I., Rodchemkov, G. Detection of JWH-018 metabolites in smoking mixture post-administration urine. Forensic Sci Intl. (2010). 200: 141-147.

[88] Li, X., Hua, T., Vemuri, K., Ho, J.H., Wu, Y. Wu, L., et. al. Crystal structure of the human cannabinoid receptor CB2. Cell. (2019). 176: 459-467.

[89] Yang, A.S. and Honig, B. An integrated approach to the analysis and modeling of protein sequences and structures. II. On the relationship between sequence and structural similarity for proteins that are not obviously related in sequence. J Mol Biol. (2000). 301: 679-689.

[90] Lin, S.W. and Sakmar, T.P. Specific tryptophan UV-absorbance changes are probes of the transition of rhodopsin to its active state. Biochemistry. (1996). 35: 11149-11159.

[91] Erlanson, D.A., McDowell, R.S., O’Brien, T. Fragment-Based Drug Discovery. Journal of Medicinal Chemistry. (2004). 47: 3463-3482.

[92] Li, Q. Application of fragment-based drug discovery to versatile targets. Front. Mol. Biosci. (2020). 7:180.

[93] Schrodinger. Glide. https://www.schrodinger.com/products/glide. Accessed October 3, 2021.

[94] Hodgson, H.H. The Sandmeyer reaction. Chemical Reviews. (1947). 251-277.

[95] Conrad, W.E., Rodriguez, K.X., Nguyen, H.H., Fettinger, J.C., Haddadin, M.J., Kurth, M.J. A one-pot-three-step route to triazolotriazepinoindazolones from oxazolino-2H-indazoles. Org Lett. (2012). 15: 3870-3873.

[96] Prieto, M., Zurita, E., Rosa, E., Munoz, L., Lloyd-Williams, P., Giralt, E. Arylboronic acids and arylpinacolboronate esters in Suzuki coupling reactions involving indoles. Partner role swapping and heterocycle protein. J Org Chem. (2004). 69(20): 6812-6820.

[97] Huo, J., Zhang, J., Zhao, B. Preparation of N-1-phenyl-3-(2-furanyl)-1H-pyrazol-5-yl carboxamide derivatives useful as agricultural fungicides and herbicides. Patent CN106083831. (2016).

[98] Okauchi, T., Itonaga, M., Minami, T., Owa, T., Kitoh, K., Yoshino, H. A general method for acylation of indoles at the 3-position with acyl chlorides in the presence of dialkylaluminum chloride. Org Lett. (2000). 10: 1485-1487.

[99] Cabri, W. and Candiani, I. Recent developments and new perspectives in the Heck reaction. Acc Chem Res. (1995). 28: 2-7.

[100] Baek, G.H., Cho, S.J., Jung, Y.S., Seong, C.M., Lee, C.W., Park, N.S. Synthesis of 3-arylpropylamine derivatives from aryl halides using Heck reation. Bull Korean Chem Soc. (1999). 20: 232-236.

[101] Vomacka, J., Korotkov, V.S., Bauer, B., Weinandy, F., Kunzmann, M.H., Krysiak, J., et. al. An aromatic hydroxyamide attenuates multiresistant staphylococcus aureus toxin expression. Chemistry- European Journal. (2016). 22: 1622-1630.

[102] Lipshutz, B.H., Wilhelm, R.S., Kozlowski, J.A. The chemistry of higher order organocuprates. Tetrahedron Letters. (1984). 40: 5005-5038.

[103] Nickerson, D.M. and Mattson, A.E. Transition metal and hydrogen bond donor hybrids: catalysts for the activation of alkylidene malonates. Chemistry. (2012). 18(27): 8310-8314.

[104] Bernard, A.M., Piras, P.P., Serra, A. Stereochemistry of decarboxylation of arylmethylene-propanedioic acids dimethyl esters. Tetrahedron Letters. (1985). 26: 4391-4392.

[105] Rathke, M.W. Beta-hydroxy esters from ethyl acetate and aldehydes or ketones: ethyl 1-hydroxycyclohexylacetate. Organic Syntheses. (1988). 53: 66.

[106] Tomoo, T., Nakatsuka, T., Katayama, T., Hayashi, Y., Fujieda, Y., Terakawa, M., et. al. Design, synthesis, and biological evaluation of 3-(1-aryl-1H-indol-5-yl)propanoic acids as new indole-based cytosolic phospholipase A2alpha inhibitors. J Med Chem. (2014). 57: 7244-7262.

[107] Cullen, M., Bastos, C.M., Parks, D., Munoz, B. Proteasome activity enhancing compounds. Patent WO2020006296. (2020).

[108] Eggers, K., Fyles, T.M., Montoya-Pelaez, J.M. Synthesis and characterization of photoswitchable lipids containing hemithioindigo chromophores. J Org Chem. (2001). 66: 2966-2977.

[109] Mori, A., Miyakawa, Y., Ohashi, E., Haga, T., Maegawa, T., Sajiki, H. Pd/C-Catalyzed chemoselective hydrogenation in the presence of diphenylsulfide. Org Lett. (2006). 8: 3279-3281.

[110] Agonist and antagonist functional data was generously provided by the National Institute of Mental Health's Psychoactive Drug Screening Program, Contract # HHSN-271-2018-00023-C (NIMH PDSP). The NIMH PDSP is Directed by Bryan L. Roth at the University of North Carolina at Chapel Hill and Project Officer Jamie Driscoll at NIMH, Bethesda MD, USA. For experimental details please refer to the PDSP web site https://pdsp.unc.edu/ims/investigator/web/.

[111] Nagai, K., Nagasawa, K., Takahashi, H., Baba, M., Fujioka, S., kondoh, E., et. al. Preparation of ring-fused compounds as inhibitors of transport protein urate transporter 1 (URAT1). Patent WO2012102405. (2012).

[112] Tantray, M.A., Khan, I., Hamid, H., Alam, M.S., Dhulap, A., Kalam, A. Synthesis of aryl anilinomaleimide based derivatives as glycogen synthase kinase-3beta inhibitors with potential role as antidepressant agents. New J Chem. (2016). 40: 6109.

[113] Baati, R., Brown, R., Dias, J., Maryan-Instone, A., Yerri, J. Preparation of 3,6-disubstituted-2-pyridinaldoxime scaffolds for use in therapy. Patent EP3696170. (2020).

[114] De Crescenzo, G.A., Rico, J.G., Boehm, T.L., Carroll, J.N., Kassab, D.J., Mischke, D.A. Preparation of sulfamato hydroxamic acid metalloprotease inhibitors. Patent WO2000046221. (2000).